U.S. DEPARTMENT OF COMMERCE
National Technical Information Service

PB-253 450

TURBULENCE MODELING AND ITS APPLICATION TO ATMOSPHERIC DIFFUSION

PART I: RECENT PROGRAM DEVELOPMENT, VERIFICATION, AND APPLICATION

AERONAUTICAL RESEARCH ASSOCIATES OF PRINCETON, INCORPORATED

PREPARED FOR
ENVIRONMENTAL SCIENCES RESEARCH LABORATORY

DECEMBER 1975

162117

EPA/600/4-75/016a
December 1975

PB 253 450

Environmental Monitoring Series

TURBULENCE MODELING AND ITS APPLICATION TO ATMOSPHERIC DIFFUSION

Part I

Environmental Sciences Research Laboratory
Office of Research and Development
U.S. Environmental Protection Agency
Research Triangle Park, N.C. 27711

TECHNICAL REPORT DATA
(Please read Instructions on the reverse before completing)

1. REPORT NO.	2.	3. RECIPIENT'S ACCESSION NO.
EPA/600/4-75/016a		

4. TITLE AND SUBTITLE
TURBULENCE MODELING AND ITS APPLICATION TO ATMOSPHERIC DIFFUSION. PART I: RECENT PROGRAM DEVELOPMENT, VERIFICATION, AND APPLICATION

5. REPORT DATE
December 1975

6. PERFORMING ORGANIZATION CODE

7. AUTHOR(S)
W. S. Lewellen and M. Teske

8. PERFORMING ORGANIZATION REPORT NO.
A.R.A.P. Report 254, Part I

9. PERFORMING ORGANIZATION NAME AND ADDRESS
Aeronautical Research Associates of Princeton, Inc.
50 Washington Road
Princeton, New Jersey 08540

10. PROGRAM ELEMENT NO.
1AA009

11. CONTRACT/GRANT NO.
EPA 68-02-1310

12. SPONSORING AGENCY NAME AND ADDRESS
Environmental Sciences Research Laboratory
Office of Research and Development
U.S. Environmental Protection Agency
Research Triangle Park, North Carolina 27711

13. TYPE OF REPORT AND PERIOD COVERED
Interim

14. SPONSORING AGENCY CODE
EPA-ORD

15. SUPPLEMENTARY NOTES
Issued as Part I of 2 Parts

16. ABSTRACT

This report details the progress made at A.R.A.P. during fiscal year 1975 towards the goal of developing a viable computer model based on second-order closures of the turbulent correlation equations for predicting the fate of nonchemically reacting contaminants released in the atmospheric boundary layer. The invariant turbulent model discussed in previous reports has been further verified by new comparisons between model predictions and experimental observations. Model capability has been extended by increasing the dimensions of the program to permit the calculation of two-dimensional, unsteady turbulent flow. A number of practical plume calculations were made and compared with standard Gaussian plume assumptions. Calculations are also made for comparison with the complementary turbulent models being developed at The Pennsylvania State University and Flow Research, Inc.

17. KEY WORDS AND DOCUMENT ANALYSIS

PRICES SUBJECT TO CHANGE

a. DESCRIPTORS	b. IDENTIFIERS/OPEN ENDED TERMS	c. COSATI Field/Group
* Turbulence		12A
* Turbulent flow		20D
* Turbulent diffusion		04A
* Atmospheric diffusion		13B
* Boundary layer		14G
* Air pollution		
* Mathematical models		

18. DISTRIBUTION STATEMENT	19. SECURITY CLASS *(This Report)*	21. NO. OF PAGES
RELEASE TO PUBLIC	UNCLASSIFIED	90
	20. SECURITY CLASS *(This page)* UNCLASSIFIED	22. PRICE $5.00 - 2.25

EPA Form 2220-1 (9-73)

EPA-600/4-75-016a
December 1975

TURBULENCE MODELING AND ITS APPLICATION TO ATMOSPHERIC DIFFUSION
PART I: RECENT PROGRAM DEVELOPMENT, VERIFICATION, AND APPLICATION

by

W. S. Lewellen and M. Teske
Aeronautical Research Associates of Princeton, Inc.
Princeton, New Jersey 08540

Contract No. 68-02-1310

Project Officer

Kenneth L. Calder
Meteorology and Assessment Division
Environmental Sciences Research Laboratory
Research Triangle Park, North Carolina 27711

U.S. ENVIRONMENTAL PROTECTION AGENCY
OFFICE OF RESEARCH AND DEVELOPMENT
ENVIRONMENTAL SCIENCES RESEARCH LABORATORY
RESEARCH TRIANGLE PARK, NORTH CAROLINA 27711

ja

DISCLAIMER

This report has been reviewed by the Environmental Sciences Research Laboratory, U.S. Environmental Protection Agency, and approved for publication. Approval does not signify that the contents necessarily reflect the views and policies of the U.S. Environmental Protection Agency, nor does mention of trade names or commercial products constitute endorsement or recommendation for use.

RESEARCH REPORTING SERIES

Research reports of the Office of Research and Development, U.S. Environmental Protection Agency, have been grouped into five series. These five broad categories were established to facilitate further development and application of environmental technology. Elimination of traditional grouping was consciously planned to foster technology transfer and a maximum interface in related fields. The five series are:

1. Environmental Health Effects Research
2. Environmental Protection Technology
3. Ecological Research
4. Environmental Monitoring
5. Socioeconomic Environmental Studies

This report has been assigned to the ENVIRONMENTAL MONITORING series. This series describes research conducted to develop new or improved methods and instrumentation for the identification and quantification of environmental pollutants at the lowest conceivably significant concentrations. It also includes studies to determine the ambient concentrations of pollutants in the environment and/or the variance of pollutants as a function of time or meteorological factors.

This document is available to the public through the National Technical Information Service, Springfield, Virginia 22161.

ic

ABSTRACT

This report details the progress made at A.R.A.P. during fiscal year 1975 towards the goal of developing a viable computer model based on second-order closure of the turbulent correlation equations for predicting the fate of nonchemically reacting contaminants released in the atmospheric boundary layer. The invariant turbulent model discussed in previous reports has been further verified by new comparisons between model predictions and experimental observations. Model capability has been extended by increasing the dimensions of the program to permit the calculation of two-dimensional unsteady turbulent flow. A number of practical plume calculations were made and compared with standard Gaussian plume assumptions. Calculations were also made for comparison with the complementary turbulent models being developed at The Pennsylvania State University and at Flow Research, Inc. of Boston, Mass.

Part II of this report contains a critical review of the current status of our A.R.A.P. invariant model, including a detailed discussion of the modeled terms, the empirical determination of the model coefficients, the validation tests, and sample applications.

This report was submitted in fulfillment of Project Number 21AUS-12, Contract Number EPA-68-02-1310 by Aeronautical Research Associates of Princeton, Inc. under the sponsorship of the Environmental Protection Agency. Work was completed as of August 1975.

TABLE OF CONTENTS

		Page
	Abstract	ii
	List of Figures	iii
I.	Conclusions	1
II	Recommendations	3
III.	Introduction	5
IV.	Program Development	8
	Introduction	8
	Transfer of Program to EPA UNIVAC 1110	8
	Development of the Two-Dimensional Unsteady Model	8
	Numerical Test Computations	13
V.	New Verification of the Basic Turbulence Model	17
VI.	Dispersion Estimates Compared with Gaussian Plume Models	23
	Introduction	23
	Ambient Turbulence Field	23
	Summary of Diffusion Model	28
	Line Source Release at Ground Level	30
	Point Source Ground Release	38
	Elevated Line Release	44
VII.	Comparison with Turbulence Models of PSU and FRI	51
VIII.	Comments on "Some Views of Modeling Dispersion and Vertical Flux" by Pasquill and Smith	58
IX.	References	60
	Nomenclature	64
	Appendix A	66
	Appendix B	71

LIST OF FIGURES

Figure No.		Page No.
1	Definition sketch for finite difference scheme	11
2	Comparison of the turbulent velocity fluctuations in the vicinity of a change of roughness as computed by the steady-state CORE program (——) and by the new PBL program (---)	15
3	Comparison of the concentration isopleths for a line source located at $x = 0$, $z = 0$ for the turbulent fields shown in Figure 2	16
4	Concentration isopleths at $x = 0.44 z_i U/w^*$ downwind of a continuous point source release into a free convective layer as simulated in a laboratory test by Deardorff and Willis[28] (——) and as predicted by our model (---). Numbers on the contours are in nondimensional units of $z_i^2 UC/Q$.	19
5	Centerline concentration isopleths downwind of a continuous point source release into a free convective layer as predicted by our model; notation as in Figure 4	21
6	Centerline concentration isopleths downwind of a continuous point source release into a free convective layer as simulated in a laboratory test by Deardorff and Willis;[28] notation as in Figure 4	22
7	Velocity and turbulence distribution predicted for a neutral, steady-state planetary boundary layer for a Rossby number $U_g/z_o f = 10^6$	24
8	Ratio of the vertical velocity variance to 10% of the wind at 10 m altitude for three different values of Rossby number	26
9	Correspondence between $\hat{R}i$ and Pasquill's stability parameter P or stability classes A-F	27
10	Ratio of the vertical velocity variance to $\hat{u}$ for different values of $\hat{R}i$ and mixed-layer depths for $Ro = 10^6$	29
11	The vertical spread σ_z as a function of distance x downwind of a line source ground release in a neutral atmosphere ($u_g = 10$ m/sec, $z_o = 10$ cm, $f = 10^{-4}$ sec^{-1})	31

Figure No.		Page No.
12	Comparison of species distribution with a Gaussian distribution for the plume of Figure 11. Normalized profiles are shown for several distances downstream of the release point. The numbers give the exponent in tens of meters; i.e., 0 is the Gaussian distribution assumed for x = 0, 2 is the profile at x = 100, etc.	32
13	Normalized surface species concentration as a function of downwind distance (——) compared with the Gaussian solution (---) for a wind assumed constant at its values at a height of 10 meters	34
14	Comparison of vertical spread in a neutral atmosphere from a line source ground release for changes in the Rossby number based on surface roughness z_o	35
15	Comparison of vertical spread from a line source ground release for different values of $\hat{R}i$ for $Ro = 10^6$ ($z_1 f/\hat{u} = 0.451$ for the unstable case)	36
16	Repeat of Figure 15 in unnormalized form for $u_g/f = 100$ km for comparison with Pasquill's Figure 6.13[30] (---)	37
17	Normalized profiles of vertical spread from a line source ground release into a stable atmosphere ($\hat{R}i = 0.134$, $Ro = 10^6$) as a function of distance downwind, denoted in powers of 10 meters (0 is Gaussian distribution assumed for x = 0)	39
18	Normalized profiles of vertical spread from a line source ground release into an unstable atmosphere ($\hat{R}i = -0.222$, $Ro = 10^6$) as a function of distance downwind, denoted in powers of 10 meters (0 is Gaussian distribution assumed for x = 0)	40
19	Concentration isopleths downwind of a point source ground release into a neutral atmosphere ($\hat{R}o = 50000$, $\hat{u}/f = 5000$ m); notation refers to tenths of maximum value, i.e., 9 is $0.9\bar{c}_{max}$, etc.	42
20	Concentration isopleths downwind of a point source ground release into a stable atmosphere ($\hat{R}i = 1.1$, $\hat{R}o = 340000$, $\hat{u}/f = 2740$ m); notation as in Figure 19	43

Figure No.		Page No.
21	Concentration isopleths downwind of a point source ground release into an unstable atmosphere ($Ri = -1.1$, $\hat{R}o = 4750$, $\hat{u}/f = 4750m$); notation as in Figure 19	45
22	Comparison of the vertical spread as a function of distance downwind of a line source for ground and elevated release into a neutral atmosphere with $Ro = 10^6$	46
23	Concentration isopleths downwind of a line source elevated release into a neutral atmosphere. Concentration levels are consistent with the numerical experiment of Lamb et al.[34]: our predictions	47
24	Concentration isopleths downwind of a line source elevated release into a neutral atmosphere. Concentration levels are consistent with the numerical experiment of Lamb et al.[34]: their results	49
25	Predictions for the mean velocity and shear stress distribution in an equilibrium, self-similar, neutral shear layer; data as observed by Wygnanski and Fiedler[40]	53
26	Predictions for the distributions of the second-order correlations of the normal velocity fluctuations in an equilibrium, self-similar, neutral shear layer; data as observed by Wygnanski and Fiedler[40]	54
27	Maximum species concentration downwind of a point source release at the center of a 200-m thick shear layer with the wind going from 6 m/sec at .4 km to 10 m/sec at .6 km	56
28	Vertical and horizontal dispersion as a function of distance downwind for the same plume as in Figure 27	57

I. CONCLUSIONS

The A.R.A.P. computer model for predicting the fate of nonchemically reacting pollutants released in the atmospheric boundary layer has been extended and its utility demonstrated by detailed calculations. The program extension to provide the capability of computing unsteady, two-dimensional turbulent flows opens up the possibility of making a wide variety of interesting calculations. A number of new comparisons between model predictions and experimental observations provides added verification of the model's fundamental validity.

Specific conclusions from the detailed model calculations are:

1) Modeling of the temperature fluctuations is given strong support by the close agreement between model predictions and experimental observations in the wake of a two-dimensional, slightly heated cylinder.

2) Comparisons between laboratory results and model predictions of turbulent fluctuations in the limiting case of free convection when the turbulence is completely produced by buoyant forces rather than mean velocity shear verify the model's basic validity.

3) Comparison of the model predictions with laboratory simulation of diffusion in a free convection, mixed layer is good, with the model able to predict the maximum concentration rising from the ground as observed in an instantaneous line release.

4) Comparison with the Gaussian plume dispersion estimates given by Pasquill shows close agreement for a line source released at ground level under neutral atmospheric conditions. But the calculations indicate that Pasquill's variation with z_o should be interpreted as a variation with Rossby number.

5) The specification of one stability parameter, a stability class or Richardson number, does not adequately specify the influence of atmospheric stability on plume dispersion. Some information on the time history of the turbulence must be provided, such as is contained in the mixing layer height.

6) For a point source release in a stable atmosphere, a strong departure from a Gaussian plume distribution is caused by variation in mean wind direction with altitude. The horizontal dispersion due to the wind veering with altitude appears much greater than that caused by horizontal wind fluctuations.

7) Comparison with the PSU model predictions for an incompressible, two-dimensional wake shows little to be gained by the incorporation of their more complex second-order closure model in its present form.

II. RECOMMENDATIONS

The process of extending the model capability concurrent with making detailed calculations with the existing model should be continued. The current model considers the pollutant as passive with no feedback on the turbulence field. We recommend that this restriction be removed by incorporating a separate momentum equation for the species. This will permit buoyant plumes and plumes with significant initial velocity to be calculated properly. This increased capability is highly desirable because of the relatively high rate of dilution which often occurs during the rising phase of real plumes.

This report gives the results of a number of detailed calculations for various atmospheric conditions. We believe such calculations should be continued, both for the purposes of further detailed verification by comparison with available measurements and to exemplify the various possible phenomena to be expected in unmeasured situations. Such calculations, using the existing A.R.A.P. programs, should also be used to provide direct technical support to EPA personnel, including the provision for utilization of A.R.A.P. programs on the EPA UNIVAC 1110 by EPA personnel.

The ultimate goal of this research is to permit the full power of the second-order closure approach to turbulent modeling to be applied to urban or regional air quality problems. At the present time, it is not clear whether this can be most fruitfully accomplished by solving the complete three-dimensional unsteady problem numerically or by approximating the problem in some fashion. A standard technique for reducing the complexity is to assume a succession of steady-state, three-dimensional, Gaussian plumes. It may be possible to use our model to parameterize non-Gaussian plume distributions for incorporation into such a model. Another, perhaps more promising, possibility is that of using vertical integrals of various moments of the desired flow properties to reduce the inherently three-dimensional, unsteady problem to a two-dimensional, unsteady problem. We believe it is time to do some preliminary investigation of these and possibly other alternative approaches to determine which appears most feasible for the urban model.

It is also desirable to continue refinements to the basic turbulence model as better data become available from experiments, either physical or numerical (such as that being conducted by Flow Research Inc. of Boston, Mass. for EPA), or as the desirability for more complicated models for various terms in the equation is established by other modeling efforts at A.R.A.P. or by the efforts of others such as Lumley or Mellor.

III. INTRODUCTION

The development of a program for practical predictions of the dispersal of pollutants in the atmosphere based on a second-order closure scheme under development at A.R.A.P. was first funded by EPA in February 1971. To our knowledge, this represented the first attempt at applying higher-order turbulence modeling to the pollutant dispersal problem. Previously, in a paper presented in January 1970[1] on the application of second-order closure modeling to the problem of clear air turbulence, it had been mentioned that there would be no real difficulty in extending such a model to permit the calculation of the dispersal of passive atmospheric pollutants in the atmospheric boundary layer under arbitrary stability conditions. Through the work at A.R.A.P.[2-9] and the work of others[10-19], the use of the explicit Reynolds stress equations to compute correlations of turbulent fluctuations with modeling techniques applied to close the system of equations has now become a viable means of solving problems involving turbulent transport. This report details the progress made at A.R.A.P. in fiscal 1975 towards utilizing a model based on such a technique to solve pollutant dispersal problems.

The computer program simulating unsteady one-dimensional (or steady two-dimensional flow that is parabolic in one direction) flow has been continually refined since its earliest version, the Clear Air Turbulence (CAT) program.[3] The CAT version included the invariantly modeled turbulence equations with known velocity and temperature gradients (functions of z only). Concurrent with this development was the construction of the Line Pollutant Dispersal (LPD) program which computed one-dimensional unsteady pollutant dispersal given all the necessary turbulent fluctuations and mean flow gradients. A typical pollutant problem was handled by assuming distributions for velocity U and temperature Θ and executing CAT to compute the steady turbulent correlations, obtained by running the CAT program to large times. These results were then used as input into the LPD program to predict the dispersal of a line source.

The first step in the refinement of CAT was Free CAT, in which the turbulent equations of motion were regrouped in the solution scheme to include the dynamic behavior of the U and

θ mean equations. The excitement these solutions generated stimulated the development of a more complete model for atmospheric flows. That model became CORE, a program for solving the complete set of one-dimensional unsteady equations, including the coriolis body force. Here the V mean velocity is included in the solution scheme, as is a pollutant species C . All of the requisite turbulent correlations are also present within the computer program. CORE was written to permit the solution of the turbulence either by their modeled differential equations or by a refinement of the superequilibrium limit[3] into the quasi-equilibrium equations[6] where the q^2 turbulent correlation is the only one solved in its complete differential form. CORE was also extended to permit solution to many of the types of laboratory flows for which A.R.A.P. verifies its turbulent modeling. One of CORE's improvements over CAT and Free CAT is the matching of the lower boundary condition into the law-of-the-wall and Monin-Obukhov relations. All of these refinements were an effort on our part to permit one-dimensional solutions in as short a computer time as possible while retaining the accuracy needed to yield a reliably predictive result.

Concurrent with the refinements in the turbulent programming and the invariant model itself came the further development of the pollutant programming. Even though the line dispersal is a valuable step towards predicting and understanding pollutant dispersal, it was realized that a really worthwhile modeling effort would have to include a point-source or "spatial" pollutant dispersal (SPD) program. The development of the initial program was funded by EPA. The numerical procedure used in the solution of the partial differential equations was an extension of the same technique used quite successfully in the one-dimensional program. SPD computes the steady three-dimensional solution of the modeled turbulent diffusion equations when the ambient velocity, temperature, and turbulent field are prescribed or previously calculated from a program such as CORE. As a part of the current effort, SPD was programmed on the EPA UNIVAC 1110. The experience gained in the transfer of this program from our META-4 computer to the UNIVAC 1110 is discussed in the next section.

In mid-1972, A.R.A.P. began a two-year effort with the Navy for the development of a submarine wake program. The rudimentary features of SPD were taken over into a model for turbulence in the two-dimensional marching framework (WAKE).[20, 21] At that time, computer availability was such that the turbulence was entirely the quasi-equilibrium form of the invariant equations. Only the q^2 turbulent energy correlation was retained in its fully differential form. Mean flow variables consisted of a density perturbation and three velocities. Due to the interaction between potential and kinetic energy

leading to horizontal and vertical velocities and internal gravity waves, it is essential to predict the perturbation pressure accurately. One of the main results of the Navy effort was the development of a solution technique to solve the Poisson equation in two dimensions.

Section IV deals with the development of a two-dimensional marching program incorporating the turbulence features of CORE, the pollutant dispersal experience of SPD, and the pressure solution of WAKE. Section V deals with new comparisons between model results and experimental observations which provide additional verification of the basic turbulence model. The results of detailed diffusion calculations for a number of different atmospheric conditions are presented in Section VI. Results for both line and point sources are compared with dispersion estimates for Gaussian plumes.

The results of comparison calculations for the complementary turbulence models currently supported by EPA at Flow Research Inc. and at The Pennsylvania State University are described in Section VII. Section VIII contains some comments on the questions related to second-order closure raised by Drs. F.B. Smith and F. Pasquill in their recent paper, "Some Views of Modeling Dispersion and Vertical Flux."[22]

Two appendices are included. Appendix A details the one-dimensional unsteady equations, together with the boundary conditions appropriate for diffusion in the planetary boundary layer. This provides a convenient reference for the complete mathematical specification of the problems solved in Section VI. Appendix B is a reprint of an AIAA paper, to be published in the AIAA Journal, giving some comparisons between model predictions and experimental observations for some variable density flows.

Part II contains a critical review of the current status of our A.R.A.P. invariant model. It contains a detailed discussion of the modeled terms, the empirical determination of the model coefficients, the validation tests, and sample applications.

IV. PROGRAM DEVELOPMENT

INTRODUCTION

One task of the current EPA contract period was the development of computer code incorporating the invariantly modeled turbulence equations for the solution of unsteady two-dimensional flows. By the incorporation of an additional advection term, this same code can be used to solve steady three-dimensional flow problems that are parabolic in one direction and thus provide one direction for numerical marching. Our thrust was directed towards a generalization of the one-dimensional unsteady CORE turbulence program, with the structure of the spatial pollutant dispersal (SPD) program as a guide.

TRANSFER OF PROGRAM TO EPA UNIVAC 1110

Since we anticipated the need for access to the EPA computer as the only substantial way to resolve the future computational demands of this large program, our first step in its development was to make the current SPD computer code operational on the Raleigh facility. In mid-November 1974, we spent a pleasant and most instructive week in Raleigh. Primed with many of the necessary manuals giving us the information we needed about conversion to the UNIVAC 1110, our task was accomplished rather painlessly. Special thanks must go to Bob Jergens and Ginger Smiley for their cooperation and helpfulness during this time. Since November we have made a number of production runs using the SPD version on the 1110. The speed ratio between our META-4 and the UNIVAC machine was 30/1, enabling us to complete a simulation in less than an hour. Our only displeasure with the set-up has been the expected one of having the machine down for maintenance quite often and of having to wait until after the dinner hour to obtain a communication line. Some of the results presented in Section VI were obtained on the UNIVAC 1110.

DEVELOPMENT OF THE TWO-DIMENSIONAL UNSTEADY MODEL

The SPD program[3] solves for the species distribution C and its turbulence correlations $\overline{cv}$, $\overline{cw}$, $\overline{c\theta}$, and $\overline{cc}$ by

solving numerically the modeled partial differential equations

$$\frac{DC}{Dt} = \nu \frac{\partial^2 C}{\partial x_j^2} - \frac{\partial \overline{cu_j}}{\partial x_j} \tag{1}$$

$$\frac{D\overline{cu_i}}{Dt} = -\overline{u_i u_j} \frac{\partial C}{\partial x_j} - \overline{cu_j} \frac{\partial u_i}{\partial x_j} + \frac{g_i}{\theta_o} \overline{c\theta} + v_c \frac{\partial}{\partial x_j} \left(q\Lambda \frac{\partial \overline{cu_i}}{\partial x_j} \right) - \frac{Aq\overline{cu_i}}{\Lambda} \tag{2}$$

$$\frac{D\overline{c\theta}}{Dt} = -\overline{u_j \theta} \frac{\partial C}{\partial x_j} - \overline{cu_j} \frac{\partial \theta}{\partial x_j} + v_c \frac{\partial}{\partial x_j} \left(q\Lambda \frac{\partial \overline{c\theta}}{\partial x_j} \right) - \frac{2bsq\overline{c\theta}}{\Lambda} \tag{3}$$

$$\frac{D\overline{cc}}{Dt} = -2\overline{cu_j} \frac{\partial C}{\partial x_j} + v_c \frac{\partial}{\partial x_j} \left(q\Lambda \frac{\partial \overline{cc}}{\partial x_j} \right) - \frac{2bsq\overline{cc}}{\Lambda} \tag{4}$$

The effort for this year has been directed towards using the same computer code structure, to be described below, to include the solution for the other turbulence variables in the y-z coordinate system, with marching direction of either x or t. These variables are u, v, w, θ, p, q^2, Λ, $\overline{uv}$, $\overline{uw}$, $\overline{vw}$, $\overline{u\theta}$, $\overline{v\theta}$, $\overline{w\theta}$, $\overline{\theta^2}$, $\overline{vv}$, and $\overline{ww}$. The modeled equations governing these variables are given in Part II of this report. They consist of 4 scalar equations, (2), (3), (26) and (29); 2 vector equations, (1) and (25); along with the tensor equation (24) representing 6 scalar equations. For convenient reference, the equations and boundary conditions are detailed in Appendix A for the one-dimensional planetary boundary layer code. The resultant computer code is called the Planetary Boundary Layer (PBL) code.

A great deal of sophisticated coding is required to transform the differential equations into finite difference form and place them within an auxiliary code that performs the many tests and numerical controls needed to maintain the solution accuracy. For our present purposes, we will attempt to give the basic information essential to the reproduction of our work. If the inclination of the reader leans elsewhere, we suggest that he now skip to the last few paragraphs of this section for a discussion of our simulation comparison.

The necessary nonlinear parabolic partial differential equations are written in finite difference form using a two-point forward analog for the marching step $\Delta t = t^{n+1} - t^n$ and a three-point centered analog for the two spatial dimensions. In order to make efficient use of a relatively modest number of mesh points and to solve accurately, not only near the lower surface but also out to large vertical z heights, we determined to continue using our unequally spaced spatial grid mesh. Thus, Δy and Δz need not be the same within the solution space and, in fact, Δz may vary by as much as two orders of magnitude from the surface to the upper level geostrophic wind. We permit the program to adjust this mesh spacing internally as the solution progresses and as high curvature regions within the flow disappear or form. The major drawback of the unequally spaced mesh is that it does not permit a second-order accurate solution scheme.

For two-dimensional flow, our finite difference scheme must be written on the cross-like mesh shown in Figure 1 where a typical first derivative (say, $\partial\overline{vv}/\partial y$) and a typical second derivative $\left(\frac{\partial}{\partial y} q\Lambda \frac{\partial \overline{vv}}{\partial y}\right)$ at the point (y_j, z_i) at time t^n would be formed as follows. We define

$$\Delta_m = y_j - y_{j-1} \qquad \Delta_p = y_{j+1} - y_j \qquad \Delta_t = \Delta_m + \Delta_p$$

$$F_m = \frac{\Delta_p}{\Delta_m \Delta_t} \qquad F_p = \frac{\Delta_m}{\Delta_p \Delta_t}$$

$$G_m = \frac{(q\Lambda)_j + (q\Lambda)_{j-1}}{\Delta_m \Delta_t} \qquad G_p = \frac{(q\Lambda)_{j+1} + (q\Lambda)_j}{\Delta_p \Delta_t}$$

and write these two example derivatives as

$$\frac{\partial \overline{vv}}{\partial y} \doteq F_p \left(\overline{vv}_{j+1} - \overline{vv}_j\right) + F_m \left(\overline{vv}_j - \overline{vv}_{j-1}\right) \qquad (5)$$

$$\frac{\partial}{\partial y}\left(q\Lambda \frac{\partial \overline{vv}}{\partial y}\right) \doteq G_p \left(\overline{vv}_{j+1} - \overline{vv}_j\right) - G_m \left(\overline{vv}_j - \overline{vv}_{j-1}\right) \qquad (6)$$

Equations (5) and (6) may be extended in a straightforward manner to yield the entire finite difference formulation of the equations for the twenty means and correlations. The first major step is now complete. The next step is to decide

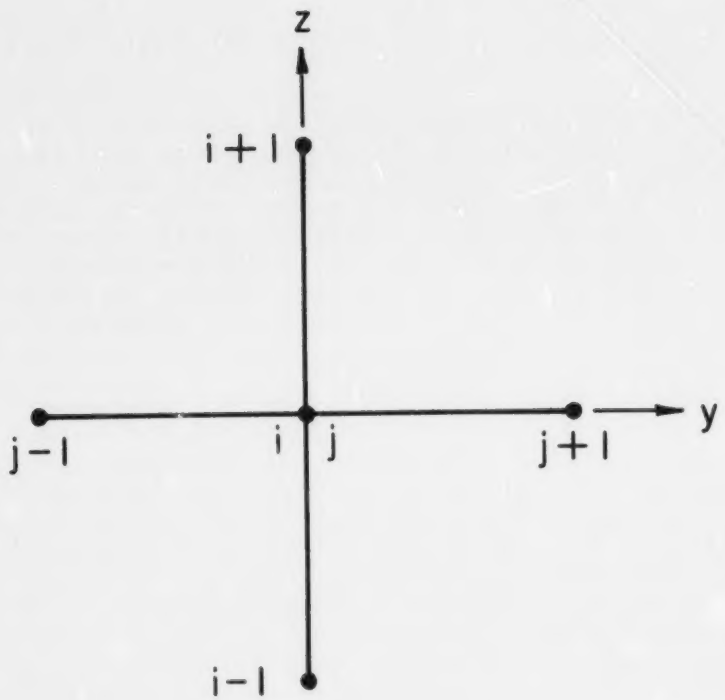

Figure 1. Definition sketch for finite difference scheme

how these equations will be solved. We elect to use the alternating-direction implicit (ADI) tridiagonal algorithm developed by Peaceman, Rachford and Douglas.[23] To do this, we divide the marching step Δt into two equal parts ($\Delta t/2$) and integrate the equations first in the z direction, then in the y. During the z integration half-step, z derivatives in the unknowns are treated implicitly, while y derivatives are evaluated explicitly with the presently known solutions. The reverse is true during the y integration half-step. The implicit algorithm requires the construction of two vector arrays and the demand for sweeping twice through the grid mesh.

Once the solutions are known at the next step, t^{n+1}, we test these solutions by determining the maximum variable change normalized by its maximum variable value. Since we wish to hold the solution to a given tolerance (2% change, for example), we then have a rather simple scheme for determining our marching step size Δt. Since curvature tests control our mesh in the y and z directions and the ADI algorithm integrates the equations, our necessary input to execute the program becomes consistent variable initial and boundary conditions. More details on the methods used for mesh control and step size are given in Reference 9.

An examination of the equations that we are solving should convince the reader that they are strongly coupled. A strict use of the ADI scheme would require the inversion of large matrices twice at every grid point per step. The computing time required would be prohibitive since we must maintain enough grid points in each direction to resolve the solution (approximately 30 points). Thus, it becomes obvious that we must not only linearize the production terms in an advantageous manner (we evaluate them at their known values from the previous step), but we must resolve the coupling inherent in the mean flow equations. For example, for v, we have, from Eq. (1) in Part II,

$$\frac{Dv}{Dt} = -\frac{\partial p}{\partial y} + \nu\nabla^2 v - \frac{\partial \overline{vv}}{\partial y} - \frac{\partial \overline{vw}}{\partial z} - f(u - u_g) \qquad (7)$$

Equation (7) shows that v is implicitly coupled to not only u but also $\overline{vv}$ and $\overline{vw}$ (p is either prescribed or obtained from a solution of the Poisson equation found by taking the divergence of the momentum equation). However, through our experience with this effect in the CORE program, it has proven advantageous to replace the $\overline{vv}$ and $\overline{vw}$ derivatives by rewriting (7) as

$$\frac{Dv}{Dt} = -\frac{\partial p}{\partial y} + \frac{\partial}{\partial y}\left[\left(\nu + \varepsilon_y\right)\frac{\partial v}{\partial y}\right] + \frac{\partial}{\partial z}\left[\left(\nu + \varepsilon_z\right)\frac{\partial v}{\partial z}\right]$$

$$- f(u - u_g) - \frac{\partial}{\partial y}\left[\overline{vv} + \varepsilon_y \frac{\partial v}{\partial y}\right] - \frac{\partial}{\partial z}\left[\overline{vw} + \varepsilon_z \frac{\partial v}{\partial z}\right] \qquad (8)$$

where $\varepsilon_y = \overline{vv}\Lambda_y/q$ and $\varepsilon_z = \overline{ww}\Lambda_z/q$ (9)

and the last two terms in (8) are evaluated explicitly. Then the second and third terms in (8) may be recast into implicit terms in v, lending a greater stability to the v equation since these terms are diffusion-like. The v equation is then coupled only to u by the coriolis body force. Similar dynamic couplings due to the buoyancy force must exist between $\overline{w\theta}$ and $\overline{\theta^2}$, and $\overline{cw}$ and $\overline{c\theta}$. Linearization of some terms by evaluation of the coefficients from the previous step permits the rest of the equations to become uncoupled from each other. The computer time to solve this equation set is tolerable — on the order of 4 minutes of META-4 time per step for a 30 × 30 mesh when the specie is not present, an extra minute when it is. A solution to Poisson's equation will add 2 or 3 minutes to the solution time per step for this size mesh.

NUMERICAL TEST COMPUTATIONS

After an extensive time spent debugging the program and uncovering several new numerical problems associated with the addition of the cross-dimension y, we have been able to test the program on two problems: the steady-state solution of a simple neutral planetary boundary layer, and the steady-state solution of flow over a simple ramp change in the surface roughness. The primary reason for choosing these two test cases is that we were able to run the CORE code, which marches in the y direction, side by side with PBL, giving us the steady-state solution for all z, and thus giving us the solutions that PBL should yield in the limit of large times. The greatest disadvantage of choosing to run PBL to steady state was that we had to interpret "steady state" somewhat loosely because of the computer time a typical run requires. Much of the difficulty may be traced to the convection terms present in the substantial derivative

$$\frac{D}{Dt} = \frac{\partial}{\partial t} + v\frac{\partial}{\partial y} + w\frac{\partial}{\partial z} \qquad (10)$$

Since our flow for v is from negative to positive y, one can see rather crudely that our time step is controlled by

$$\frac{v\Delta t}{\Delta y} \leq 1 \qquad (11)$$

so that the solution does not move so fast past the y grid points that it cannot be resolved in the time step we are taking. This is the so-called Courant condition.[23] It restricts our step size in the marching direction even with a careful selection of v and Δy.

After imposing this cross-velocity step-size restriction, we were able to approach the "steady" solution predicted by the CORE program for the neutral planetary boundary layer run.

The second test was the more stringent — that of a ramp change in surface roughness. For this case, we held the geostrophic wind at 10 m/sec and $z_o = 0.0001$ m for $y \leq -10$ m, $z_o = 0.1$ m for $y \geq +10$ m, and a linear z_o in between. The solution was begun everywhere with the steady-state CORE solution for $z_o = 0.0001$ m. Readjustment occurred rapidly. The Courant condition, for $\Delta y = 10$ m, required us to restrict $\Delta t \sim 2$ sec (liberally). After several hundred seconds, we compared the PBL prediction for turbulent energy q^2 with the "steady" solution from CORE over this same ramp change. The two curves are given in Figure 2. The agreement is rather encouraging. The slight differences are probably due to the relatively larger mesh spacing of the PBL program.

Further work with PBL will include more solution comparison but also simulation of flows we cannot in fact compute other ways. Once the pressure loop is implemented, along with the differential equation solutions of both the cross-plane velocities v and w, we will be able to simulate a wide variety of fundamentally interesting flows.

For this test case, we have also included the computation of diffusion from a line source at $x = 0$. Comparison between the predicted concentration isopleths for the two programs are given in Figure 3. Again, the results of the CORE program should be more accurate since it uses a much finer mesh. The accuracy of the new PBL appears acceptable, but more tests will be made on it before it is declared operational.

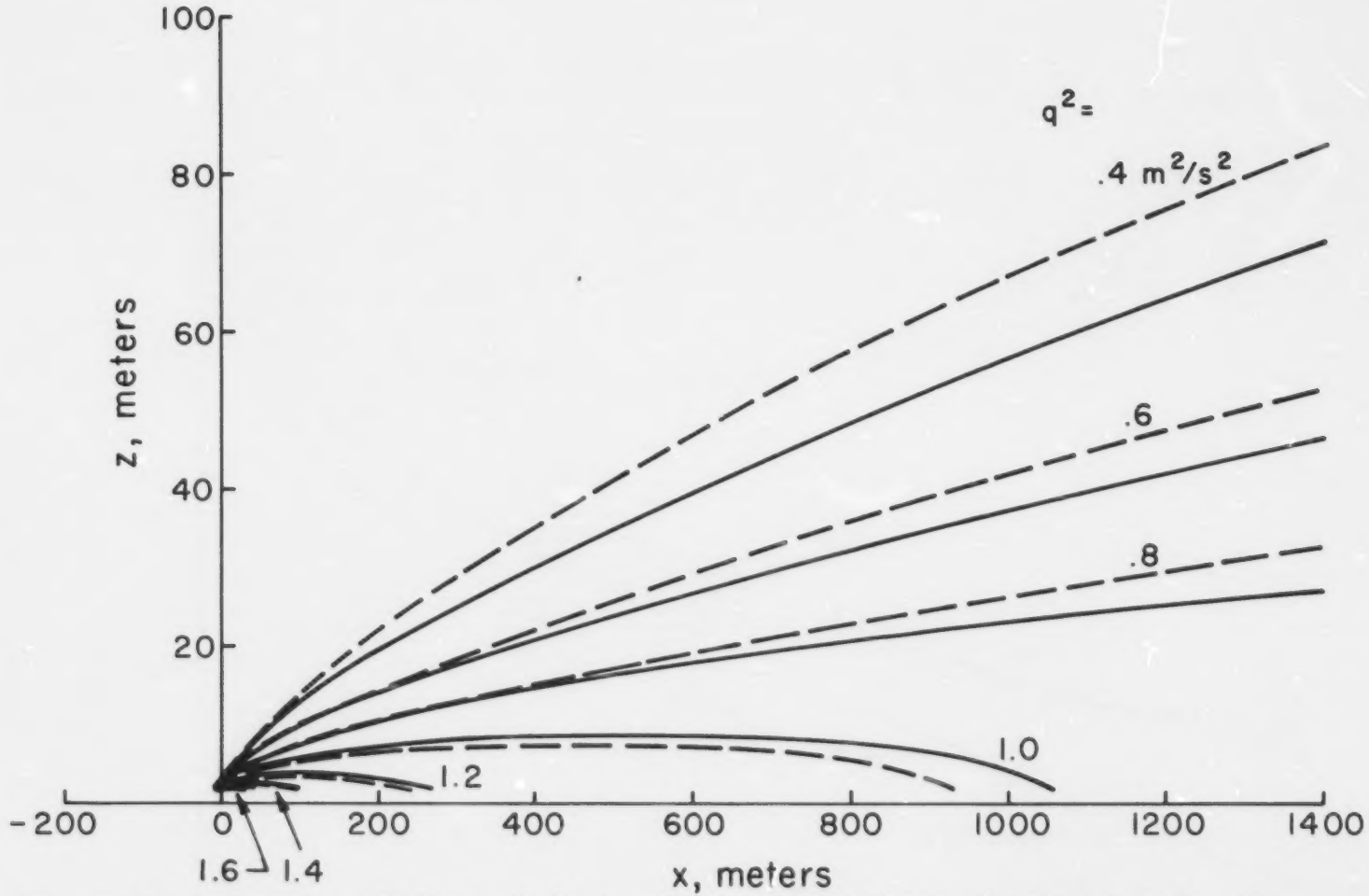

Figure 2. Comparison of the turbulent velocity fluctuations in the vicinity of a change of roughness as computed by the steady-state CORE program (——) and by the new PBL program (---)

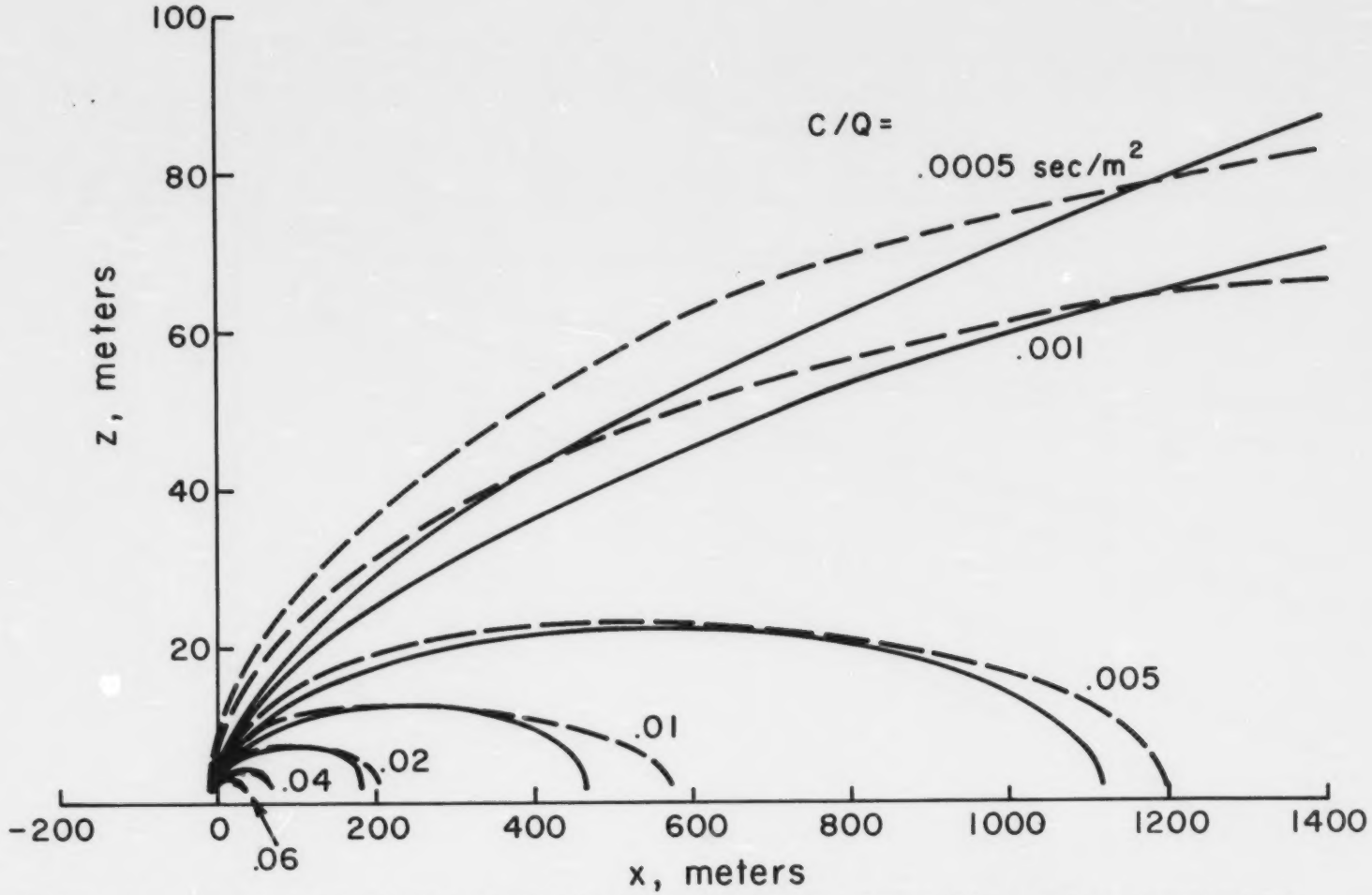

Figure 3. Comparison of the concentration isopleths for a line source located at x = 0, z = 0 for the turbulent fields shown in Figure 2

V. NEW VERIFICATION OF THE BASIC TURBULENCE MODEL

The wide variety of flow geometries to which the model has been successfully applied is detailed in Part II. Here we want only to describe two new validation tests made during the last year under this EPA contract. One of these is a comparison with laboratory measurements of temperature fluctuations in the wake of a heated cylinder. The second is a comparison with laboratory measurements of both the basic turbulence field and the resulting dispersion of a passive species which occurs in free convection bounded by a stable temperature gradient. The principal results of these two comparisons were included in a recent AIAA paper[24] which is included herein as Appendix B.

Since the modeling involved in the temperature correlation equations had previously been validated only by comparison with atmospheric surface layer data[5], it was desirable to check the results for a flow problem which did not involve either boundaries or stability influences. Such is the case far downstream of a slightly heated cylinder. Freymuth and Uberoi[25] and, more recently, LaRue and Libby[26] have made measurements of the temperature variance and mean temperature increments obtained in the self-similar region of the wake. The corresponding self-similar profiles predicted by our model are compared with the data of LaRue and Libby in Figure 1 of Appendix B. The normalizing length z_{50} is fixed by comparison with the mean velocity profile (see Section VII for a comparison of the velocity profiles). The agreement is quite good, particularly in view of the fact that no new constants or adjustment coefficients are required (or permitted) in this comparison. The centerline value of the temperature variance normalized by the mean temperature increment predicted by the model is 0.276. This agrees with the value of 0.28 observed by LaRue and Libby rather than the value of 0.21 reported by Freymuth and Uberoi.

Free convection is a flow that is quite different from the flows used to determine the model coefficients. In this case, the turbulence is produced by the unstable buoyancy force without being influenced by any mean shear stress. Willis and Deardorff[27] have measured the velocity and temperature

fluctuations in an unstable layer bounded above by a stable temperature gradient and below by a surface with a positive heat flux. Their experiment called for establishing an initial stable temperature gradient between two surfaces and then applying constant heat flux to the region through the lower surface. With mean velocities restricted to a minimum, free convection occurs in a mixed layer above the lower surface. The thickness of this mixed layer increased with time, but the turbulent correlations were observed to exhibit self-similarity when normalized by the characteristic velocity

$$w^* = \left(\frac{g\overline{w\theta}_o z_i}{\theta} \right)^{1/3}$$

where $\overline{w\theta}_o$ = surface heat flux

z_i = depth of the mixed layer

Model predictions for the normalized plots of $\overline{ww}/w^{*2}$, $\overline{uu}/w^{*2}$, $\overline{\theta^2}w^{*2}/(\overline{w\theta})_o^2$, and $\overline{wq^2}/2w^{*3}$ are compared with the laboratory observations in Figures 3, 4, 5, and 6, respectively, of Appendix B. The comparison of the vertical velocity fluctuation is very good. The horizontal velocity observations show modest peaks near the top and bottom of the mixed layer that are not predicted by the model, but the prediction for the center half of the layer is in good agreement. The temperature variance predicted by the model and observed in the experiment is the same except near the top of the mixed layer where the observations show a much stronger local maximum than is predicted. The inertial oscillations existing in this region do not appear to be correctly simulated by the model.

The favorable comparisons of Figures 3, 4, and 5 of Appendix B are in spite of the fact that the modeled vertical flux of kinetic energy is significantly different from the experimental observations, as shown in Figure 6. This is consistent with our basic assumption that the second-order correlations calculated from their conservation equations are given more accurately than the accuracy to which the third-order correlations are approximated.

Deardorff and Willis[28] have also simulated diffusion in a free convection mixed layer by tracking the release of a large number of small, neutrally buoyant particles in their convection tank. Figure 4 shows our model predictions for the ensemble averaged pollutant concentration distribution a distance $x = 0.44 z_i U/w^*$ downwind of the continuous point source. For this calculation, we have taken U to be a constant between $z = 0$ and z_i to correspond to the fact that the experiment was actually performed as an instantaneous

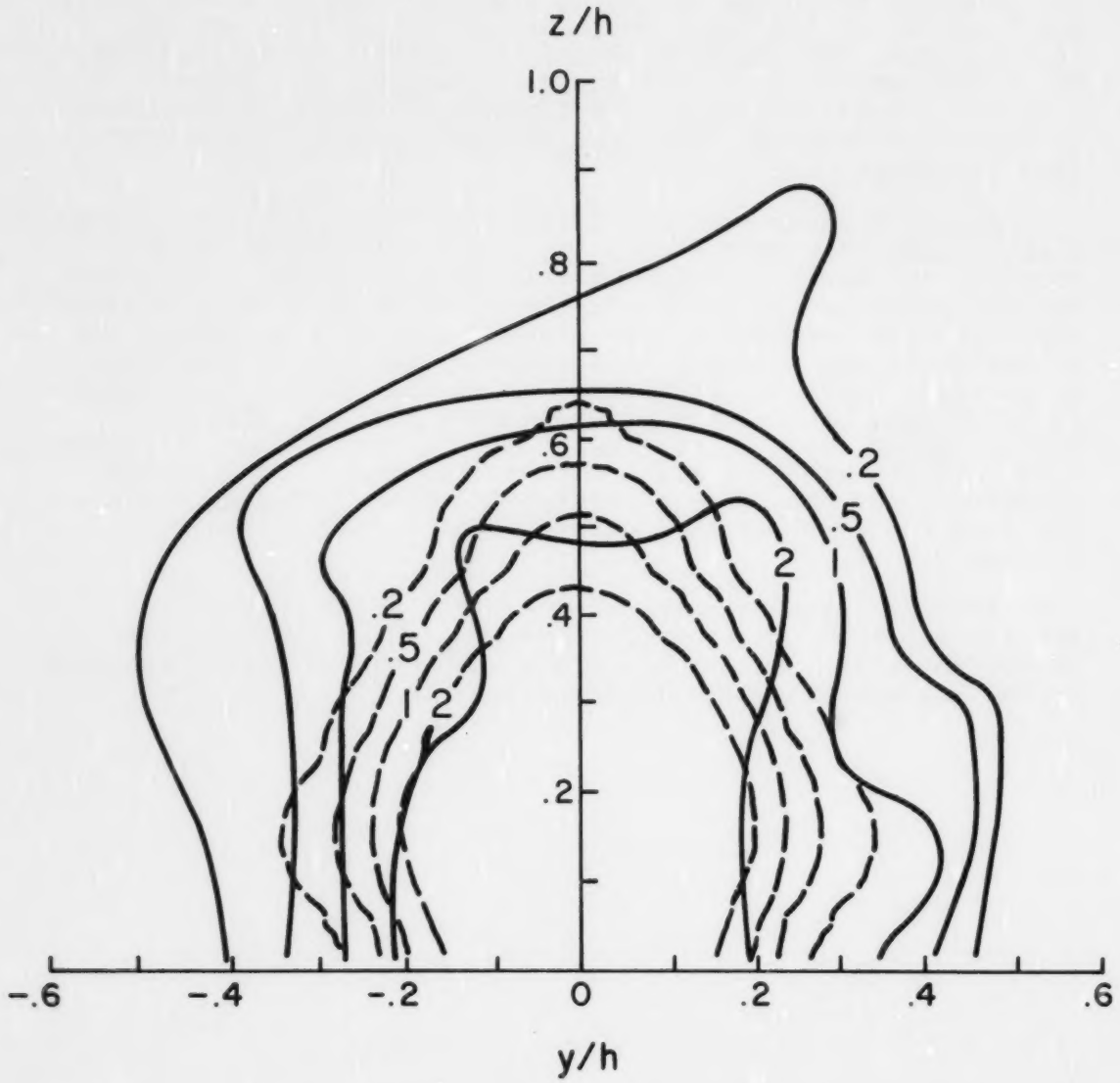

Figure 4. Concentration isopleths at $x = 0.44 z_i U/w^*$ downwind of a continuous point source release into a free convective layer as simulated in a laboratory test by Deardorff and Willis[28] (——) and as predicted by our model (---). Numbers on the contours are in nondimensional units of $z_i^2 UC/Q$.

line source experiment. Figure 4 also shows the average concentration distribution from their five experiments. The asymmetry about the $y = 0$ axis is apparently a measure of the sampling error due to basing their average on a relatively small number of samples. For both the predictions and the observations, the concentration is normalized by multiplying by $z_i^2 U/Q$ where Q is the source strength. The correspondence between the model predictions and their observations is quite encouraging. Even the lateral spread is in reasonable agreement.

Figure 5 shows our predictions for the centerline concentration isopleths in the plane $y = 0$. Their experimental contours are shown in Figure 6. In both the model predictions and the experimental contours, the altitude of maximum concentration rises downwind of the ground release. As pointed out by Deardorff and Willis,[28] this result could not be simulated by either a Gaussian plume model or an eddy coefficient model. In our model, this effect could be increased slightly by increasing d to a value significantly greater than 1. Note also that the experimental contours are taken from only one experiment and thus should be expected to be somewhat different from the curve which would be obtained for an ensemble average.

Although some discrepancies between model predictions and experimental observations have been noted in these new validation tests, taken as a group they provide strong evidence to the fundamental correctness of the model.

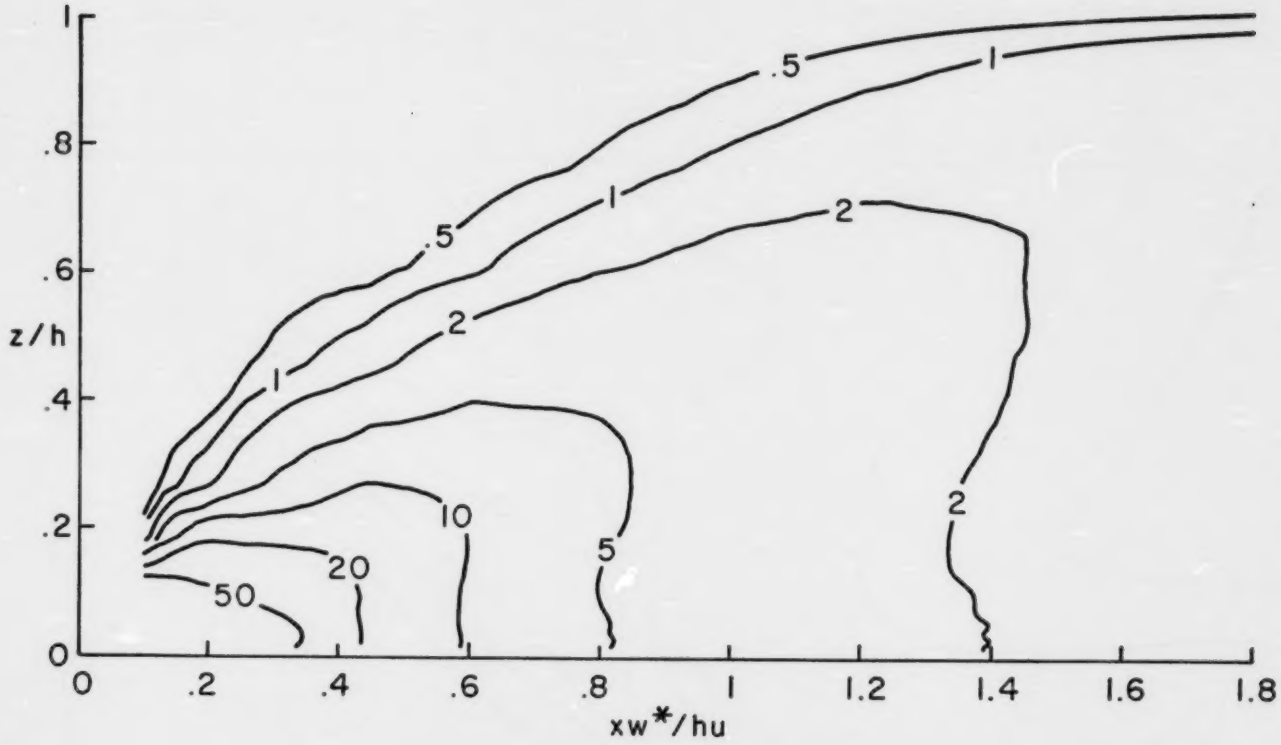

Figure 5. Centerline concentration isopleths downwind of a continuous point source release into a free convective layer as predicted by our model; notation as in Figure 4

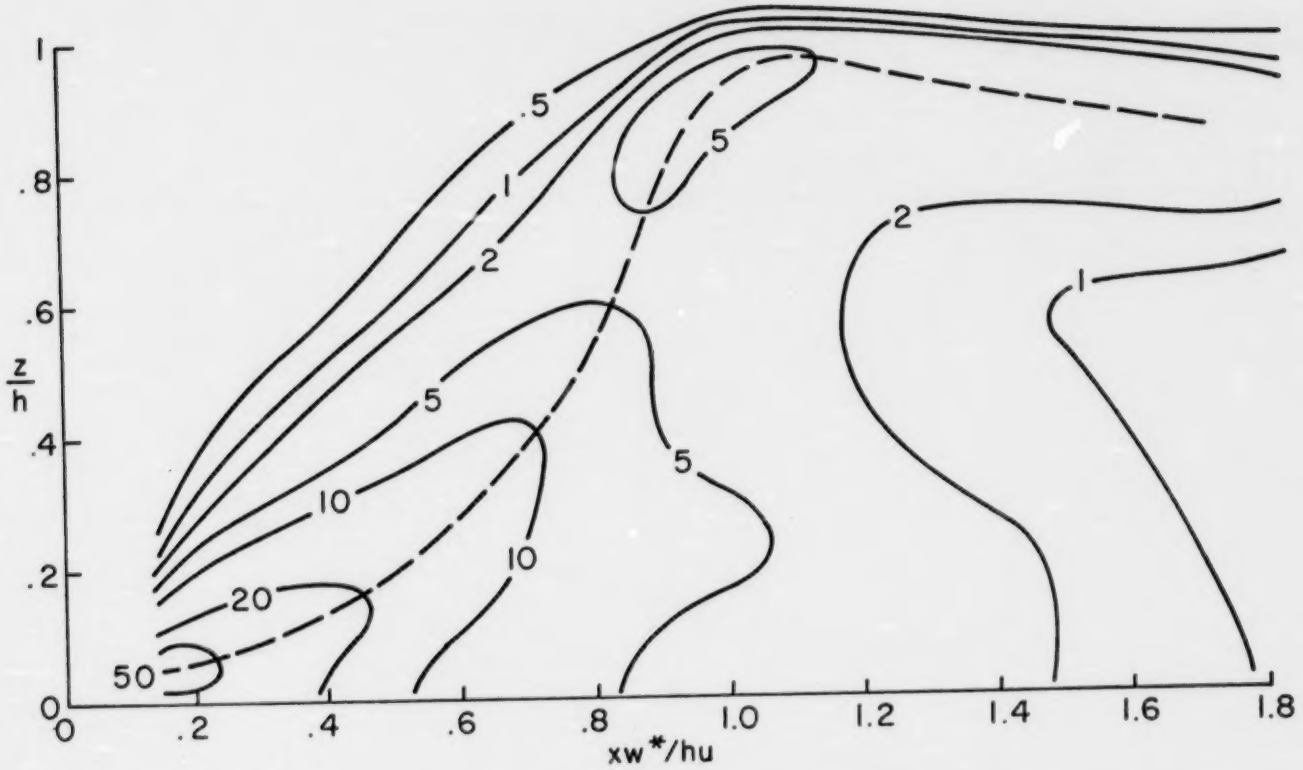

Figure 6. Centerline concentration isopleths downwind of a continuous point source release into a free convective layer as simulated in a laboratory test by Deardorff and Willis;[28] notation as in Figure 4

VI. DISPERSION ESTIMATES COMPARED WITH GAUSSIAN PLUME MODELS

INTRODUCTION

A popular method for estimating pollutant dispersal is to assume a steady-state Gaussian plume with the spatial dispersion of the plume given empirically.[29] The purpose of this chapter is to compare the predictions of our model with the latest recommendations for Gaussian plumes as given by Pasquill.[30]

AMBIENT TURBULENCE FIELD

The details of the turbulence model used herein are identical to what is used in Reference 6. All of the turbulent velocity fields are computed solving the full set of equations (Eqs. 2.1-2.3 and 2.24-2.26 of Part II) with the one-dimensional unsteady CORE program. These equations and boundary conditions are repeated here in Appendix A. The only difference from the quasi-equilibrium solution used in Reference 6 is in the inclusion of all the diffusion terms, since we will be dealing here with near-equilibrium turbulent conditions.

The complete velocity field predicted for a neutral, steady-state, planetary boundary layer is given in Figure 7. The governing equations show that the only dimensionless parameter required to completely define this flow is some form of the Rossby number. Figure 7 is shown for $U_g/z_o f = 10^6$. A more easily measured velocity than the geostrophic wind in practical cases may be the velocity at a set height, say 10 m. A popular theoretical choice for a normalizing velocity is the surface shear stress velocity u^*. Here we will use $\hat{u}$ = 10% of the wind velocity at the 10 m height. This completely arbitrary choice has the advantage of being easier to measure than either U_g or u^* and numerically is the same order of magnitude as u^*.

We will not show all of the turbulence variables for all of the diffusion calculations to be discussed in this chapter. But in order to show the flavor of the variation with

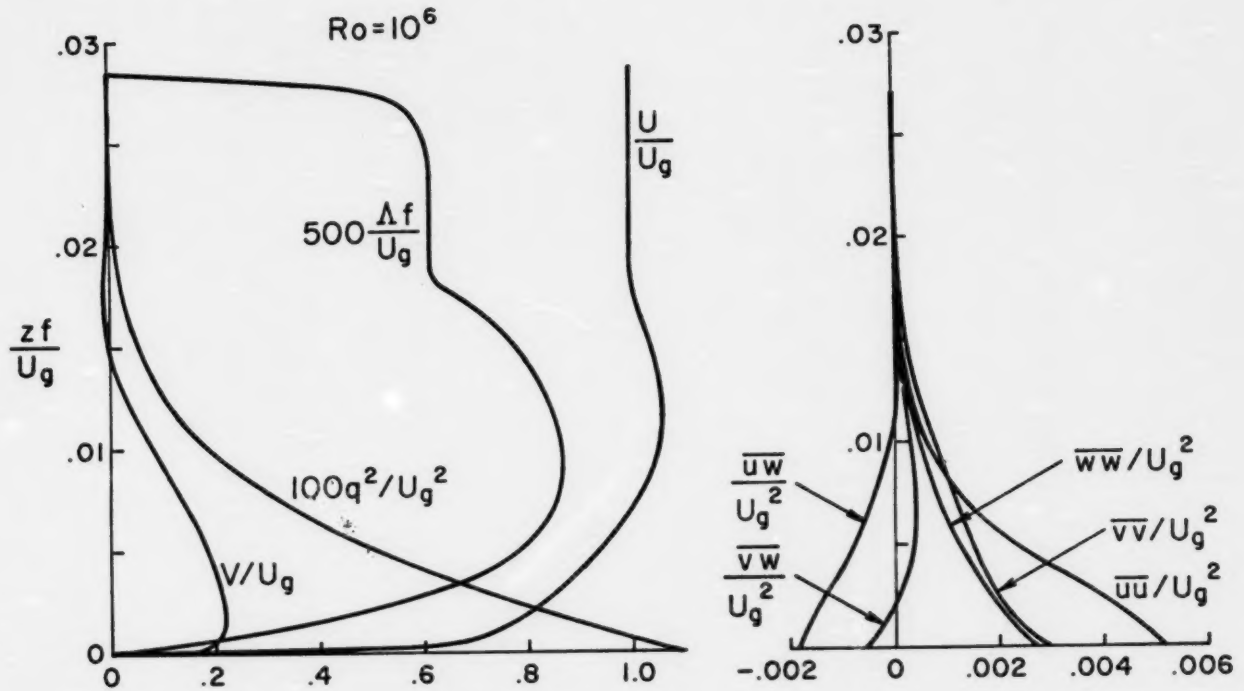

Figure 7. Velocity and turbulence distribution predicted for a neutral, steady-state, planetary boundary layer for a Rossby number $U_g/z_o f = 10^6$

$\hat{R}o = \hat{u}/z_o f$, Figure 8 shows $(\overline{ww})^{1/2}/\hat{u}$ for three different values.

The influence of stability introduces at least one more parameter – some measure of the stability such as a Richardson number or Monin-Obukhov length. Usually one must also know something about the time history of the PBL. Certainly in the unstable case, some specification of the height of the inversion, i.e., depth of the mixed layer, must be given since, in this case, no steady-state turbulence velocity field is possible. The depth of the mixed layer and consequently the whole turbulence field will continue to evolve in time. But as shown in Section V and in Appendix B, a quasi-steady turbulence can occur for a given inversion height z_i . In our program, z_i is not a rigid lid but is defined as the altitude at which the maximum values of $\overline{\theta^2}$ occur as the temperature inversion is approached.

Here we have chosen to measure the stability by the Richardson number based on the potential temperature and wind velocity taken 10 m above the surface:

$$\hat{R}i = \frac{g(\theta_{10\ m} - \theta_o)(1\ m)}{\theta_o \hat{u}^2} \tag{12}$$

Again, we have sacrificed theoretical neatness in order to choose a parameter which may be easily measured. The Richardson number defined this way is roughly equal to the gradient Richardson number at the 10 m height. When the logarithmic profiles for u and θ are appropriate, the relationship may be written exactly as

$$\hat{R}i = \frac{g}{\theta_o}\left[\frac{(\partial\theta/\partial z)}{(\partial u/\partial z)^2}\,\frac{100}{z\ \ell n\ z/z_o}\right]_{z=10\ m} \tag{13}$$

The correspondence between $\hat{R}i$ and Pasquill's stability parameter P is shown in Figure 9. For convenience, we have also shown the correspondence between P and Pasquill's former stability classes.

The implication in the discussion of Figure 6.13 in Reference 30 is that the influence of surface heat flux on turbulent fluctuations is uncoupled from the influence of z_o . This does not appear to be the case. The curve in Figure 9 is drawn for $z_o = 10$ cm. If the definition of P remained fixed, as defined in Figure 6.13 of Reference 30,

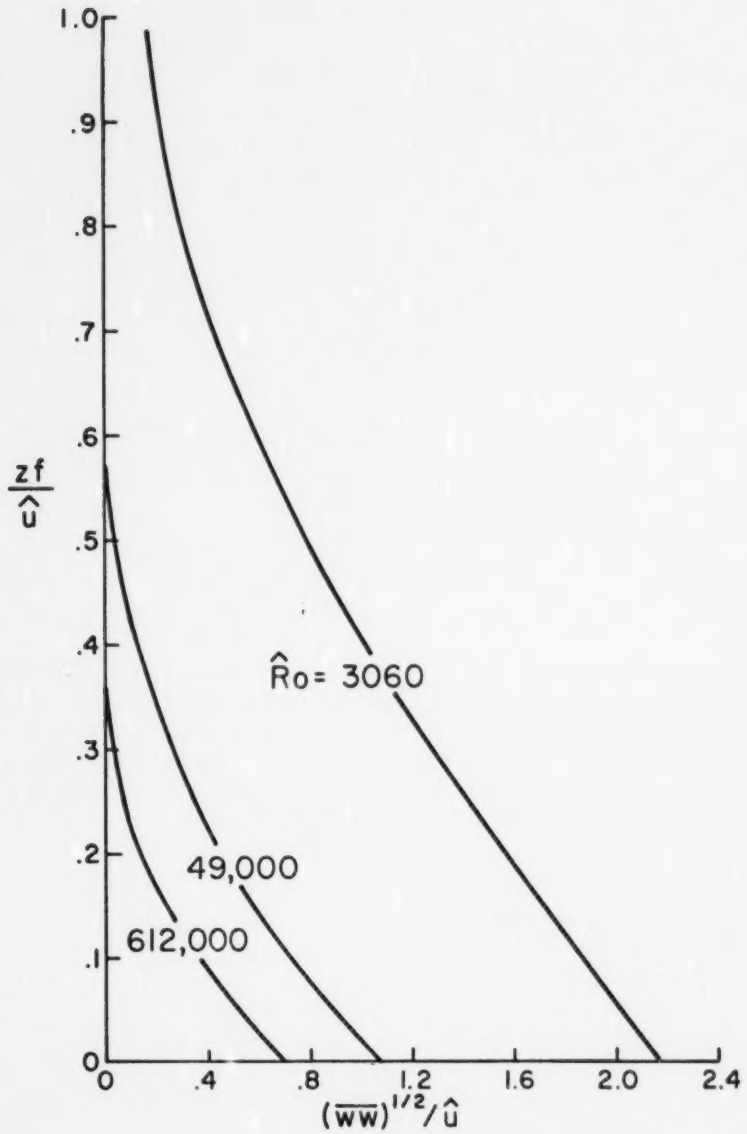

Figure 8. Ratio of the vertical velocity variance to 10% of the wind at 10 m altitude for three different values of Rossby number

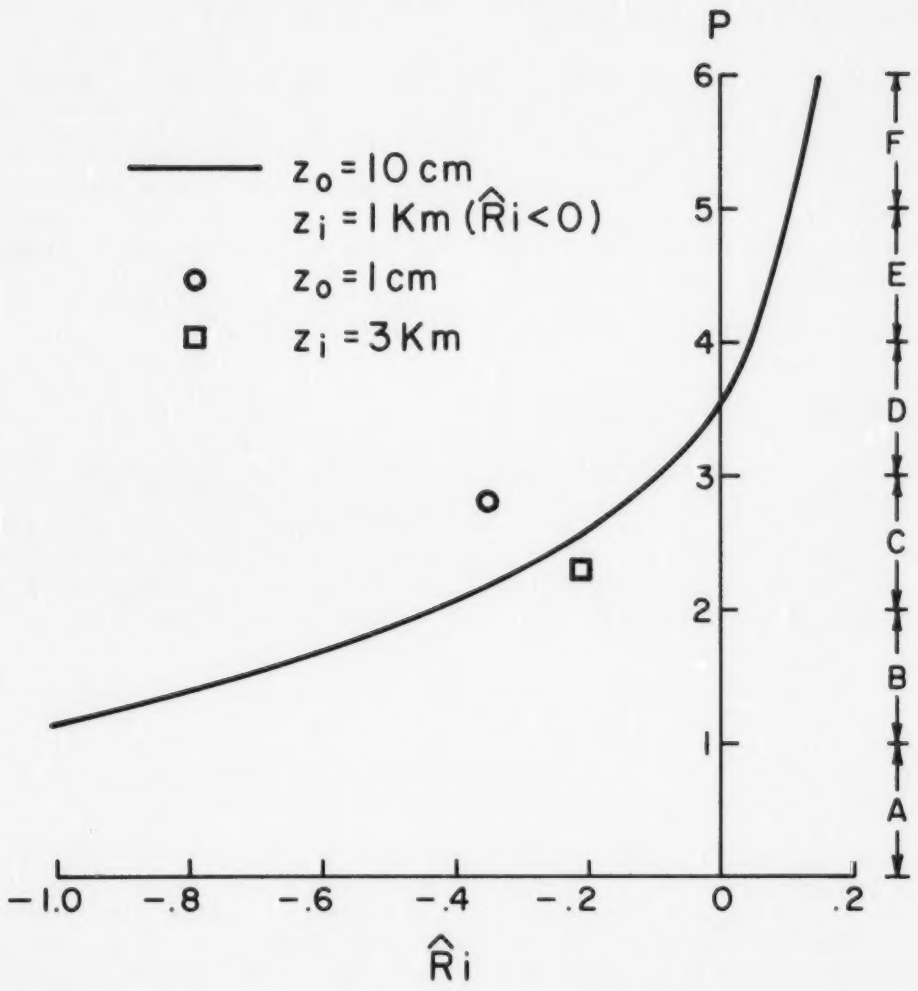

Figure 9. Correspondence between $\hat{R}i$ and Pasquill's stability parameter P or stability classes A-F

for other values of z_o, then the points in Figure 9 indicate a nonuniqueness between P and $\hat{R}i$. However, it seems more desirable to have P defined so that at a fixed altitude $\overline{ww}/U^2$ is determined uniquely. This would require the definition sketch of P (Fig. 6.13, Ref. 30) to shift with z_o and should make the relationship between P and $\hat{R}i$ contain less scatter.

Figure 10 shows $(\overline{ww})^{1/2}/\hat{u}$ for four different values of $\hat{R}i$ and two different values of the dimensionless inversion height $z_i f/\hat{u}$. The inversion height represents additional information supplementary to the surface meteorological conditions and must be known if estimates of dispersion very far from the source are to be made. It may typically vary diurnally from something less than 100 m near sunrise to a few kilometers near sunset.[32] Note that for $z/z_i \gtrsim 0.1$, the two curves for essentially the same $\hat{R}i$, but different z_i's, show a significantly different value of $(\overline{ww})^{1/2}$.

SUMMARY OF DIFFUSION MODEL

As developed in References 3 and 6, the diffusion of a passive species calls for the solution of the species continuity equation, the species turbulent flux equation, and the species-temperature correlation equation (Eqs. (1)-(4) from Section IV) with the velocity turbulence field known from a prior decoupled calculation. In these equations,

$$q_p = q_t(\Lambda_p/\Lambda_t)^{1/3} \tag{14}$$

where the subscript t represents the value of q or Λ obtained from the prior turbulence calculation.

The greatest difficulty in using Eqs. (1) through (4) is in properly setting the pollutant velocity scale q_p and length Λ_p. When the size of the plume is large in comparison to the most energetic turbulent eddies, q_p and Λ_p may be taken as equal to the same scales used in computing the turbulence. However, when the plume scale is much less than the most energetic eddies, then both the velocity and length scales of the plume may be significantly smaller than the companion scales for the turbulent velocity field. Our approach takes the plume scale proportional to the spread of the species plume

$$\Lambda_p = d\sigma \tag{15}$$

subject to the constraint

$$\Lambda_p \leq \Lambda_t \tag{16}$$

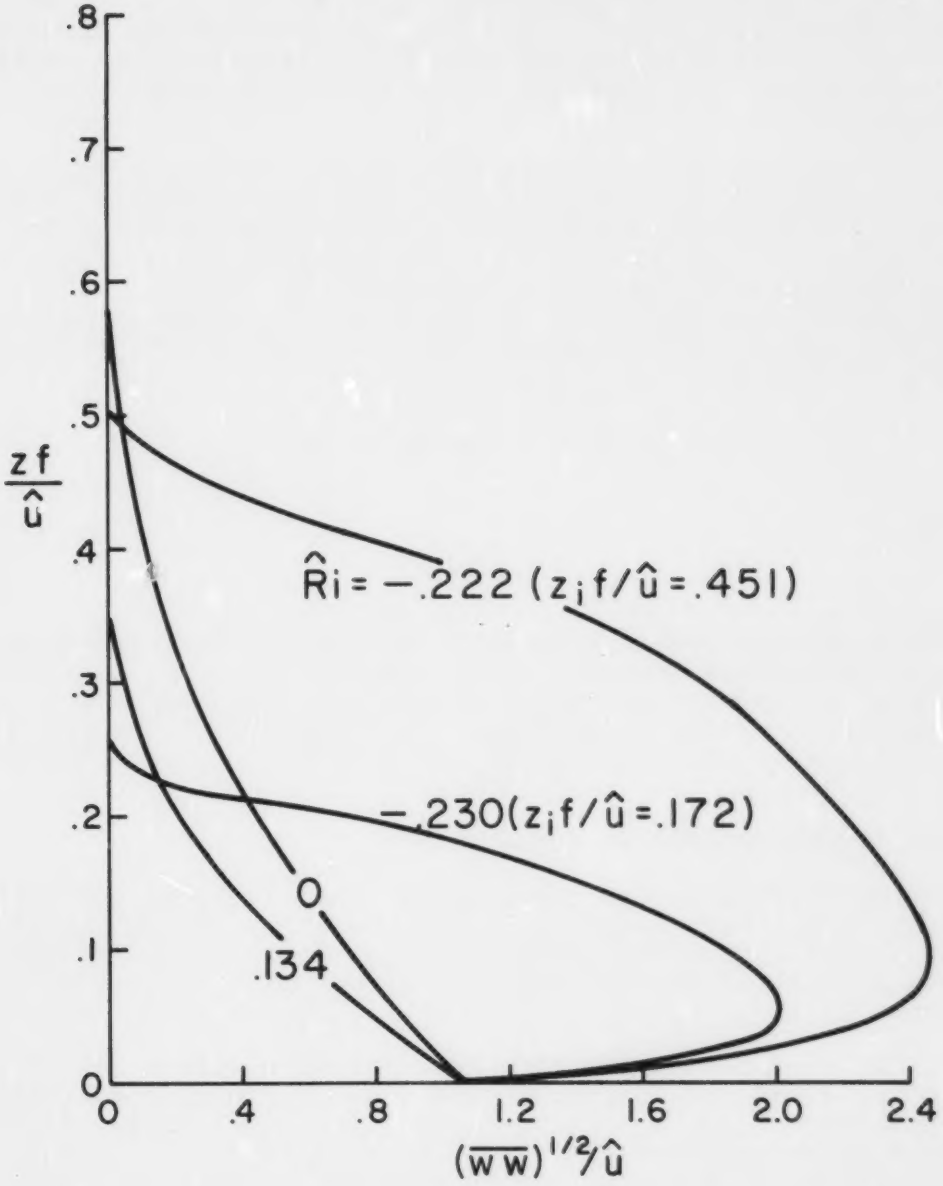

Figure 10. Ratio of the vertical velocity variance to $\hat{u}$ for different values of $\hat{R}i$ and mixed-layer depths for $Ro = 10^6$

That is, the mixing scale cannot be larger than the ambient turbulent scale. The proportionality factor d is a model input coefficient. It is the only new coefficient introduced in the species equation that has not previously been determined and used in computing the velocity and temperature distributions.

A discussion of the relation of our model equations to K theory has been given in the chapter on Super-Equilibrium Theory in Reference 3. The validity of K theory requires that the convective terms (those on the left-hand side of Eq. (2)) and the diffusion term (the term with the second-order derivative) be negligible in comparison with the remaining terms. For a one-dimensional problem with neutral stability, this reduces to

$$\overline{wc} = - \frac{\overline{ww}\Lambda}{Aq} \frac{\partial C}{\partial z} \tag{17}$$

i.e.,

$$K_z = \frac{4}{3} \frac{\overline{ww}\Lambda}{q} \tag{18}$$

This should be reasonably valid near the surface under neutral conditions where the expression reduces to $K_z = (0.52)u^*z$. We wish to emphasize that this reduction is valid only under these very special conditions. At higher altitudes and/or for non-neutral conditions, other terms in Eq. (2) are important.

LINE SOURCE RELEASE AT GROUND LEVEL

We first consider cases where sensitivity to the coefficient d is very weak. In close proximity to the ground, the scale of the turbulence is proportional to the distance from the ground so that Eq. (16) rather than (15) will limit Λ_p.

Figure 11 is a plot of the vertical variance σ_z for the two-dimensional problem of a line source perpendicular to the surface wind in a neutral atmosphere with Rossby number based on the geostrophic wind, $Ro = u_g/fz_o = 10^6$. The difference between σ_z for $d = 1$ and an extreme value of $d = 1000$ is slight. Also shown for comparison is Pasquill's latest recommendation for use with Gaussian plume models obtained from a combination of eddy diffusivity calculations and empirical data (Ref. 30, Fig. 6.13b).

Figure 12 compares the vertical distribution of species concentration at several downwind distances with the Gaussian

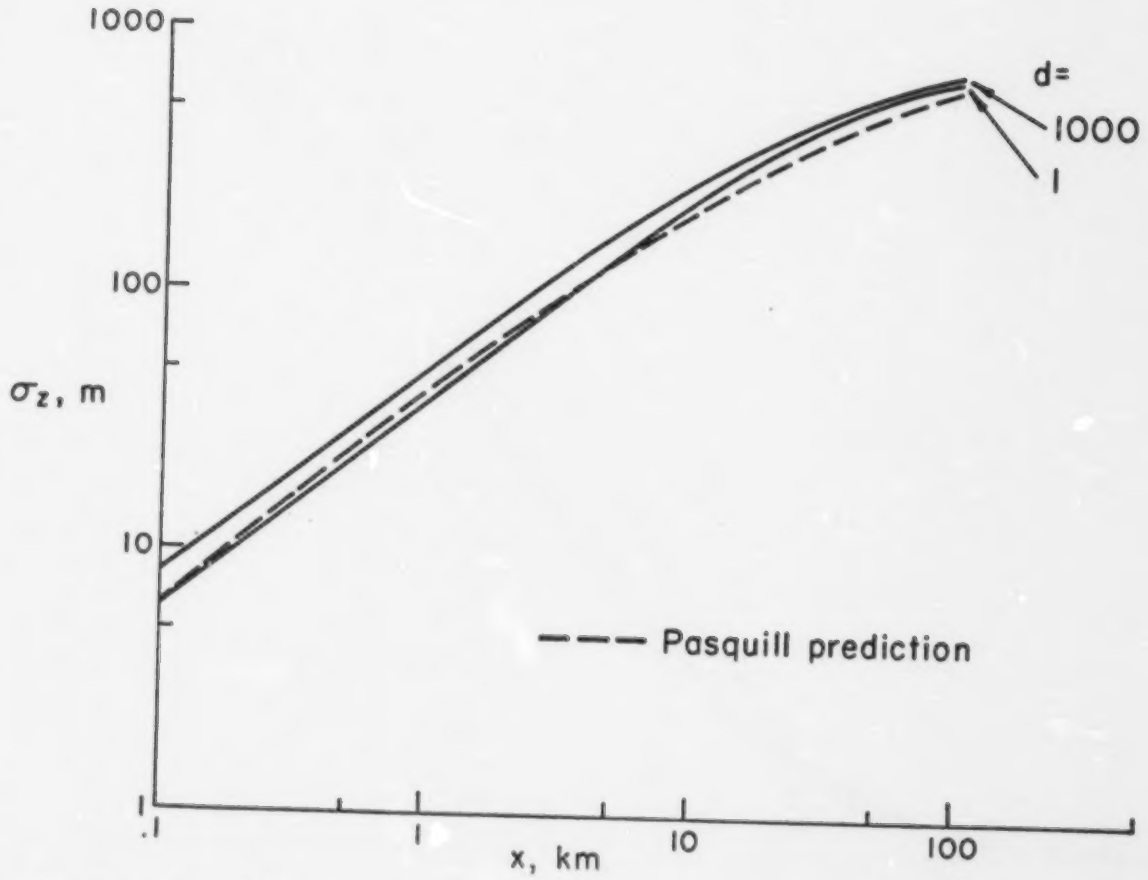

Figure 11. The vertical spread σ_z as a function of distance x downwind of a line source ground release in a neutral atmosphere (u_g = 10 m/sec, z_o = 10 cm, $f = 10^{-4}$ sec^{-1})

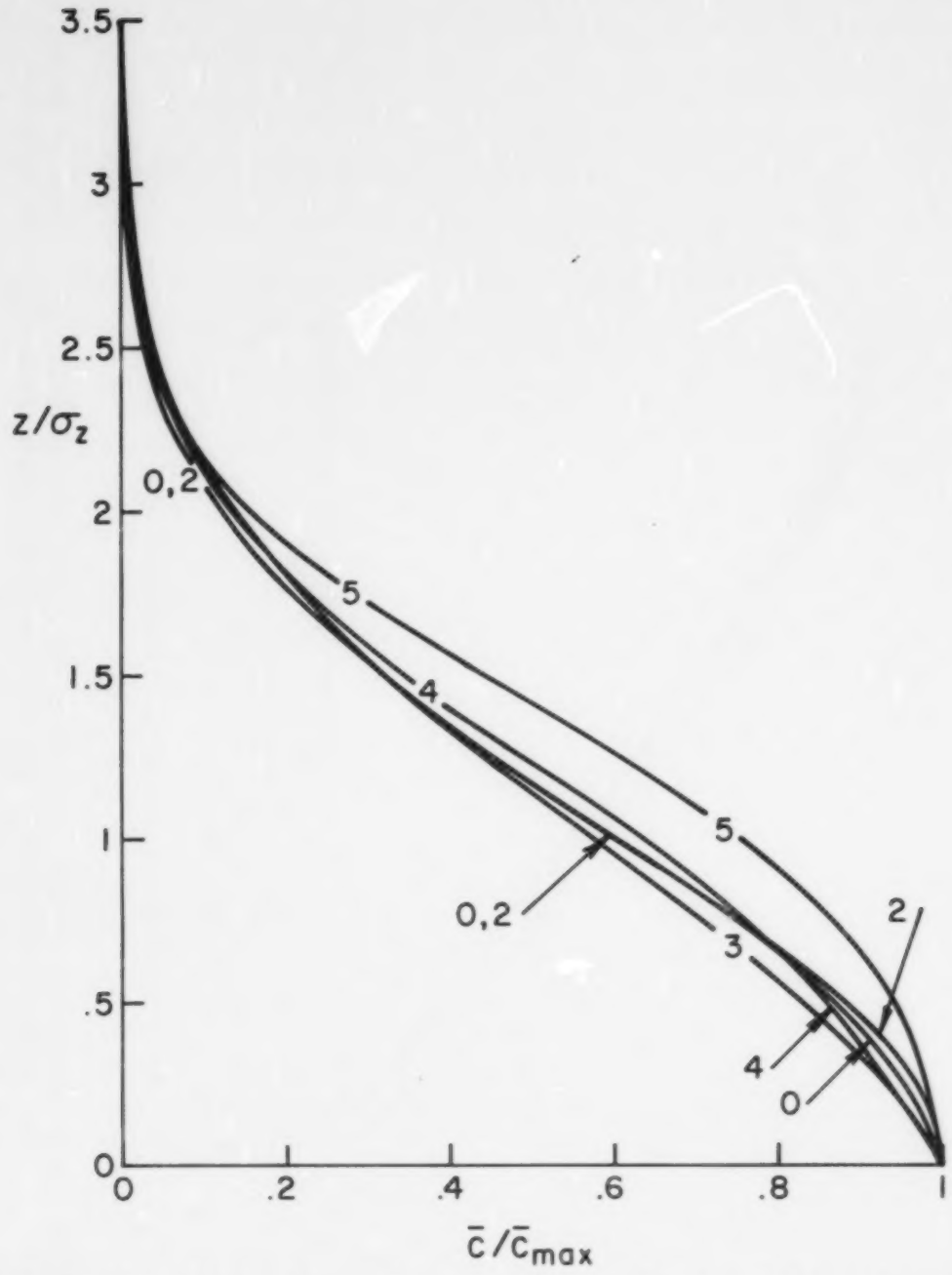

Figure 12. Comparison of species distribution with a Gaussian distribution for the plume of Figure 11. Normalized profiles are shown for several distances downwind of the release point. The numbers give the exponent in tens of meters; i.e., 0 is the Gaussian distribution assumed for x = 0, 2 is the profile at x = 100, etc.

distribution. In spite of the shear existing in the wind profile, the normalized results do not depart strongly from Gaussian. However, Figure 13 shows that this should not be interpreted as verification of the commonly used Gaussian plume approximation for determination of the surface concentration, because this approximation ordinarily assumes a uniform wind. If the 10-meter value of the wind is used in the Gaussian plume model, Figure 13 shows that it would predict a lower value of surface concentration close to the source and a higher value at a distance, even when the empirical σ_z variation is used.

Pasquill's Figure 6.13d[30] shows the growth of σ_z for various values of z_o but with no indication of variation with geostrophic wind or coriolis parameter. Our modeled turbulence equations indicate that the proper dimensionless parameter for this neutral case is the Rossby number. A normalized curve for a variation of two orders of magnitude in the Rossby number is shown in Figure 14. These curves should not be used for estimating σ_z quite close to the source since we arbitrarily start with $\sigma_z = 1$ m at $x = 0$. The dependence on Rossby number is slightly stronger than that implied by Pasquill's Figure 6.13.

The influence of stability on vertical spread is much stronger than the influence of Rossby number. In Figure 15 the stability is measured by the Richardson number defined in Eq. (1). On the unstable side ($\hat{R}i < 0$), σ_z is capped by the presence of the temperature inversion layer at the top of the unstable layer of thickness z_i. This yields an upper bound on σ_z of $\sigma_z \approx 0.6 z_i$.

An unexpected feature of Figure 15 is that normalization of the lengths by $\hat{u}/f$ scales the curves such that they tend to converge at low x. If the lengths were normalized by u_g/f instead, there would be more spread between the unstable and stable cases. Exact comparison between the influence of stability, as predicted by Figure 15 and that predicted by Pasquill, is difficult because no normalization is given for his lengths. The implication in his curves is that for specified z_o and stability class, there is no dependence of spread rate on wind velocity, as mentioned in the discussion of Figure 9. If we interpreted his plots as made for a geostrophic wind of 10 m/sec and $f = 10^{-4}\ \text{sec}^{-1}$ so that $u_g/f = 100$ km, as was done in Figure 11, then a direct comparison can be made. This yields the comparison shown in Figure 16. On this basis, Figure 16 shows a stronger effect of stability on σ_z on the unstable side and a weaker effect on the stable side than that implied by Pasquill.

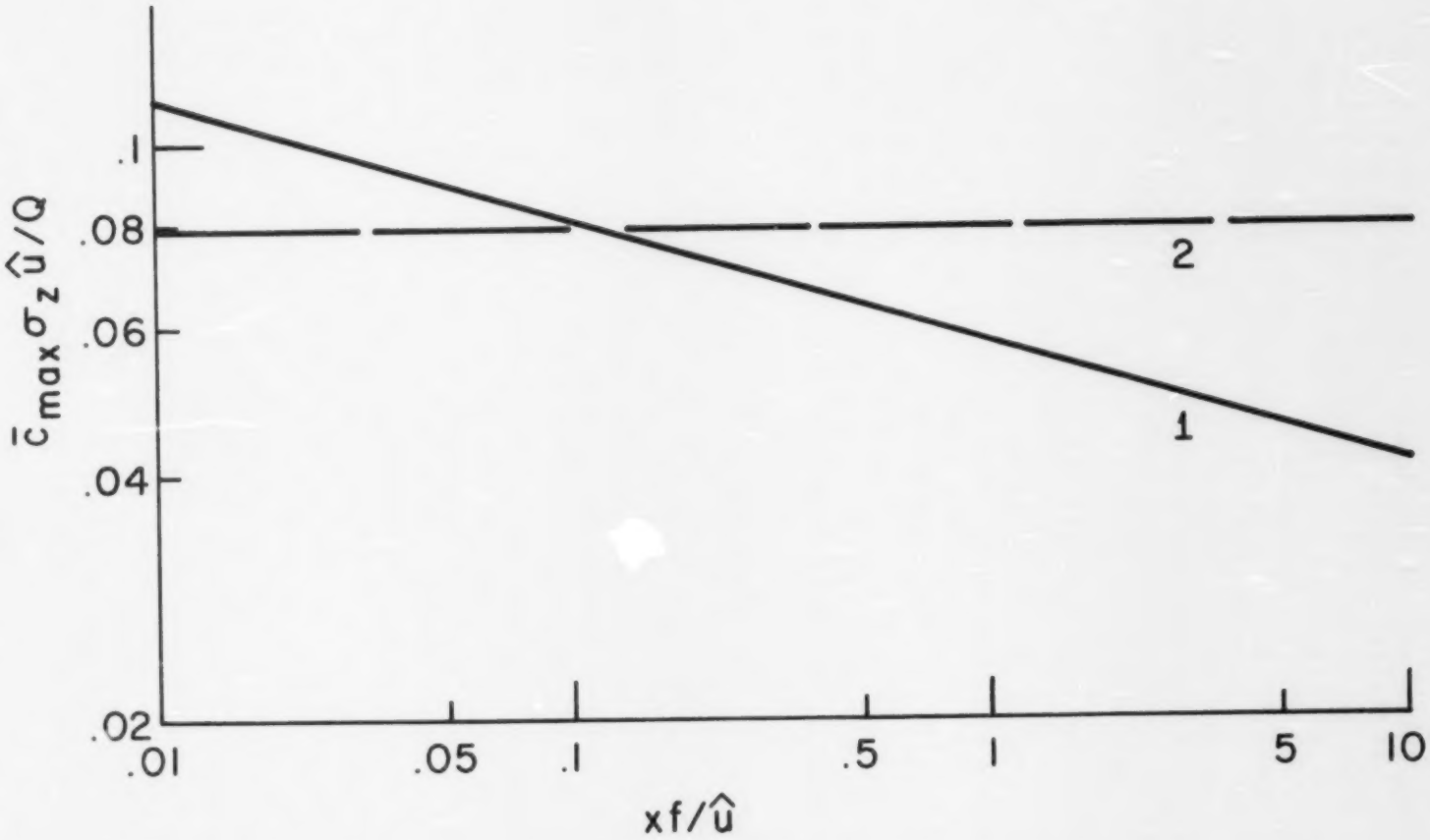

Figure 13. Normalized surface species concentration as a function of downwind distance (——) compared with the Gaussian solution (---) for a wind assumed constant at its value at a height of 10 meters

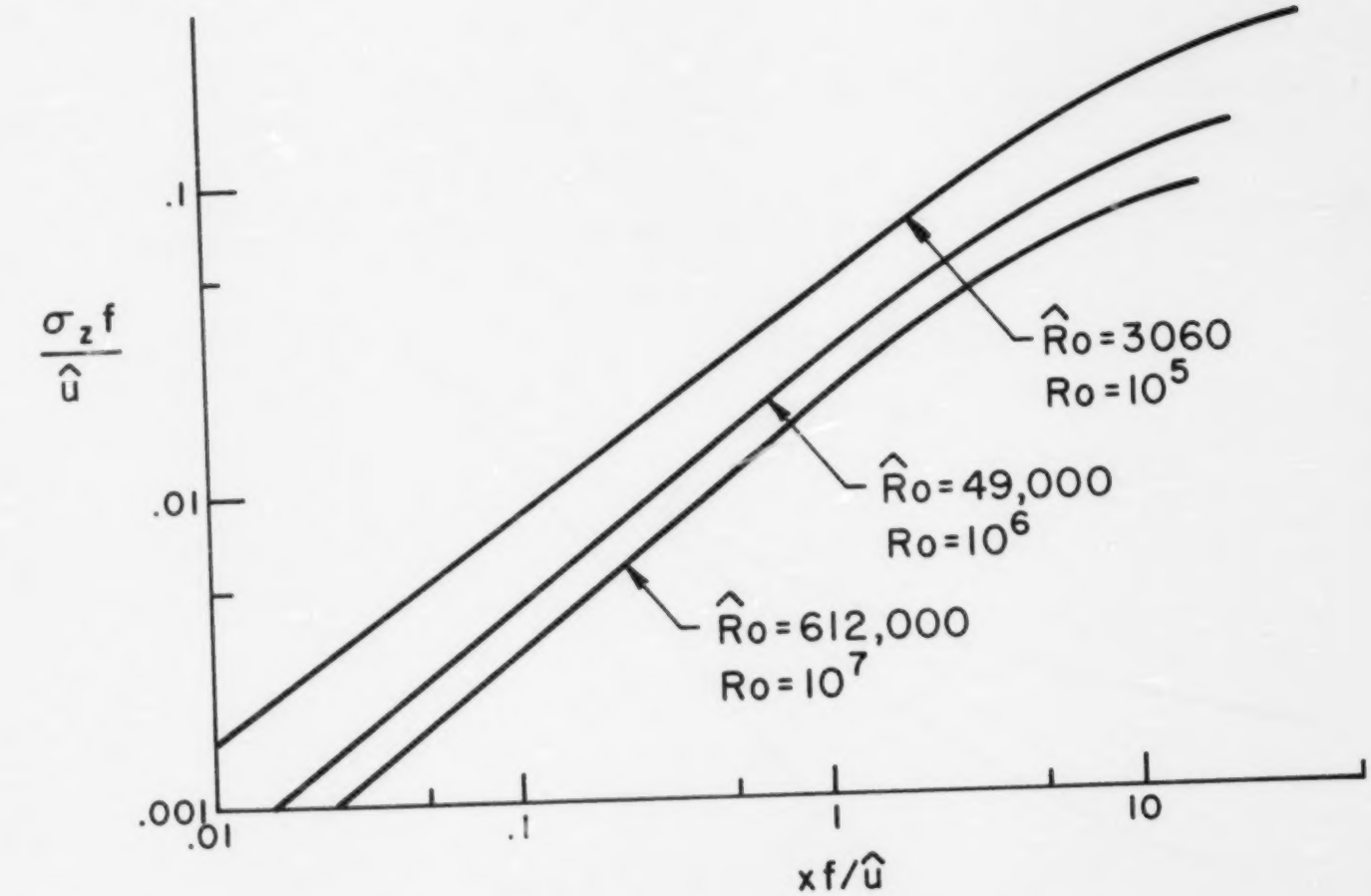

Figure 14. Comparison of vertical spread in a neutral atmosphere from a line source ground release for changes in the Rossby number based on surface roughness z_o

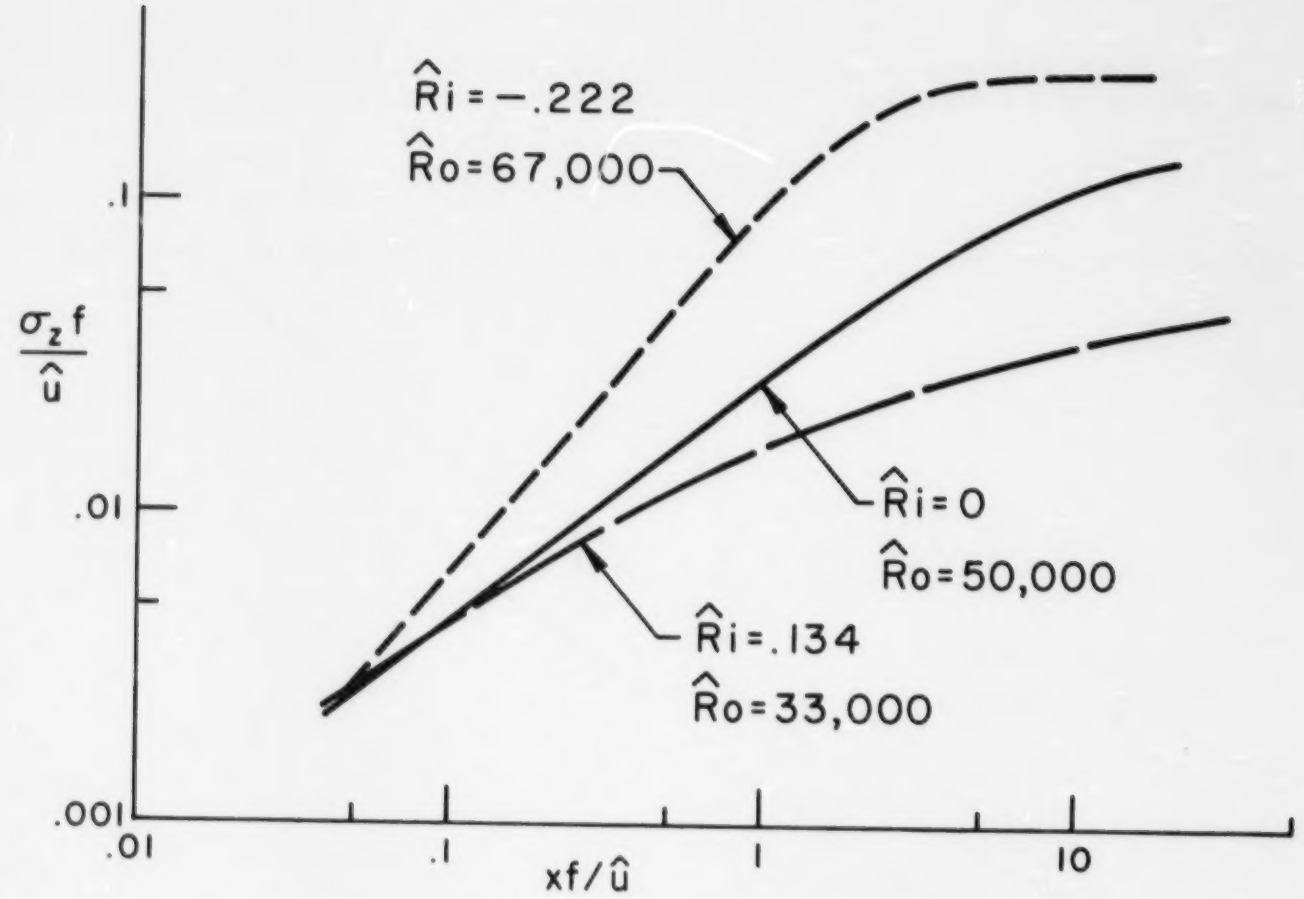

Figure 15. Comparison of vertical spread from a line source ground release for different values of $\hat{R}i$ for $Ro = 10^6$ ($z_1 f/\hat{u} = 0.451$ for the unstable case)

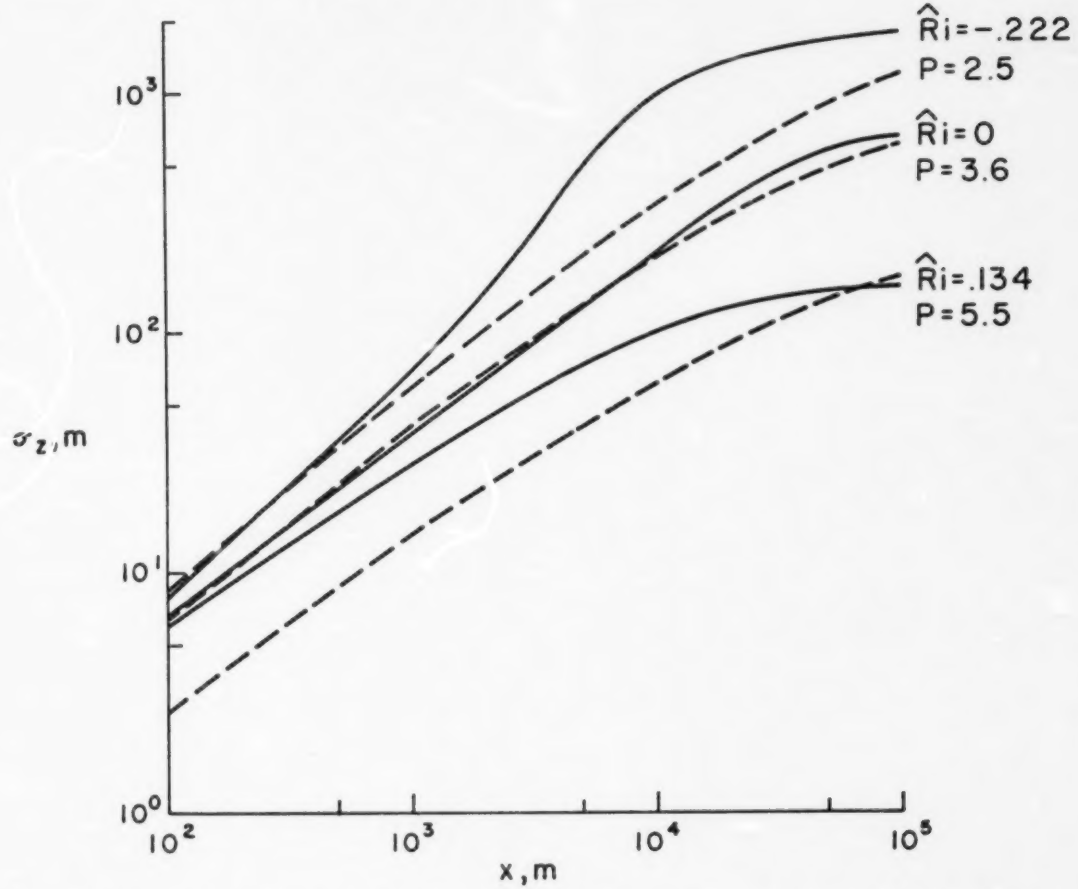

Figure 16. Repeat of Figure 15 in unnormalized form for u_g/f = 100 km for comparison with Pasquill's Figure 6.13[30] (---)

Neglecting any influence of u_g or f on the variation of σ_z with z_o in Pasquill's Figure 6.13 is probably not too serious for practical calculations, because this will lead to no more than an order of magnitude uncertainty in Ro, which translates into less than a factor of two in the estimate of σ_z. However, neglecting any influence of the mixed layer depth on σ_z estimates in unstable atmospheres can potentially lead to more error. The influence of differing mixed layer heights at similar unstable values of P can lead to significantly different values of turbulence even relatively near the ground, and thus to significantly different dispersion values. This will be the case when

$$\frac{w^*}{u^*} = \left(-\frac{kz_i}{L}\right)^{1/3} \gtrsim 1$$

When this condition is met, diffusion above $z/z_i \gtrsim 0.1$ cannot be determined by stability class alone.

The concentration profiles are compared with the normalized Gaussian distribution for $Ri \neq 0$ in Figures 17 and 18. The distributions for stable conditions remain similar to the Gaussian but, in unstable conditions there are strong departures. Note that at $x = 10$ km, the maximum concentration occurs significantly above ground level. After the vertical spread is effectively capped by the inversion, the concentration asymptotically approaches a uniform distribution between the ground and the inversion, with a sharp drop-off at the bottom of the inversion layer. When the Gaussian plume model is modified by the method of images to account for the presence of a lid in air quality modeling, it is possible to approach the uniform distribution between the ground and the inversion. However, it will not permit the maximum concentration to rise above ground level. The ratio of the ground concentration to that which would be predicted by a simple Gaussian plume transported by a constant wind departs remarkably little for $Ri \neq 0$ from that shown in Figure 13 for the neutral case. The plume for the stable case shows a concentration ratio approximately 10% higher at $xf/\hat{u} = 10$, while the unstable is approximately 10% lower. Apparently the wind shear is the dominant variable in determining this concentration ratio, and $\hat{u}$ fairly effectively measures this influence.

POINT SOURCE GROUND RELEASE

To this point we have shown results that assumed no variation in the y direction. The more interesting problem in practice is usually the three-dimensional plume involving lateral as well as vertical dispersion. Any theory attempting

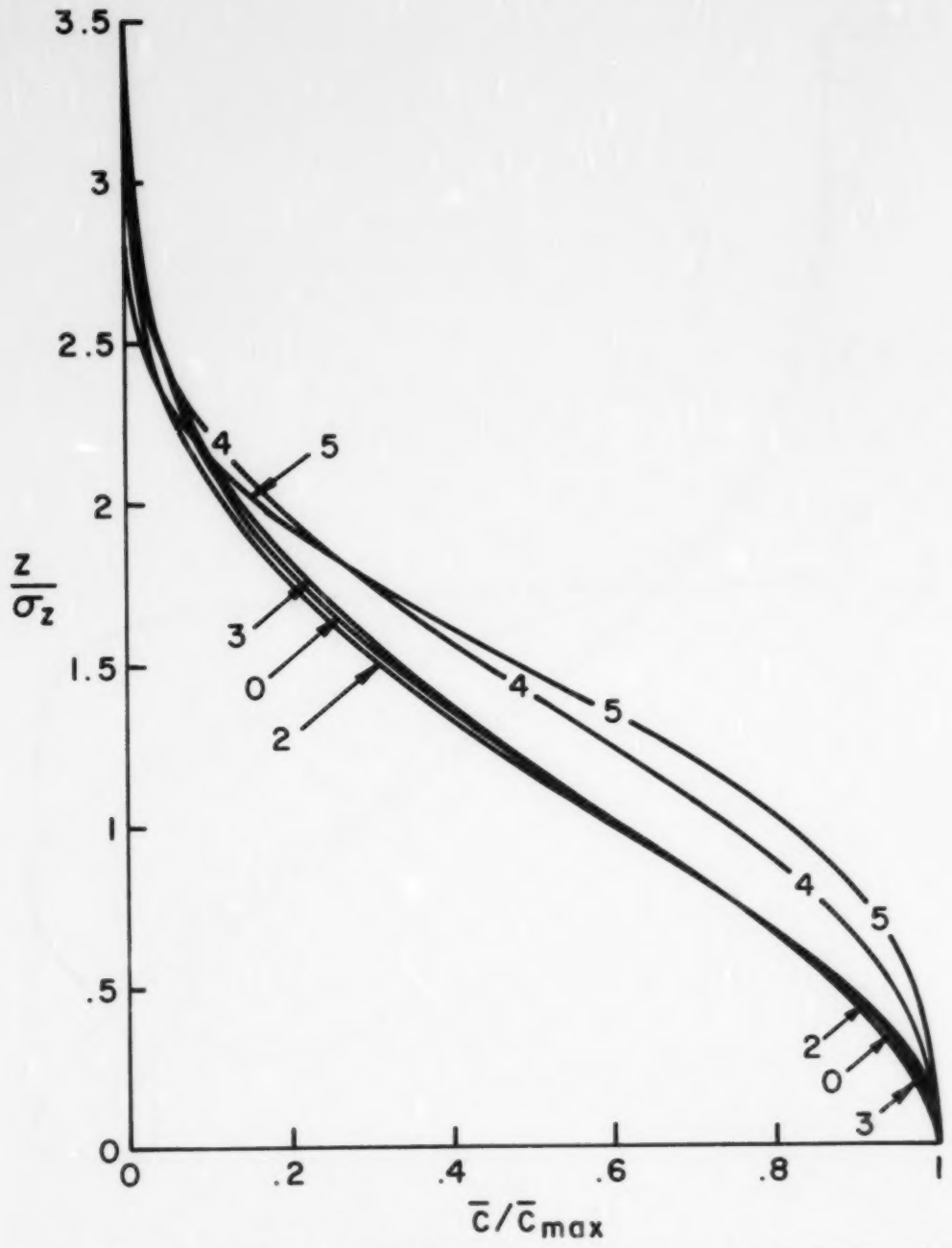

Figure 17. Normalized profiles of vertical spread from a line source ground release into a stable atmosphere (R_i = 0.134, Ro = 10^6) as a function of distance downwind, denoted in powers of 10 meters (0 is Gaussian distribution assumed for x = 0)

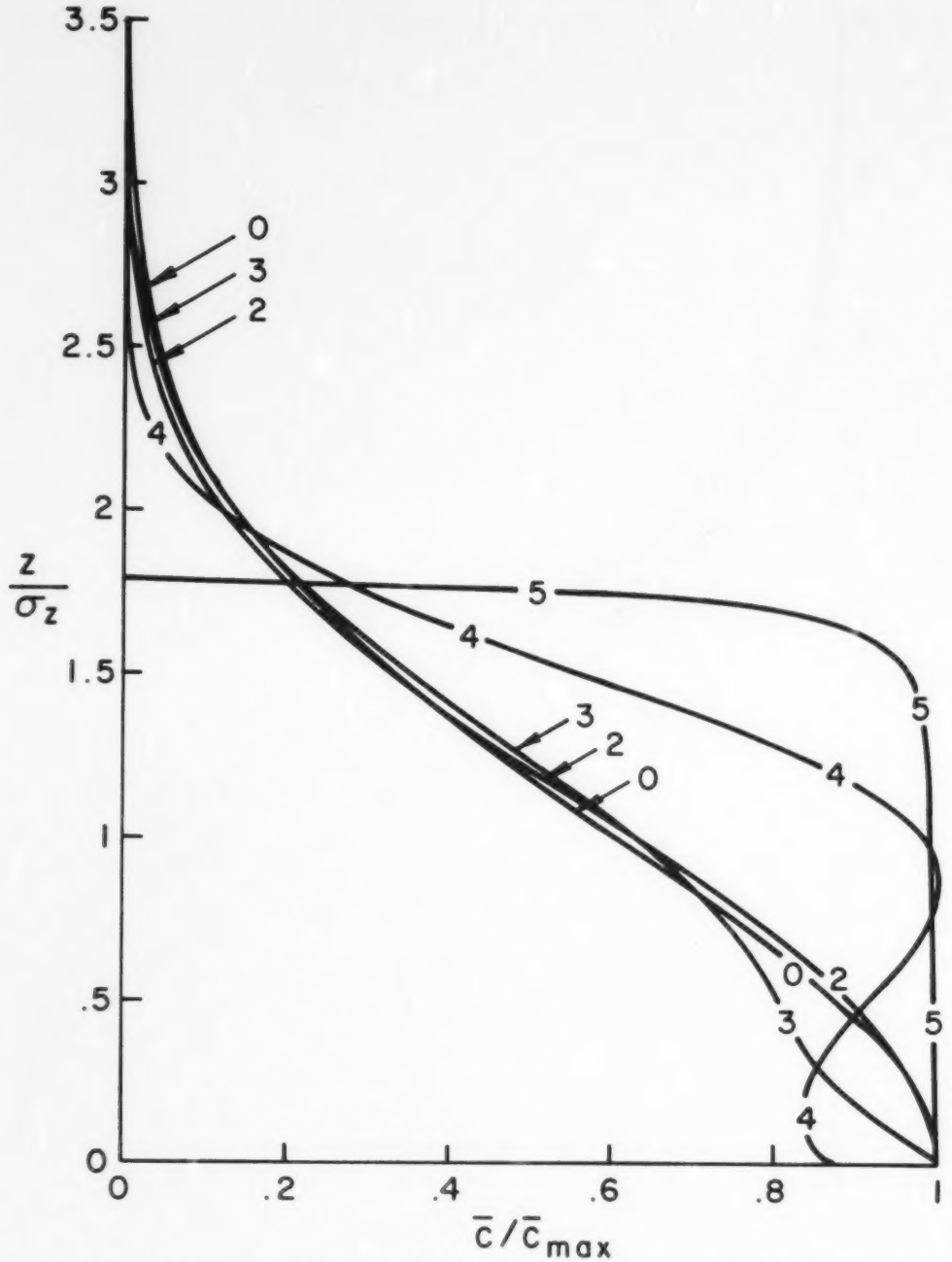

Figure 18. Normalized profiles of vertical spread from a line source ground release into an unstable atmosphere ($Ri = -0.222$, $Ro = 10^6$) as a function of distance downwind, denoted in powers of 10 meters (0 is Gaussian distribution assumed for $x = 0$)

to compute three-dimensional dispersion must first be able to predict any valid differences between vertical and lateral velocity variances. In the neutral boundary layer, our model predicts the two variances to be equal. Most investigators believe the lateral to be larger, but there is considerable uncertainty. Panofsky[32] quotes ratios anywhere from 1.2 to 2.4. Our basic turbulence model probably needs an additional term representing the influence of mean strain on the modeling of the terms involving pressure fluctuations, as has been suggested by several investigators (for example, Lumley and Khajeh-Nouri,[14] Naot[33]). However, with the large uncertainty in the empirical data, it is difficult to make any such adjustments with confidence. Even with a model which correctly predicts the lateral fluctuations in an ideal homogeneous boundary layer, inhomogeneities in terrain appear to have such a large influence on the low frequency lateral velocity fluctuations that a confident prediction in a real situation will be difficult. Notwithstanding these difficulties, we do believe it is enlightening to proceed with calculations that show the influence of stability on the three-dimensional plume.

In this three-dimensional case, there are two different values of σ: σ_y and σ_z. Therefore, Eq. (15) must be generalized to determine the plume. For present purposes, the Λ's appearing in the diffusion terms of Eqs. (2) through (4) are specified by either $d\sigma_y$ or $d\sigma_z$, depending on the direction of the diffusion, while the Λ^z's appearing in the tendency-towards-isotropy terms are given by an average value:

$$\Lambda = d\,\frac{2\sigma_y^2\sigma_z}{(\sigma_y^2 + \sigma_z^2)} \qquad (19)$$

In any case, the constraint in Eq. (16) is still applied and, therefore, there is very little sensitivity of the results to the particular form of Eq.(19) in the problem of ground release.

Concentration isopleths downwind of a point source at ground level in a neutral atmosphere are shown in Figure 19. The notable distortion from a Gaussian distribution apparent in Figure 19 appears to be principally caused by the Ekman spiral of the principal wind deviation with altitude.

The influence of the Ekman spiral is much more pronounced for the case of a point release at ground level in a stable atmosphere, as shown in Figure 20. This is primarily due to the fact that the angle between the surface wind and the upper level geostrophic wind is 30° more for this stable case

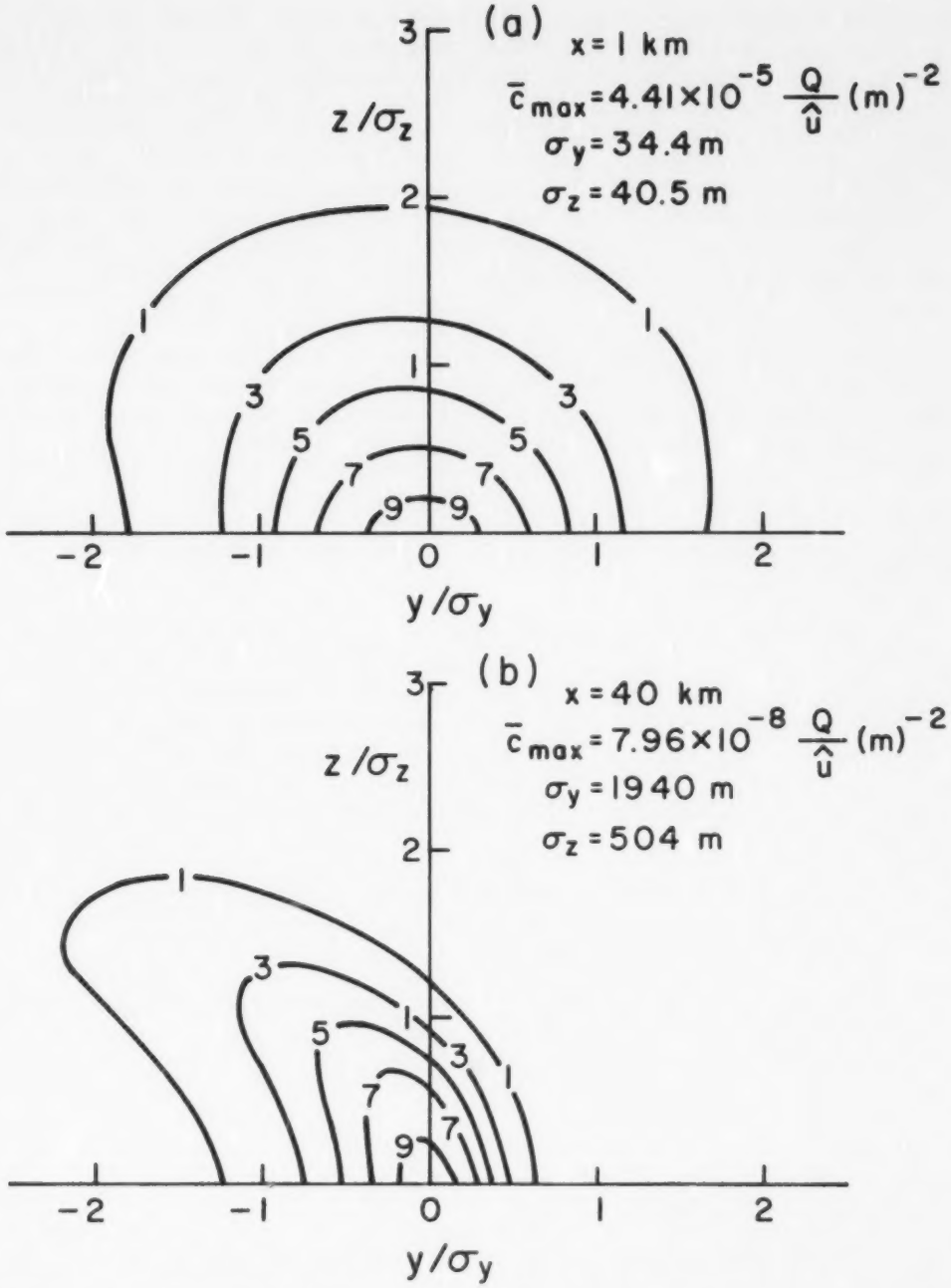

Figure 19. Concentration isopleths downwind of a point source ground release into a neutral atmosphere ($\hat{R}o$ = 50,000, $\hat{u}/f$ = 5000 m); notation refers to tenths of maximum value, i.e., 9 is $0.9\bar{c}_{max}$, etc.

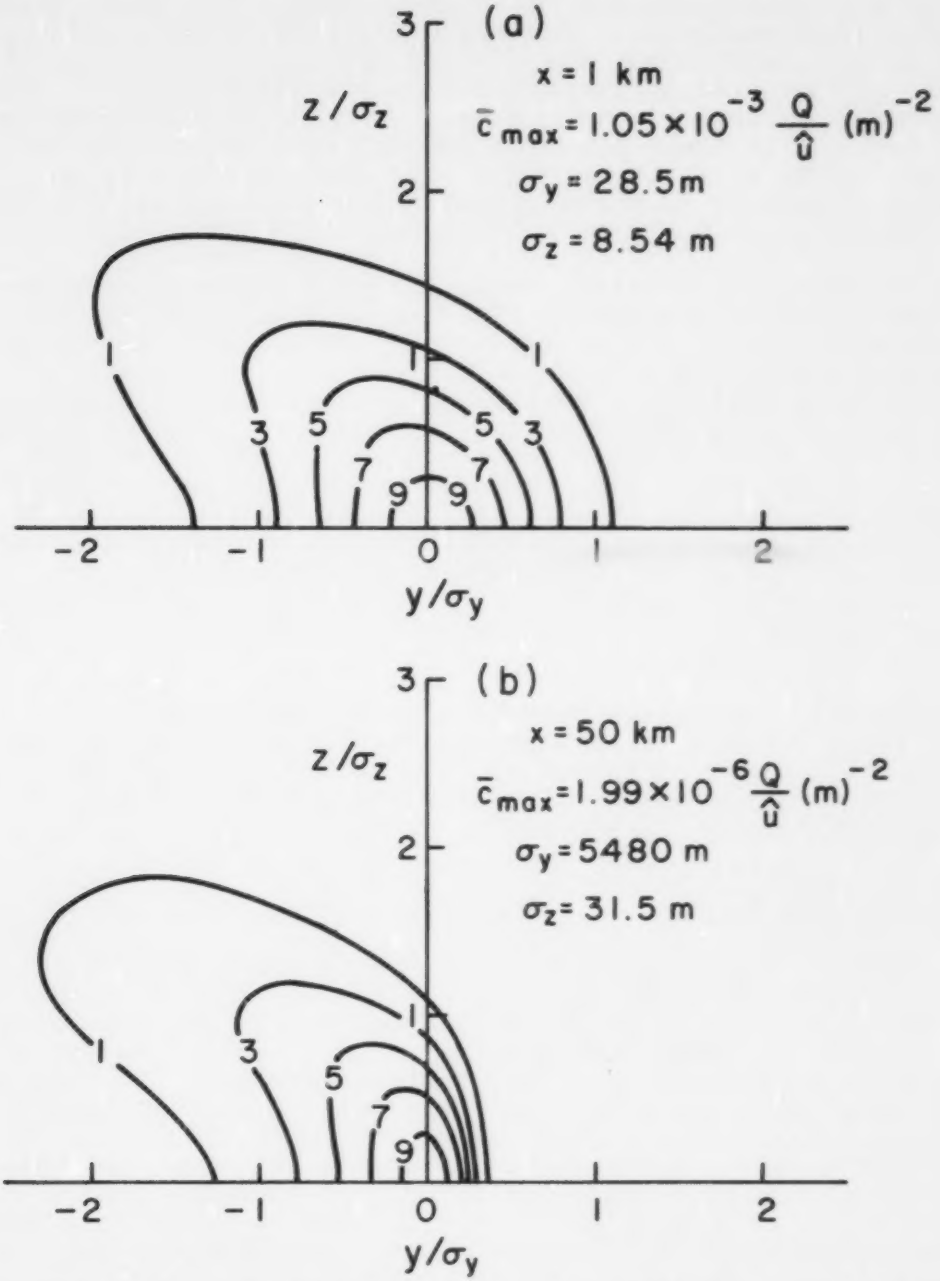

Figure 20. Concentration isopleths downwind of a point source ground release into a stable atmosphere (Ri = 1.1. Ro = 340,000, u/f = 2740 m); notation as in Figure 19.

($\hat{R}i = 1.1$) than it is for the neutral case. The Ekman layer is also much shallower. The maximum ground level concentration occurs immediately downwind of release, even though the plume is distorted asymmetrically by the Ekman spiral. The uncertainty present in the lateral velocity fluctuations is overshadowed in these plots by the enhanced lateral spreading caused by the wind veering with altitude. Therefore, we believe Figure 20 is a valid prediction although we have not yet uncovered reliable data to compare with its predictions.

Figure 21 is a complementary plot of a ground release into an unstable atmosphere ($Ri = -1.1$) with an inversion layer occurring at 3.8 km ($z_i = 0.355u^*/f$). For this level of instability, there is very little effect of the wind veering with altitude. Note that the upper level inversion behaves very much like a reflecting boundary (similar to the ground boundary) in the distribution at 10 km. This is a result of the model, since we have not specified any such boundary condition. As seen in Appendix A, the same boundary condition on the species is specified for all stability conditions as $z \to \infty$. Further downwind of the release, the concentration will continue to be quite homogeneous between the ground and the inversion layer, but with an ever-increasing lateral spread.

Direct comparisons between vertical spread rates for two- and three-dimensional plume calculations show relatively little difference. Estimating σ_z on the basis of two-dimensional calculations appears valid even when the plume is three-dimensional.

ELEVATED LINE RELEASE

Results for dispersal downwind of a continuous line source at an elevation which is a significant fraction of the neutral planetary boundary layer are shown in Figures 22 and 23. Figure 22 shows the influence of the release height on the vertical spread rate. The vertical velocity fluctuation is less at altitude than near the ground, and the mean wind is larger, but these effects are partly counterbalanced by the fact that the turbulent scale is significantly larger. The net effect is a reduction in σ_z of approximately a factor of 2 at $xf/\hat{u} = 10$. This difference would disappear asymptotically as σ_z becomes greater than the release height z_r.

In Figure 23, the concentration isopleths have been normalized to make them directly comparable to the results of a numerical experiment performed by Lamb et al.,[34] i.e.,

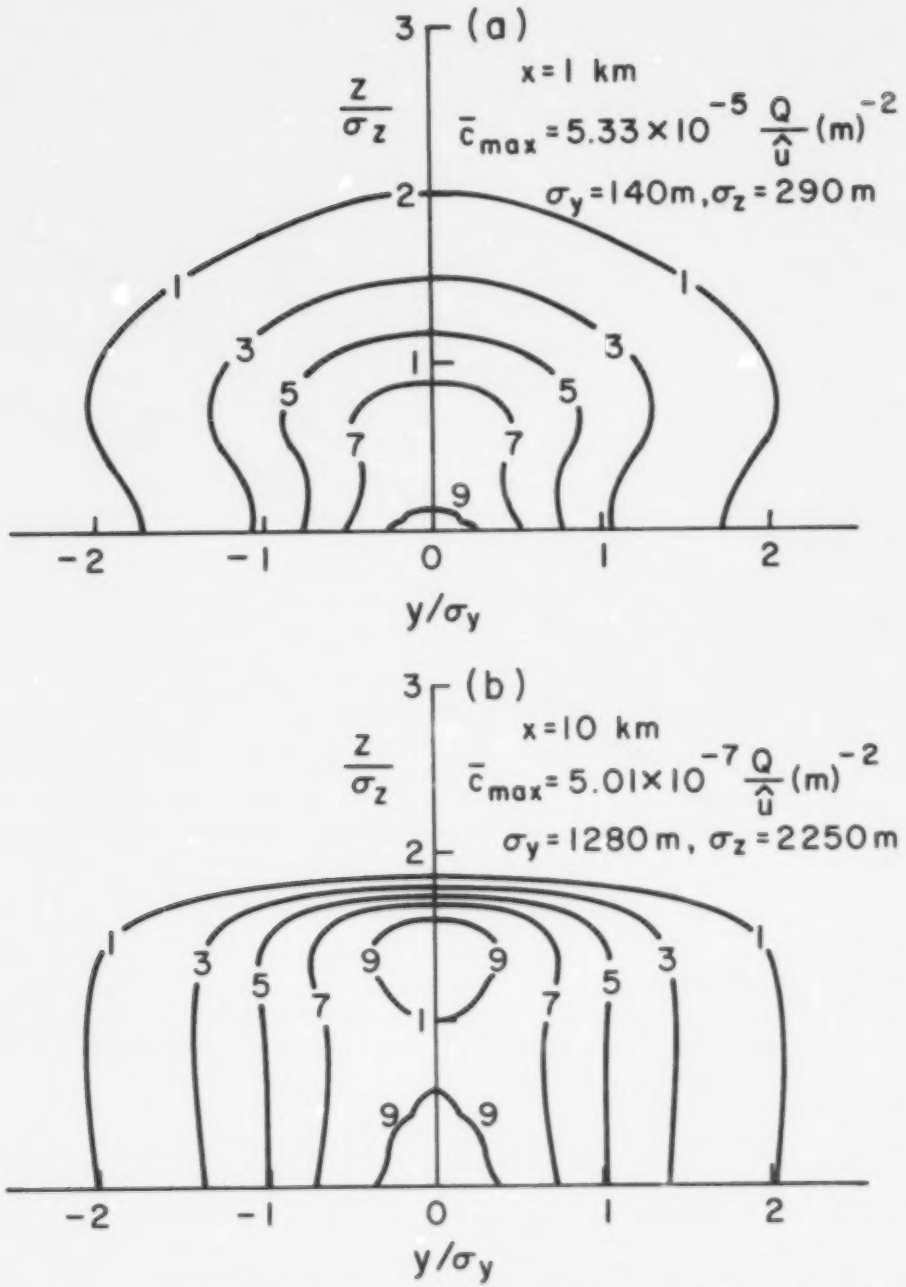

Figure 21. Concentration isopleths downwind of a point source ground release into an unstable atmosphere ($\hat{R}i$ = -1.1, Ro = 4750, $\hat{u}/f$ = 4750 m); notation as in Figure 19

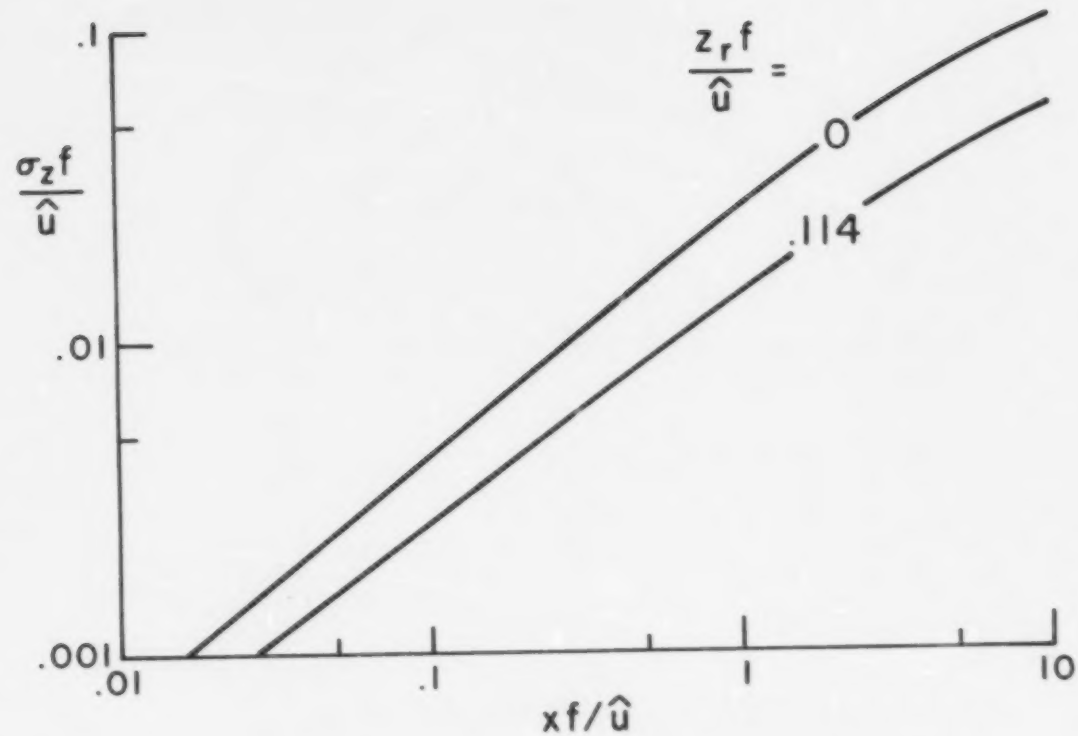

Figure 22. Comparison of the vertical spread as a function of distance downwind of a line source for ground and elevated release into a neutral atmosphere with Ro = 10^6

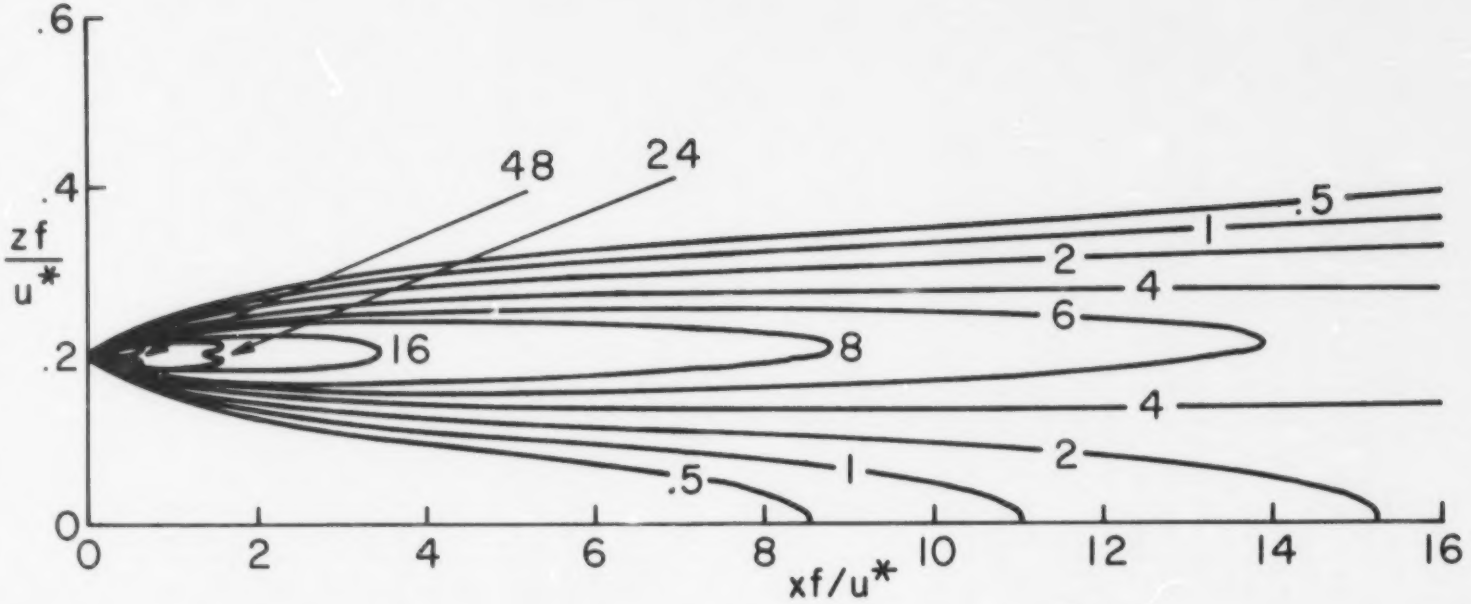

Figure 23. Concentration isopleths downwind of a line source elevated release into a neutral atmosphere. Concentration levels are consistent with the numerical experiment of Lamb et al.[34] : our predictions

$CU_r u^*/fQ$ where U_r is the mean velocity at the release height. In their numerical experiment, they released ideal numerical particles into the three-dimensional, unsteady velocity field computed by Deardorff[35] for a neutral atmosphere. Their results are presented in Figure 24. The greatest discrepancies between Figure 23 (our prediction) and Figure 24 occur close to the source where the plume calculated by Lamb et al.[34] shows a wider spread than is predicted by our model. Because of the time step involved in Deardorff's original model,[35] the smallest resolvable normalized Δx is $\Delta x = 0.2u^*/f$[†] so that details of the concentration distribution in the immediate neighborhood of the source are not expected to be valid. This leaves the unanswered question of how accurate their concentration distribution is at their first downstream point. Since the problem is an initial value problem, it would seem that any uncertainties in the early distribution would remain for some finite time in the calculation.

An interesting phenomenon occurs near the source in our model calculations. The plume appears to split and then reform, with the centerline concentration value at a position $x < 2$ km downwind of the source being much less than the value above or below it. This is a result of the wave nature of Eqs. (1) and (2) when the plume scale is much less than the turbulent scale. Physically, this is a manifestation of the meandering which is often evident when viewing a small plume in strong turbulence. Since our distributions represent an ensemble average of such plumes, the meandering instantaneous plume spends more time at a distance from the downwind centerline of the averaged plume than it does on the centerline. This meandering phase has been previously discussed.[6]

It is interesting to note that the computer output for the experiment of Lamb et al. (supplied to us by Lamb) shows a value of concentration on the centerline of the plume at $xf/u^* = 0.2$ which is only approximately 10% of the value at the z station above or below the centerline. However, for the reasons stated earlier, this cannot be used to quantitatively verify the meander problem.

It is in determining this early meander phase of the plume that the coefficient d in Eq. (14) has its largest influence. The sensitivity disappears when the plume size reaches the scale of the ambient turbulence. Better data or numerico-empirical analyses able to determine the early-time behavior of a plume will be required for further adjustment of this parameter.

[†]Private communication from R.G. Lamb

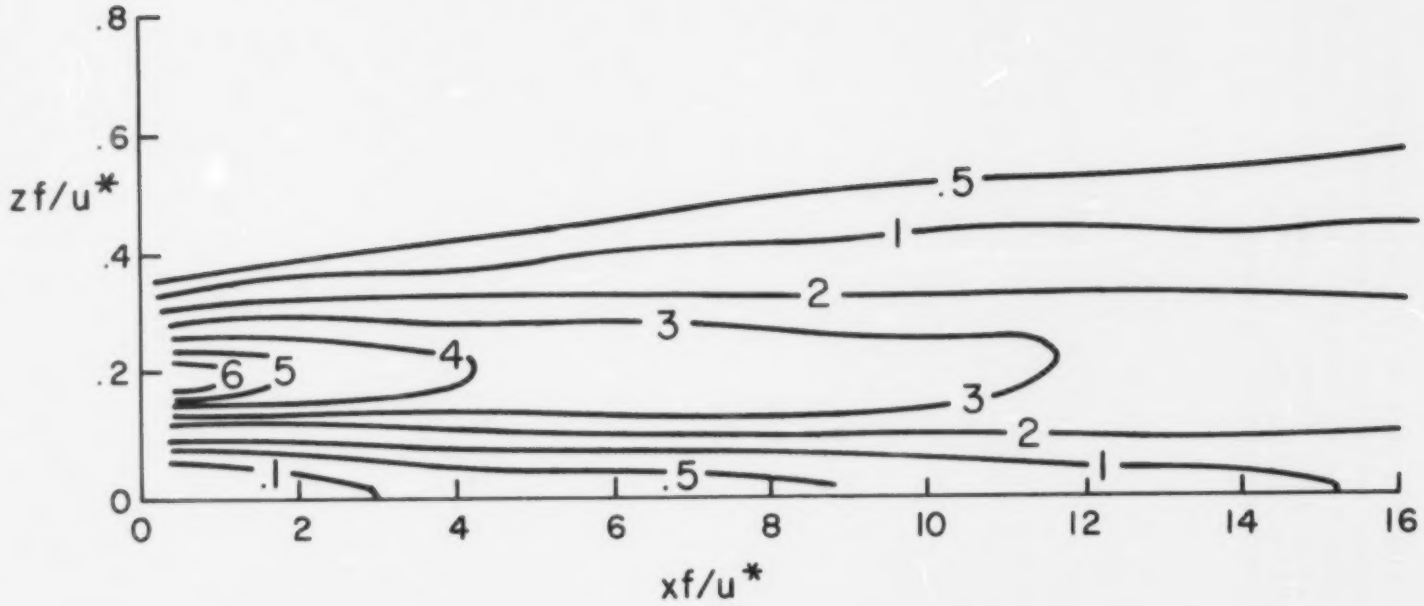

Figure 24. Concentration isopleths downwind of a line source elevated release into a neutral atmosphere. Concentration levels are consistent with the numerical experiment of Lamb et al.[34]: their results

Model results for elevated point source plumes, for both stable and unstable conditions, have been presented in Reference 6. That report also contains model predictions of point source plume dispersion from different stack heights for unstable conditions which show the dependence (close to a -2 power law) of maximum ground concentration on effective stack height.

VII. COMPARISON WITH TURBULENCE MODELS OF PSU AND FRI

The Environmental Protection Agency is currently funding two other research groups on complementary turbulence modeling studies. The general nature of second-order closure and an attempt to develop a completely rational model are being pursued by a group at The Pennsylvania State University under the direction of John Lumley. Calculations which will hopefully provide validation information for closure models are being attempted by Flow Research Inc. under the direction of Steven Orszag. The purpose of this chapter is to show the interrelationship between these efforts and that at A.R.A.P. and to provide some comparison calculations.

As outlined in Reference 14, Lumley and his colleagues are attempting to develop models for second-order closure as rigorously as possible. The inherent generality of this approach leads to a large number of coefficients which must be determined. In fact, as Lumley states in Reference 36, a "dizzying array" of possible terms appears. In contrast, our approach has been to use a relatively simple closure model and only add complexity as comparisons between model predictions and experimental data prove it desirable to do so. As a result, the PSU approach and the A.R.A.P. approach are quite complementary. PSU has explored a greater variety of closure assumptions, while A.R.A.P. has explored a wider variety of flows with our simple closure assumptions.

One flow which Lumley has calculated is that of a two-dimensional incompressible wake.[14] Comparison between his model prediction for the self-similar region of this flow and that predicted by the A.R.A.P. model is presented in Figure 4.3 of Part II, along with Townsend's[37] wake measurements. Both model predictions agree with the mean velocity measurements and predict a maximum shear stress approximately 20% less than Townsend's values. Both models also predict longitudinal turbulence intensity that is 20% to 30% higher than Townsend's values. However, Lumley's model, which contains many more terms and coefficients (some evaluated for this particular flow), does show marginally better agreement of the lateral and transverse velocity fluctuations with the observations of Townsend. It should also be noted that there

is some uncertainty in the data since Thomas[38] reports measurements of the longitudinal rms intensity which are about one-third higher than Townsend's reported values.

In Figure 1 of Appendix B we compare our predictions for the temperature fluctuations in this two-dimensional wake flow with the observations of LaRue and Libby.[26] The agreement is very good. This is a calculation Lumley and his colleagues indicate they expect to make in the future.

Although we do expect that Lumley's approach will eventually lead to model terms that will be an improvement over our current simple model, particularly for the pressure-strain correlation, the preceding comparisons indicate that at present his complex model has no significant advantage over ours.

Second-order closure modeling requires reliable empirical information for the numerical evaluation of the modeled terms. As may be noted by the many discrepancies between data observed by different investigators, good reliable data are extremely difficult to obtain. An alternative to physical experiments is numerical experiments. Exact numerical calculations of the Navier-Stokes equations at realistic Reynolds numbers for atmospheric flows are beyond the state of the art of computer technology for the foreseeable future.[39] However, since turbulence in high Reynolds number flow tends to become independent of Reynolds number, it does appear possible to make detailed computations at relatively moderate Reynolds numbers to simulate atmospheric flow and diffusion. Such computations are being attempted at Flow Research Inc.

In consultation with Dr. Arthur Bass of FRI, we defined a problem for mutual computations and comparison between A.R.A.P. and FRI. The problem agreed upon is that of the turbulent field and pollutant dispersal in a simulated, neutral atmospheric shear layer above the influence of the ground. We specified the shear layer to be 200 m thick with $\Delta U = 4$ m/sec and centered at 0.5 km when the wind is 8 m/sec. A point source of pollutant was to be released into the turbulence field generated by this shear layer. Such a neutral shear layer will, of course, spread in time, but for purposes of this comparison calculation, we have chosen to hold the velocity field as frozen at the equilibrium turbulent conditions occurring for this ΔU and Δz while the diffusion calculation is made.

Figures 25 and 26 show the A.R.A.P. predictions for the mean velocity distribution and the mean values of the second-order velocity correlations. To date, no results have been received from FRI for comparison. We have included laboratory shear layer data as reported by Wygnanski and Fiedler[40] although

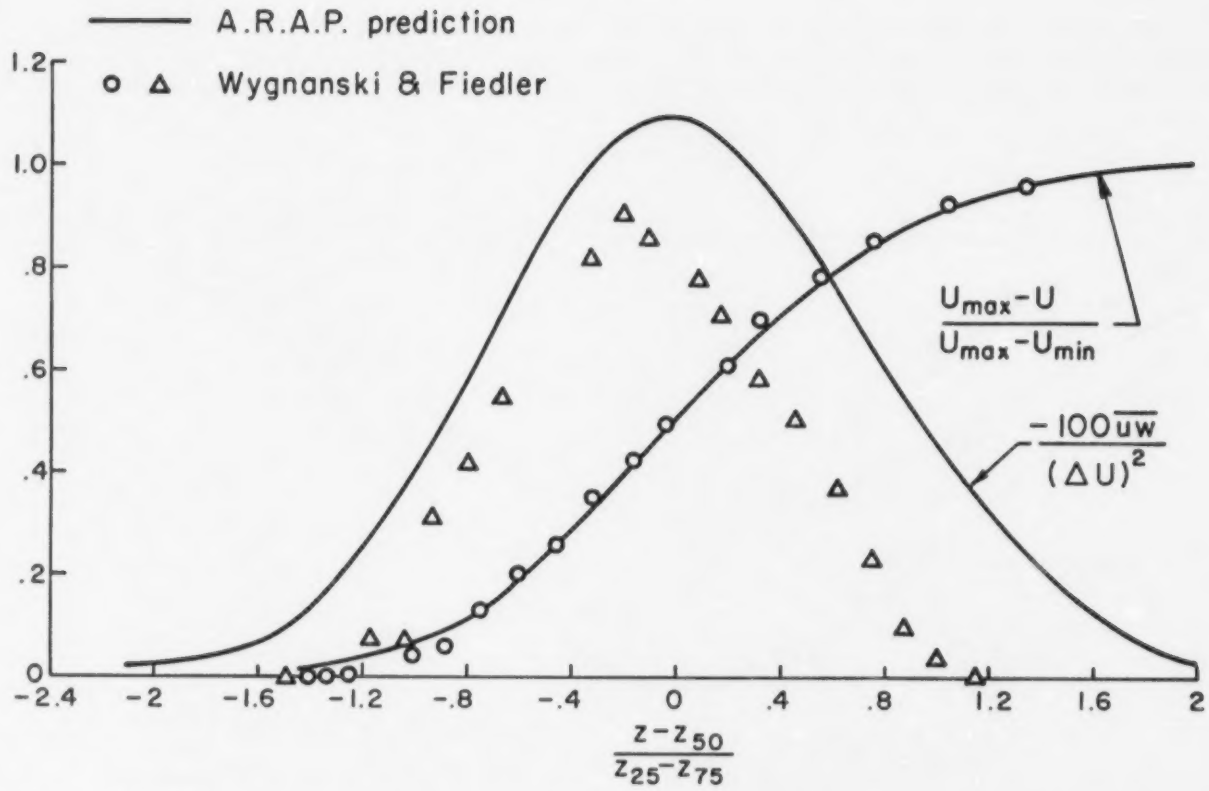

Figure 25. Predictions for the mean velocity and shear stress distribution in an equilibrium, self-similar, neutral shear layer; data as observed by Wygnanski and Fiedler[40]

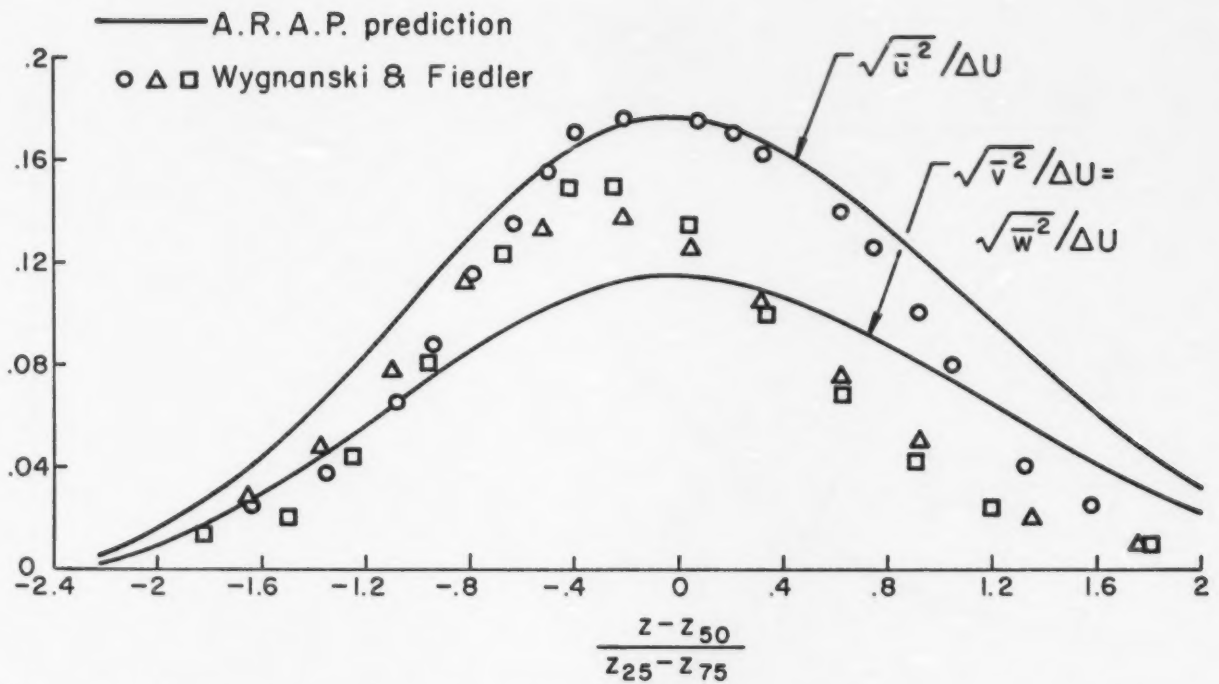

Figure 26. Predictions for the distributions of the second-order correlations of the normal velocity fluctuations in an equilibrium, self-similar, neutral shear layer; data as observed by Wygnanski and Fiedler[40]

there is considerable uncertainty surrounding the data as reported in Reference 41.

Two computations of the average distributions of the diffusing species were made for values of $d = 1$ and $d = 10^3$. Since d represents a model coefficient which should be determined empirically, good numerical results by FRI would provide us with the opportunity for fixing this coefficient. Figure 27 shows a plot of maximum species concentration downwind of the source for the two different values of d. The vertical and horizontal dispersion of the species are shown in Figure 28. For ease of computation, we started with an initial Gaussian distribution with $\sigma = 10$ m at $x = 0$. At this time, it is unclear as to what the quality of the FRI diffusion computations will be. High quality results would permit us to select a more definitive value of d than the value of 1 used throughout most of this report. Otherwise, we must await high quality experimental results before completing this refinement.

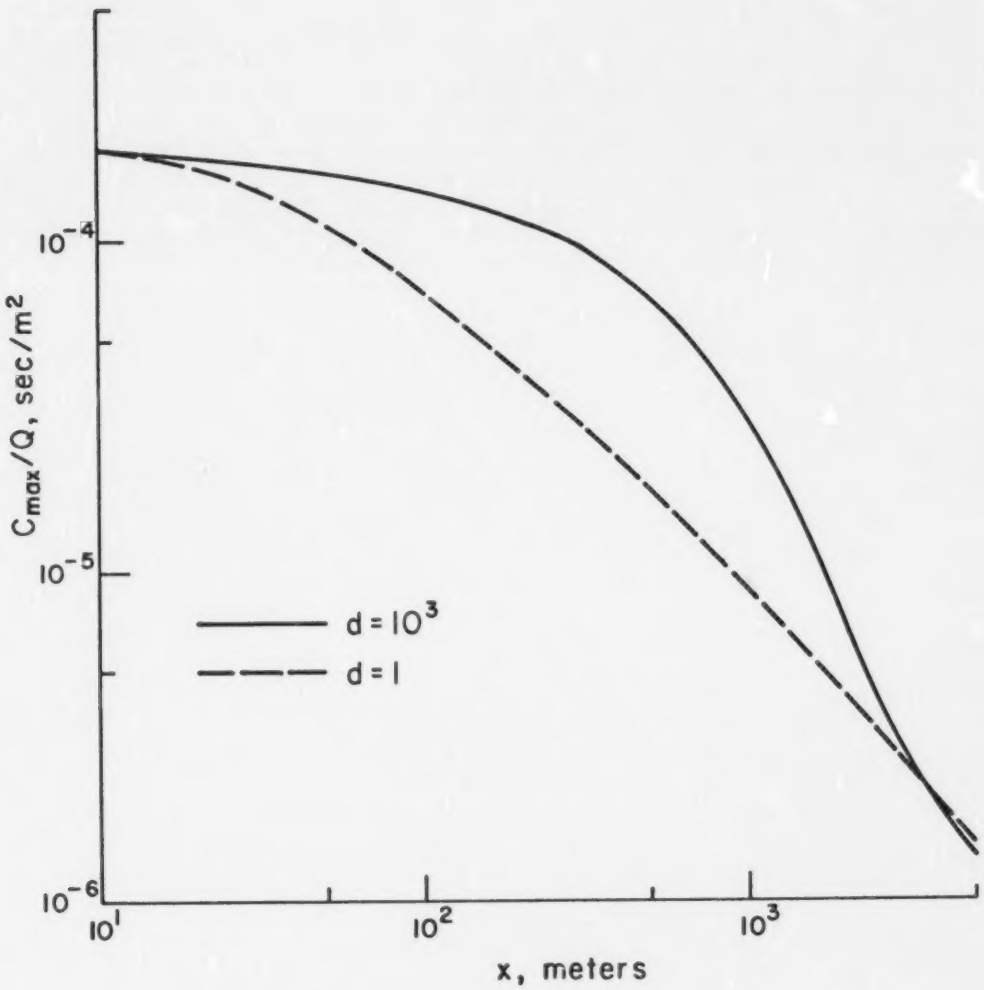

Figure 27. Maximum species concentration downwind of a point source released at the center of a 200-m thick shear layer with the wind going from 6 m/sec at .4 km to 10 m/sec at .6 km

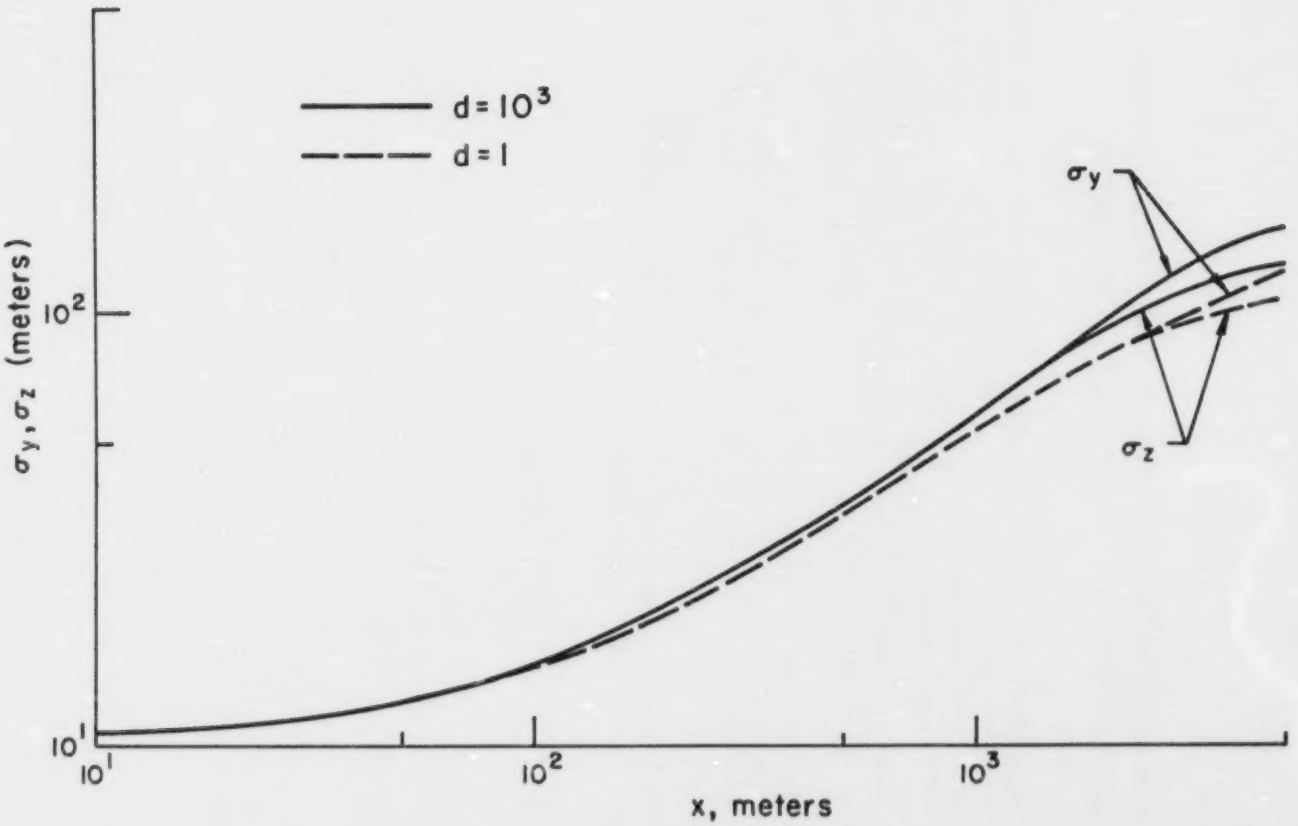

Figure 28. Vertical and horizontal dispersion as a function of distance downwind for the same plume as Figure 27

VIII. COMMENTS ON "SOME VIEWS OF MODELING DISPERSION AND VERTICAL FLUX" BY PASQUILL AND SMITH

In a note published in Reference 22, Pasquill and Smith raised objections to the use of second-order conservation equations in turbulent modeling. They expressed belief that closure assumptions would have to be valid to an unobtainably high accuracy. After an exchange of letters, this objection has been partially retracted in Pasquill's latest report,[42] but he still expresses some reservations about the approach.

Their objection is based on the observation that for some flows, particularly ground-level evaporation during a typical diurnal cycle, the time rate of change of species turbulent flux will be much smaller than the flux production term; i.e., in Eq. (2), the terms on the left-hand side may be orders of magnitude smaller than the largest terms on the right. Pasquill[42] gives an estimate of

$$\frac{\partial \overline{wc}}{\partial t} \Big/ \overline{ww}\,\frac{\partial C}{\partial z} \approx 10^{-4} \qquad (20)$$

at 10 m altitude for the time between sunrise and noon with $\overline{ww} \approx 2$ m/sec. Based on this, their original argument was that the modeled terms which provide the balance on the right-hand side of Eq. (2) must therefore be modeled to an accuracy of 1 part in 10^4. In the latest report, Pasquill[42] does admit that when the flux equation is modeled in the form given in Eq. (2), the explicit dependence of the modeled terms on $\overline{wc}$ provides stability to the equation so that $\overline{wc}$ can be evaluated even in the stationary case.

However, Pasquill still raises the question of whether adequate "settling down" time will be possible to obtain an adequately accurate value of $\overline{wc}$ in typical cases. He proceeds to consider a spatially varying case where Λ/q is order 1 minute, while the ratio of the characteristic dimension of an area source to the streaming velocity may be less than an hour, and suggests that in such a case the accuracy required in the modeling may be difficult to obtain due to inadequate "settling time." A check on the ratio of the

left-hand side of Eq. (2) to the last term in Eq. (2) shows that when this ratio R ceases to be much less than 1 is exactly when a dynamic equation for $\overline{wc}$ is required.

$$R = u \frac{\partial \overline{wc}}{\partial x} \Big/ Aq \frac{\overline{wc}}{\Lambda} \sim \frac{\Lambda}{Aq} \frac{u}{x} \qquad (21)$$

That is, whenever the characteristic time scale of the turbulent mixing becomes significant in comparison with a typical transit time over an area source of pollution, then an equilibrium balance of the terms on the right-hand side of Eq. (2) is not adequate, and the dynamic balance including the left-hand side must be used to obtain a valid estimate of $\overline{wc}$.

By his estimates of the two different conditions, Pasquill has shown that a reliable diffusion model must be able to compute $\overline{wc}$ accurately whether the time rate of change of $\overline{wc}$ (or the spatial convection of $\overline{wc}$) is significant or not. We believe Eq. (2) has this capability. Whenever $R \ll 1$, then a computation using Eq. (2) will rapidly approach an equilibrium between the terms on the right-hand side and yield an appropriate estimate of $\overline{wc}$ even if the initial value of $\overline{wc}$ used for the computation was grossly in error. On the other hand, when $R \not\ll 1$, the dynamic balance shows the influence of the initial conditions of $\overline{wc}$ must be retained, and a simple equilibrium balance between the right-hand side terms would lead to errors. Stated another way, when $R \ll 1$, superequilibrium diffusion theory which reduces to a type of K theory[3] should be approximately valid, but when R is not much less than 1, such theories are not valid. Although $R \ll 1$ typically in the homogeneous atmospheric surface layer, this is not the case in spatially inhomogeneous cases and will not always be the case at altitude in the typical homogeneous diurnal boundary layer.

IX. REFERENCES

1. Donaldson, C.duP., R.D. Sullivan, and H. Rosenbaum. "A Theoretical Study of the Generation of Atmospheric Clear Air Turbulence." AIAA Journal. 10:162-170, February 1972.

2. Donaldson, C.duP. "Calculation of Turbulent Shear Flows for Atmospheric and Vortex Motions." AIAA Journal. 10:4-12, January 1972.

3. Donaldson, C.duP. "Atmospheric Turbulence and the Dispersal of Atmospheric Pollutants." In: *AMS Workshop on Micrometeorology*, Haugen, D.A. (ed.). Boston, Science Press, 1973. pp. 313-390.

4. Lewellen, W.S., M.E. Teske, and C.duP. Donaldson. "Application of Turbulent Model Equations to Axisymmetric Wakes." AIAA Journal. 12:620-625, May 1974.

5. Lewellen, W.S. and M.E. Teske. "Prediction of the Monin-Obukhov Similarity Functions from an Invariant Model of Turbulence." J. Atmos. Sciences. 30:1340-1345, 1973.

6. Lewellen, W.S., M.E. Teske, R.M. Contiliano, G.R.Hilst, and C.duP. Donaldson. "Invariant Modeling of Turbulent Diffusion in the Planetary Boundary Layer." Aeronautical Research Associates of Princeton, Inc. Report No. EPA-650/4-74-035. Environmental Protection Agency, Raleigh, NC. September 1974.

7. Donaldson, C.duP. "The Relationship Between Eddy Transport and Second-Order Closure Models for Stratified Media and for Vortices." In: *Free Turbulent Shear Flows*. NASA SP-321, Volume 1, 1973. pp. 233-255.

8. Varma, A.K., R.A. Beddini, R.D. Sullivan, and C.duP. Donaldson. "Application of an Invariant Second-Order Closure Model to Compressible Turbulent Shear Layers." (Presented at AIAA 7th Fluid and Plasma Dynamics Conference, Palo Alto, June 17-19, 1974.) AIAA Paper No. 74-592.

9. Sullivan, R.D. "A Program to Compute the Behavior of a Three-Dimensional Turbulent Vortex." Aeronautical Research Associates of Princeton, Inc. Report No. ARL-

TR-74-0009. Aerospace Research Labs., Wright-Patterson AFB, Ohio. 1973.

10. Harlow, F.H. (ed.). "Turbulence Transport Modeling." AIAA Selected Reprint Series, Volume XIV, 1973.

11. Launder, B.E. and D.B. Spalding. *Mathematical Models of Turbulence*. New York, Academic Press, 1972.

12. Mellor, G.L. "Analytic Prediction of the Properties of Stratified Planetary Surface Layers." J. Atmos. Sciences. 30:1061-1069. 1973.

13. Launder, B.E. "On the Effects of a Gravitational Field on the Turbulent Transport of Heat and Momentum." J. Fluid Mechanics. 67 (Part 3):569-581, 1975.

14. Lumley, J.L. and B. Khajeh-Nouri. "Computational Modeling of Turbulent Transport." *Advances in Geophysics*, Volume 18A. New York, Academic Press, 1974.

15. Zeman, D. and H. Tennekes. "A Self-Contained Model for the Pressure Terms in the Turbulent Stress Equations of the Atmospheric Boundary Layer." J. Atmos. Sciences. 32:1808-1813, 1975.

16. Shir, C.C. "A Preliminary Numerical Study of Atmospheric Turbulent Flows in the Idealized Planetary Boundary Layer." J. Atmos. Sciences. 30:1327-1339. 1973.

17. Mellor G.L. and T. Yamada. "A Hierarchy of Turbulence Closure Models for Planetary Boundary Layers." J. Atmos. Sciences. 31:1791-1806. 1974.

18. Wyngaard, J.C., O.R. Coté, and K.S. Rao. "Modeling the Atmospheric Boundary Layer." *Advances in Geophysics*, Volume 18A. New York, Academic Press, 1974.

19. Wyngaard, J.C. and O.R. Coté. "The Evolution of a Convective Planetary Boundary Layer - A Higher-Order Closure Model Study." Boundary Layer Meteorology. 7:289. 1974.

20. Lewellen, W.S., M.E. Teske, and C.duP. Donaldson. "Second-Order Turbulent Modeling Applied to Momentumless Wakes in Stratified Fluids." Aeronautical Research Associates of Princeton, Inc. Report No. 206. 1973.

21. Lewellen, W.S., M.E. Teske, and C.duP. Donaldson. "Turbulent Wakes in a Stratified Fluid." Aeronautical Research Associates of Princeton, Inc. Report No. 226. 1974.

22. Pasquill, F. and F.B. Smith. "Some Views on Modeling Dispersion and Vertical Flux." In: *Proceedings of the 5th Meeting of the Expert Panel on Air Pollution Modeling*. Roskilde, Denmark, Danish Atomic Energy Commission, 1974.

23. Roache, P.J. *Computational Fluid Dynamics.* Albuquerque, Hermosa Publishers, 1972. pp. 91-95.

24. Lewellen, W.S., M.E. Teske, and C.duP. Donaldson. "Variable Density Flows Computed by a Second-Order Closure Description of Turbulence." AIAA Journal (to be published).

25. Freymuth, P. and M.S. Uberoi. "Structure of Temperature Fluctuations in the Turbulent Wake Behind a Heated Cylinder." Physics of Fluids. 14:2574-2580, December 1971.

26. LaRue, J.C. and P.A. Libby. "Temperature Fluctuations in the Plane Turbulent Wake." Physics of Fluids. 17:1956-1975, November 1974.

27. Willis, G.E. and J.W. Deardorff. "A Laboratory Model of the Unstable Planetary Boundary Layer." J. Atmos. Sciences. 31:1297-1307, 1974.

28. Deardorff, J.W. and G.E. Willis. "Physical Modeling of Diffusion in the Mixed Layer." In: *Proceedings of a Symposium on Atmospheric Diffusion and Air Pollution.* Santa Barbara, American Meteorological Society, September 1974. pp. 387-391.

29. Turner, D.B. "Workshop on Atmospheric Dispersion Estimates." Office of Air Programs, Environmental Protection Agency, Publication No. AP-26 (5th printing), 1972.

30. Pasquill, F. *Atmospheric Diffusion.* 2nd edition. New York, John Wiley & Sons, Inc., 1974.

31. Lewellen, W.S., M.E. Teske, and C.duP. Donaldson. "Turbulence Model of Diurnal Variations in the Planetary Boundary Layer." In: *Proceedings of the 1974 Heat Transfer and Fluid Mechanics Institute,* Davis, L.R. and R.E. Wilson (eds.). Stanford, Stanford University Press, 1974. pp. 301-319.

32. Panofsky, H.A. "The Atmospheric Boundary Layer Below 150 Meters." In: *Annual Review of Fluid Mechanics.* Palo Alto, Annual Reviews, Inc., 1974. pp. 147-177.

33. Naot, D., A. Shavit, and M. Wolfshtein. "Two-Point Correlation Model and the Redistribution of Reynolds Stress." Physics of Fluids. 16:738. June 1973.

34. Lamb, R.G., W.H. Chen, and J.H. Seinfeld. "Numerico-Empirical Analyses of Atmospheric Diffusion Theories." In: *Proceedings of a Symposium on Atmospheric Diffusion and Air Pollution.* Santa Barbara, American Meteorological Society, September 1974. pp. 317-324.

35. Deardorff, J.W. "Numerical Investigation of Neutral and Unstable Planetary Boundary Layers." J. Atmos. Sciences. 29:91-115, 1972.

36. Lumley. J.L. "Prediction Methods for Turbulent Flows." The Pennsylvania State University. In a lecture series presented at Von Karman Institute, Rhode-St.-Genese, Belgium, March 3-7, 1975.

37. Townsend, A.A. *The Structure of Turbulent Shear Flow.* Cambridge, Cambridge University Press, 1956,

38. Thomas, R.M. "Conditional Sampling and Other Measurements in a Plane Turbulent Wake." J. Fluid Mechanics. 57 (Part 3):549-582, 1973.

39. Orszag, S.A. "Numerical Simulation of Turbulent Flows." Massachusetts Institute of Technology. Presented at University of Tennessee Space Institute Short Course on Fundamentals and Applications of Turbulence, April 1975.

40. Wygnanski, I. and H. Fiedler. "The Two-Dimensional Mixing Region." J. Fluid Mechanics. 41 (Part 1):327-361, 1970.

41. Birch, S.F. and J.M. Eggers. "A Critical Review of the Experimental Data for Developed Free Turbulent Shear Layers." In: *Free Turbulent Shear Flows*, Volume I. NASA SP-321, 1973 (also see Volume II).

42. Pasquill, F. "Some Topics Relating to Modeling of Dispersion in Boundary Layers." Report No. EPA-650/4-75-015. Environmental Protection Agency, Raleigh, N.C. April 1975.

NOMENCLATURE

A, a, b	model constants
C	mean species concentration
c	species concentration fluctuations about the mean
D	laminar diffusion coefficient
d	model constant relating plume spread to plume turbulent scale, see Eq. (15)
f	Coriolis parameter = $2\Omega \sin \phi$
g	gravitational acceleration
k	von Karman's constant = $-u^*/(z\ \partial u/\partial z)_o$ in the neutral surface layer
L	Monin-Obukhov length = $-\theta_o u^{*3}/kg(\overline{w\theta})_o$
n	decay rate for grid turbulence
P	mean pressure (also Pasquill's stability parameter)
p	pressure fluctuation
q	square root of twice the turbulent kinetic energy
Q	source strength
Ri	Richardson number
$\hat{Ri}$	characteristic Richardson number defined in Eq. (12)
Ro	Rossby number based on geostrophic conditions = U_g/fz_o
$\hat{Ro}$	characteristic Rossby number = $\hat{u}/fz_o$
s	model constant
s_0, s_1, s_2	constants in scale equation
t	time
t_c	Brunt-Väisälä period
U_i	mean fluid velocity in the ith direction
U_g	geostrophic wind velocity
u_i	fluctuating fluid velocity in the ith direction
u^*	surface shear stress velocity

$\hat{u}$	characteristic surface velocity equal to 0.1 times the wind velocity at 10 meters
v_c	model turbulent diffusion coefficient
W	mean vertical velocity
w	fluctuating vertical velocity
w*	free convective velocity scale = $[gz_i(\overline{w\theta})_o/\theta_o]^{1/3}$
x_i, x_j, x_k	Cartesian coordinates
z	vertical coordinate
z_i	temperature inversion height above an unstable layer
z_o	surface roughness height
z_{50}	distance to 1/2 the centerline value
z_r	plume release height
ε	dissipation function
θ	mean potential temperature
θ	fluctuating potential temperature
Λ	model macroscale length
λ	model microscale length = $\Lambda/[a + bq\Lambda/\nu]^{1/2}$
ν	kinematic viscosity
ρ	density
ϕ	latitude
Ω_i	angular velocity of the coordinate system
σ	plume spread

Superscript:

$\overline{\quad}$	denotes ensemble average

Subscript:

o	denotes surface value
g	denotes geostrophic condition
p	denotes plume value
t	denotes ambient turbulence value

APPENDIX A

SUMMARY OF ONE-DIMENSIONAL UNSTEADY EQUATIONS AND BOUNDARY CONDITIONS FOR DIFFUSION IN THE PLANETARY BOUNDARY LAYER

As a convenience to the reader, the equations solved for the mean flow variables and turbulence field are summarized here for the one-dimensional unsteady case. The mean flow equations are:

$$\frac{DU}{Dt} = f(V - V_g) + \nu_o \frac{\partial^2 U}{\partial z^2} - \frac{\partial}{\partial z} \overline{uw} \tag{A.1}$$

$$\frac{DV}{Dt} = -f(U - U_g) + \nu_o \frac{\partial^2 V}{\partial z^2} - \frac{\partial}{\partial z} \overline{vw} \tag{A.2}$$

$$\frac{D\theta}{Dt} = \nu_o \frac{\partial^2 \theta}{\partial z^2} - \frac{\partial}{\partial z} \overline{w\theta} \tag{A.3}$$

To these are added the equations for the six independent Reynolds stresses:

$$\frac{D\overline{uu}}{Dt} = 4\Omega(\overline{uv} \sin \phi - \overline{uw} \cos \phi) - 2\overline{uw} \frac{\partial U}{\partial z} + \nu_c \frac{\partial}{\partial z}\left[\Lambda q \frac{\partial \overline{uu}}{\partial z}\right]$$

$$- \frac{q}{\Lambda}\left(\overline{uu} - \frac{q^2}{3}\right) + \nu_o \frac{\partial^2}{\partial z^2} \overline{uu}$$

$$- \frac{2\nu_o}{3\lambda^2} q^2 \tag{A.4}$$

$$\frac{D\overline{vv}}{Dt} = -4\Omega\overline{uv}\sin\phi - 2\overline{vw}\frac{\partial V}{\partial z} + v_c\frac{\partial}{\partial z}\left[\Lambda q\frac{\partial\overline{vv}}{\partial z}\right] - \frac{q}{\Lambda}\left(\overline{vv} - \frac{q^2}{3}\right) + \nu_o\frac{\partial^2}{\partial z^2}\overline{vv} - \frac{2\nu_o}{3\lambda^2}q^2 \qquad (A.5)$$

$$\frac{D\overline{ww}}{Dt} = 4\Omega\overline{uw}\cos\phi + \frac{2g}{\theta_o}\overline{w\theta} + v_c\frac{\partial}{\partial z}\left[\Lambda q\frac{\partial\overline{ww}}{\partial z}\right] - \frac{q}{\Lambda}\left(\overline{ww} - \frac{q^2}{3}\right) + \nu_o\frac{\partial^2}{\partial z^2}\overline{ww} - \frac{2\nu_o}{3\lambda^2}q^2 \qquad (A.6)$$

$$\frac{D\overline{uv}}{Dt} = 2\Omega(\overline{vv}\sin\phi - \overline{vw}\cos\phi - \overline{uu}\sin\phi) - \overline{uw}\frac{\partial V}{\partial z} - \overline{vw}\frac{\partial U}{\partial z} + v_c\frac{\partial}{\partial z}\left[\Lambda q\frac{\partial\overline{uv}}{\partial z}\right] - \frac{q}{\Lambda}\overline{uv} + \nu_o\frac{\partial^2}{\partial z^2}\overline{uv} \qquad (A.7)$$

$$\frac{D\overline{uw}}{Dt} = 2\Omega(\overline{vw}\sin\phi - \overline{ww}\cos\phi + \overline{uu}\cos\phi) - \overline{ww}\frac{\partial U}{\partial z} + \frac{g}{\theta_o}\overline{u\theta} + v_c\frac{\partial}{\partial z}\left[\Lambda q\frac{\partial\overline{uw}}{\partial z}\right] - \frac{q}{\Lambda}\overline{uw} + \nu_o\frac{\partial^2}{\partial z^2}\overline{uw} \qquad (A.8)$$

$$\frac{D\overline{vw}}{Dt} = 2\Omega(-\overline{uw}\sin\phi + \overline{uv}\cos\phi) - \overline{ww}\frac{\partial V}{\partial z} + \frac{g}{\theta_o}\overline{v\theta}$$

$$+ \nu_c \frac{\partial}{\partial z}\left[\Lambda q \frac{\partial \overline{vw}}{\partial z}\right] - \frac{q}{\Lambda}\overline{vw}$$

$$+ \nu_o \frac{\partial^2}{\partial z^2}\overline{vw} \qquad (A.9)$$

the equations for the three components of the heat flux vector:

$$\frac{D\overline{u\theta}}{Dt} = 2\Omega(\overline{v\theta}\sin\phi - \overline{w\theta}\cos\phi) - \overline{uw}\frac{\partial\Theta}{\partial z} - \overline{w\theta}\frac{\partial U}{\partial z}$$

$$+ \nu_c \frac{\partial}{\partial z}\left[\Lambda q \frac{\partial \overline{u\theta}}{\partial z}\right] - \frac{Aq}{\Lambda}\overline{u\theta} + \nu_o \frac{\partial^2}{\partial z^2}\overline{u\theta} \qquad (A.10)$$

$$\frac{D\overline{v\theta}}{Dt} = -2\Omega\overline{u\theta}\sin\phi - \overline{vw}\frac{\partial\Theta}{\partial z} - \overline{w\theta}\frac{\partial V}{\partial z} + \nu_c \frac{\partial}{\partial z}\left[\Lambda q \frac{\partial \overline{v\theta}}{\partial z}\right]$$

$$- \frac{Aq}{\Lambda}\overline{v\theta} + \nu_o \frac{\partial^2}{\partial z^2}\overline{v\theta} \qquad (A.11)$$

$$\frac{D\overline{w\theta}}{Dt} = 2\Omega\overline{u\theta}\cos\phi - \overline{ww}\frac{\partial\Theta}{\partial z} + \frac{g}{\theta_o}\overline{\theta^2} + \nu_c \frac{\partial}{\partial z}\left[\Lambda q \frac{\partial \overline{w\theta}}{\partial z}\right]$$

$$- \frac{Aq}{\Lambda}\overline{w\theta} + \nu_o \frac{\partial^2}{\partial z^2}\overline{w\theta} \qquad (A.12)$$

the equation for the temperature variance:

$$\frac{D\overline{\theta^2}}{Dt} = -2\overline{w\theta}\,\frac{\partial\Theta}{\partial z} + \nu_c\,\frac{\partial}{\partial z}\left[\Lambda q\,\frac{\partial\overline{\theta^2}}{\partial z_j}\right] + \nu_o\,\frac{\partial^2\overline{\theta^2}}{\partial z^2} - 2\nu_o s\,\frac{\overline{\theta^2}}{\lambda^2} \qquad \text{(A.13)}$$

and the equation for the turbulent macroscale:

$$\frac{D\Lambda}{Dt} = -s_1\,\frac{\Lambda}{q^2}\left(\overline{uw}\,\frac{\partial U}{\partial z} + \overline{vw}\,\frac{\partial V}{\partial z}\right) - s_2\,\frac{\nu_o\Lambda}{\lambda^2} + \nu_c\,\frac{\partial}{\partial z}\left(q\Lambda\,\frac{\partial\Lambda}{\partial z}\right)$$

$$- \frac{s_3}{q}\left(\frac{\partial q\Lambda}{\partial z}\right)^2 + \frac{s_4\Lambda}{q^2}\,\frac{g\overline{w\theta}}{\Theta_o} \qquad \text{(A.14)}$$

These fourteen equations are solved for the turbulence field and the results used as inputs into Eqs. (1) through (4) to solve for the species distribution.

The general boundary conditions applied to these equations at the top of the boundary layer are that as $z \to \infty$

$$\left.\begin{aligned} U &= U_g \\ V &= V_g \end{aligned}\right\} \text{ geostrophic wind}$$

$$\frac{\partial\theta}{\partial z} = \text{constant (difference between the adiabatic lapse rate and the ambient lapse rate)}$$

$$\overline{u_i u_j} = \overline{u_i\theta} = \overline{\theta\theta} = 0$$

Rather than compute all the way to the surface with these equations, which would, in general, require computing the flow around various roughness elements, the surface boundary conditions are applied at z_o, the effective aerodynamic roughness height. At $z = z_o$

$$U = V = 0$$

$$\Theta = \Theta_{surface} \quad (\text{or } \overline{w\theta} = \overline{w\theta}_{surface})$$

$$\frac{\partial \overline{u_i u_j}}{\partial z} = \frac{\partial \overline{u_i \theta}}{\partial z} = \frac{\partial \overline{\theta\theta}}{\partial z} = 0$$

The flow is now completely specified when initial conditions on all the variables are specified. The dimensionless parameters governing the flow may be obtained by normalizing the equations and boundary conditions. For a characteristic velocity, let us choose U_g, with the coordinate system aligned so that $V_g = 0$. Then, if we normalize all lengths by z_o and time by f^{-1}, Eqs. (A.1) and (A.2) introduce two parameters: a Reynolds number $U_g z_o/\nu$ and a Rossby number $U_g/z_o f$. For the high Reynolds numbers applicable for atmospheric flows, the Reynolds number dependence can usually be ignored. When the flow is neutral (i.e., θ = constant everywhere), then the only other parameter introduced by the remaining equations or the boundary conditions is cot ϕ.

If temperature is normalized by $\Delta\theta$, not yet specified, then the equations introduce one more parameter: a bulk Richardson number, $Ri_b = g\Delta\theta z_o/\theta_o U_g^2$. For stable conditions, $\Delta\theta$ may be taken as the temperature difference across the boundary layer, while for unstable conditions, it would appear reasonable to take it as the height of the inversion layer times $(\partial\theta/\partial z)_\infty$. However, there is a rather strong dependence on initial conditions involved when the influence of stability is introduced. In fact, our previous work[6] shows that for typical daily variations in the planetary boundary layer, a hysteresis-type pattern is followed for the turbulence field. In spite of this complication, in Section VI we have considered the quasi-steady conditions which will exist after conditions of roughly the same stability have been maintained for some time. Under stable conditions, such a quasi-steady turbulence field may be characterized by a single stability parameter. In Section VI, we choose a bulk Richardson number based on the temperature and velocity differences between the surface and 10 meters. However, unstable conditions appear to require two stability parameters even under quasi-steady conditions. To the bulk Richardson number, we add the ratio of the inversion height, z_i, to $\hat{u}/f$. For this purpose, z_i is defined as the altitude near the top of the boundary where the temperature variance reaches a local maximum (see Fig. B.5).

APPENDIX B

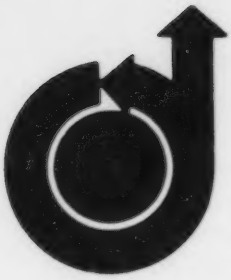

AIAA PAPER No. 75-871

EXAMPLES OF VARIABLE DENSITY FLOWS COMPUTED BY A SECOND-ORDER CLOSURE DESCRIPTION OF TURBULENCE

by
W. S. LEWELLEN, M. E. TESKE,
and
COLEMAN duP. DONALDSON
Aeronautical Research Associates of Princeton, Inc.
Princeton, New Jersey

AIAA 8th Fluid and Plasma Dynamics Conference

HARTFORD, CONNECTICUT/JUNE 16-18, 1975

For permission to copy or republish, contact the American Institute of Aeronautics and Astronautics, 1290 Avenue of the Americas, New York, N.Y. 10019.

EXAMPLES OF VARIABLE DENSITY FLOWS COMPUTED BY A SECOND-ORDER CLOSURE DESCRIPTION OF TURBULENCE*

W. S. Lewellen,** M. E. Teske,† and Coleman duP. Donaldson††
Aeronautical Research Associates of Princeton, Inc.
Princeton, New Jersey

Abstract

An incompressible fluid, with the influence of the variable density coming through a Boussinesq buoyancy term, is considered using a second-order closure approach to turbulent flow. This technique successfully incorporates the strong influence of stratification for a number of flows. Particular flows which are computed and compared with experimental data are: a) stratified shear flow with homogeneous turbulence; b) free convection bounded by a stable density gradient; c) wakes in a medium with a stable density gradient; and d) the atmospheric boundary layer where the flow oscillates from stable to unstable conditions in a typical day.

Nomenclature

F_D	wake Froude number based on diameter
g_i	general acceleration vector
k	coefficient of laminar diffusion for temperature perturbation
p	pressure fluctuation
P	mean pressure
Pr_t	turbulent Prandtl number
q	square root of twice the turbulent kinetic energy
Ri	Richardson number
t	time
t_c	Brunt-Väisälä period; defined in (12)
u^*	surface shear velocity
u_i	fluctuating velocity
U_i	mean velocity
w^*	free convection velocity scale; defined in (11)
x_i	direction
z_i	temperature inversion height above an unstable layer
z_{50}	distance to one-half the centerline velocity value
ϵ	energy dissipation
θ	fluctuating temperature
θ	mean temperature
κ	von Kármán constant
A	macroscale length
ν	coefficient of viscosity
ρ	density
Ω_j	angular velocity of the coordinate system
superscript —	denotes time average
subscript a	denotes ambient value

1. Introduction

Small changes in density are sufficient to have a strong effect on turbulent flows in the presence of a gravitational acceleration. Such flows are extremely difficult to predict with eddy viscosity approaches. This paper describes a second-order closure approach to turbulent flow which has been found to successfully incorporate the influence of stratification for a number of different flows. Our approach is to use the Reynolds stress equations to compute the turbulent fluctuations with invariant modeling techniques applied to close the system of equations. Details of this approach have been given by Donaldson.[1,2] The basic assumption is that the dependence of third-order correlations of the velocity fluctuations on the second-order correlations, the mean flow properties, and their derivatives is invariant with respect to changes in flow geometry. This permits data from relatively simple flow experiments to be used in evaluating the necessary coefficients in the modeled terms.

Similar approaches to stratified flows have been taken by Mellor,[3] Daly and Harlow,[4] Wyngaard et al.,[5] and Launder.[6] However, the particular model representations of the terms required for closure of the Reynolds stress transport equations are somewhat different in each case. Limited comparisons between models have been made by Meroney.[7] This paper will not give comparisons between various models but will

*This research has been partially funded with Federal funds from the Environmental Protection Agency under contract number EPA 68-02-1310 and the Defense Advanced Research Projects Agency of the Department of Defense as monitored by ONR under contract number N00014-72-C-0413. The content of this paper does not necessarily reflect the views or policies of any agency of the U.S. Government.
**Senior Consultant; Member, AIAA
† Associate Consultant
††President and Senior Consultant; Associate Fellow, AIAA

Copyright © American Institute of Aeronautics and Astronautics, Inc., 1975. All rights reserved.

National Technical Information Service is authorized to reproduce and sell this report.

be restricted to a brief description of a model and its application to a number of different flows involving buoyancy.

2. Model Equations

When the flow variables are decomposed into mean and fluctuating quantities, the mean flow equations may be written as

$$\frac{\partial U_i}{\partial t} + U_j \frac{\partial U_i}{\partial x_j} = - \frac{\partial \overline{u_i u_j}}{\partial x_j} + \frac{\partial}{\partial x_j}\left(\nu \frac{\partial U_i}{\partial x_j}\right) - \frac{1}{\rho}\frac{\partial P}{\partial x_i} + \frac{g_i(\theta - \theta_a)}{\theta} - 2\epsilon_{ijk}\Omega_j U_k \qquad (1)$$

$$\frac{\partial U_i}{\partial x_i} = 0 \qquad (2)$$

$$\frac{\partial \theta}{\partial t} + U_j \frac{\partial \theta}{\partial x_j} = - \frac{\partial \overline{u_i \theta}}{\partial x_i} + \frac{\partial}{\partial x_i}\left(k \frac{\partial \theta}{\partial x_i}\right) \qquad (3)$$

The flow has been assumed incompressible but with small variations in density due to changes in temperature. With the Boussinesq approximation, the effect of the density variation enters only in the gravitational body force term in the momentum equation, Eq. (1). The last term in (1) is due to coriolis forces present in a coordinate system rotating with angular velocity Ω. It is included here in anticipation of atmospheric applications. Equation (3) is a diffusion equation for the temperature perturbation.

This system of equations is not complete due to the presence of the Reynolds stress terms. Exact equations for these correlations may be derived as outlined by Donaldson.[7]

$$\frac{\partial \overline{u_i u_j}}{\partial t} + U_k \frac{\partial \overline{u_i u_j}}{\partial x_k} = - \overline{u_i u_k}\frac{\partial U_j}{\partial x_k} - \overline{u_j u_k}\frac{\partial U_i}{\partial x_k} + \frac{g_i \overline{u_j \theta}}{\theta} + \frac{g_j \overline{u_i \theta}}{\theta} - 2\epsilon_{ik\ell}\Omega_k \overline{u_\ell u_j} - 2\epsilon_{jk\ell}\Omega_\ell \overline{u_k u_i} + \nu \frac{\partial^2 \overline{u_i u_j}}{\partial x_k^2} - \frac{\partial}{\partial x_k}(\overline{u_k u_i u_j}) - \overline{\frac{u_i}{\rho}\frac{\partial p}{\partial x_j}} - \overline{\frac{u_j}{\rho}\frac{\partial p}{\partial x_i}} - 2\nu \overline{\frac{\partial u_i}{\partial x_k}\frac{\partial u_j}{\partial x_k}} \qquad (4)$$

$$\frac{\partial \overline{u_i \theta}}{\partial t} + U_j \frac{\partial \overline{u_i \theta}}{\partial x_j} = - \overline{u_i u_j}\frac{\partial \theta}{\partial x_j} - \overline{u_j \theta}\frac{\partial U_i}{\partial x_j} + \frac{g_i \overline{\theta^2}}{\theta} - 2\epsilon_{ijk}\Omega_j \overline{u_k \theta} - \frac{\partial \overline{u_i u_j \theta}}{\partial x_j} - \overline{\frac{\theta}{\rho}\frac{\partial p}{\partial x_i}} + \nu \overline{\theta \frac{\partial^2 u_i}{\partial x_j^2}} - k \overline{u_i \frac{\partial^2 \theta}{\partial x_j^2}} \qquad (5)$$

$$\frac{\partial \overline{\theta^2}}{\partial t} + U_j \frac{\partial \overline{\theta^2}}{\partial x_j} = - 2\overline{u_j \theta}\frac{\partial \theta}{\partial x_j} + k \frac{\partial^2 \overline{\theta^2}}{\partial x_j^2} - \frac{\partial}{\partial x_j}\overline{u_j \theta^2} - 2k \overline{\frac{\partial \theta}{\partial x_j}\frac{\partial \theta}{\partial x_j}} \qquad (6)$$

Closure of the system of equations at this second-order level requires modeling the last four terms in Eqs. (4) and (5) and the last two terms in Eq. (6). The terms required for (4) have been previously discussed in Refs. 2 and 8. These remain unchanged for a variable density flow; the terms required for Eqs. (5) and (6) are modeled in a similar fashion. The two new coefficients introduced with these variable density terms were evaluated using data from the atmospheric surface layer.[9] With the introduction of the model terms and the numerical coefficients, Eqs. (4)-(6) are represented for high Reynolds number flow as

$$\frac{\partial \overline{u_i u_j}}{\partial t} + U_k \frac{\partial \overline{u_i u_j}}{\partial x_k} = - \overline{u_i u_k}\frac{\partial U_j}{\partial x_k} - \overline{u_j u_k}\frac{\partial U_i}{\partial x_k} + \frac{g_i \overline{u_j \theta}}{\theta} + \frac{g_j \overline{u_i \theta}}{\theta} - 2\epsilon_{ik\ell}\Omega_k \overline{u_\ell u_j} - 2\epsilon_{jk\ell}\Omega_\ell \overline{u_k u_i} + 0.3\frac{\partial}{\partial x_k}\left(q\Lambda \frac{\partial \overline{u_i u_j}}{\partial x_k}\right) - \frac{q}{\Lambda}\left(\overline{u_i u_j} - \delta_{ij}\frac{q^2}{3}\right) - \delta_{ij}\frac{q^3}{12\Lambda} \qquad (7)$$

$$\frac{\partial \overline{u_i \theta}}{\partial t} + U_j \frac{\partial \overline{u_i \theta}}{\partial x_j} = - \overline{u_i u_j}\frac{\partial \theta}{\partial x_j} - \overline{u_j \theta}\frac{\partial U_i}{x_j} + \frac{g_i \theta^2}{\theta} - 2\epsilon_{ijk}\Omega_j \overline{u_k \theta} + 0.3\frac{\partial}{\partial x_j}\left(q\Lambda \frac{\partial \overline{u_i \theta}}{\partial x_j}\right) - \frac{0.75q}{\Lambda}\overline{u_i \theta} \qquad (8)$$

$$\frac{\partial \overline{\theta^2}}{\partial t} + U_j \frac{\partial \overline{\theta^2}}{\partial x_j} = -2\overline{u_j \theta}\frac{\partial \theta}{\partial x_j} + 0.3\frac{\partial}{\partial x_j}\left(q\Lambda \frac{\partial \overline{\theta^2}}{\partial x_j}\right) - \frac{0.45q\overline{\theta^2}}{\Lambda} \qquad (9)$$

To complete closure, it is still necessary to determine the model turbulent scale Λ. It could be specified empirically based on gross features of the particular flow geometry.[2,8] Here it will be predicted from a semi-empirically modeled, dynamic

differential equation. As Bradshaw[10] and Mellor and Herring[11] have pointed out, the form of the A equation is similar, whether one begins with the two-point velocity correlation to define an integral scale, the dissipation function $\epsilon = q^3/8A$, or the vorticity fluctuations q/A. The principal difference is in the diffusion terms. The form of the A equation used here is

$$\frac{DA}{Dt} = 0.35 \frac{A}{q^2} \overline{u_i u_j} \frac{\partial U_i}{\partial x_j} + 0.075q + 0.3 \frac{\partial}{\partial x_i}\left(qA \frac{\partial A}{\partial x_i}\right) - \frac{0.375}{q}\left(\frac{\partial qA}{\partial x_i}\right)^2 + \frac{0.8A}{q^2} \frac{g_i \overline{u_i \theta}}{\theta} \qquad (10)$$

A detailed accounting of these coefficients may be found in Ref. 12. The coefficient of the second term on the right-hand side of (10) is set by comparison with turbulence decay behind a grid; that of the third term by analogy with the diffusion terms in (7)-(9); that of the last term by comparison with atmospheric surface layer data; and the other two by computer fit to a number of different simple flows.

Equation (10) cannot command as much confidence as (7)-(9) because of the need to model all of the terms in the equation. This is true whether dealing with equations for ϵ, A, or q/A. It is also necessary to impose boundary conditions appropriate to the particular flow situation.

3. Example Calculations

With the model set, verification may be achieved by comparing predictions and observations for example flows which were not involved in the determination of the model coefficients. Several such example flows are considered here.

3.1 Temperature fluctuations in a two-dimensional wake

The modeling of Eqs. (8) and (9) may be independently checked without involving stability influences by calculating the temperature fluctuations in a plane turbulent wake when the fluctuations are sufficiently weak for the gravitational terms to be neglected. Measurements behind a slightly heated cylinder have been made by Freymuth and Uberoi[13] and LaRue and Libby.[14] Figure 1 shows a comparison between the measured distributions far downstream of the cylinder and the self-similar profiles predicted by the model. The normalizing length z_{50} is fixed by comparison with the mean velocity profile. The agreement is quite good, particularly in the concurrence of the amplitude and position of the maximum temperature fluctuation. The centerline value of $(\overline{\theta^2})^{1/2}/\Delta\theta$ is given as 0.28 by LaRue and Libby in contrast to the value of 0.21 reported by Freymuth and Uberoi. The present model predicts a self-similarity value of 0.276.

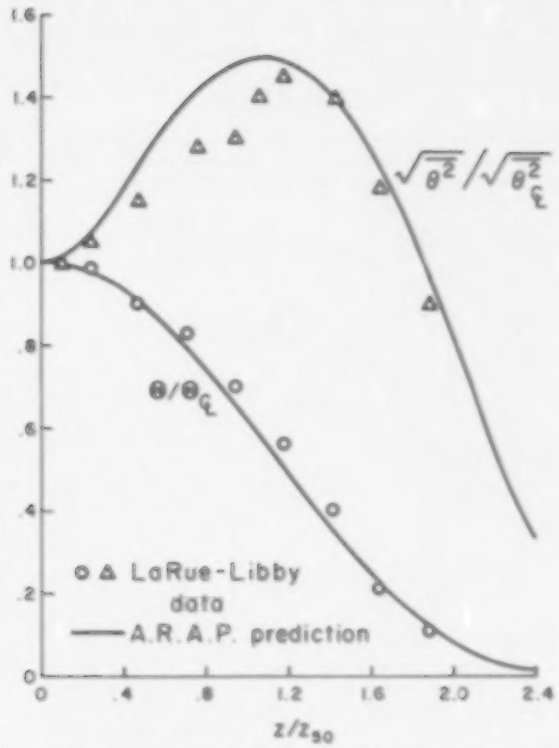

Figure 1. Temperature similarity profiles of mean temperature increment and temperature variance in a two-dimensional wake; data from Ref. 14

3.2 Stratified homogeneous turbulent shear flow

If an equilibrium flow with constant gradients in mean velocity and temperature can be established so that the turbulent correlations are homogeneous, Eqs. (7)-(9) reduce to algebraic relations between the turbulence and the mean flow gradients. Webster[15] attempted to produce such a homogeneous, stratified flow in a heated wind tunnel. Apparently, he did not achieve this goal completely since his turbulent correlations show a dependence on the streamwise direction. In spite of this acknowledged deficiency, we compare in Figure 2 the turbulent Prandtl number dependence on stratification predicted by Eqs. (7)-(9) with that reported by Webster at his most downstream station. The prediction of Launder's second-order closure model[5] is also indicated. Launder uses Webster's data to estimate some of his model coefficients.

The agreement between theory and observations in Figure 2 should only be interpreted as qualitative verification of the dependence on stability. The Prandtl number is normalized by its neutral value because of

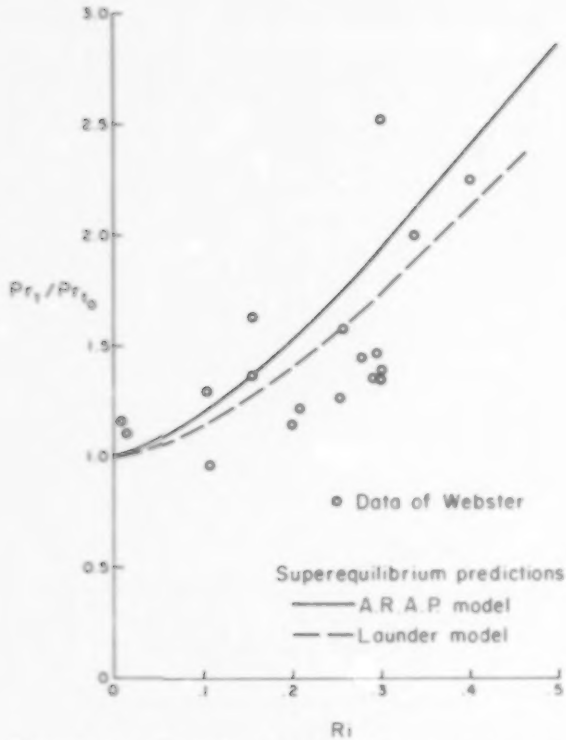

Figure 2. Turbulent Prandtl number dependence on stratification in a homogeneous stratified fluid. Data from Ref. 15; comparison prediction from Ref. 6

the large uncertainty in its reported values by Webster, varying by a factor of 3 from measurements at one station to the next.

Reliable turbulence data under stable conditions are difficult to obtain. Probably the best measured conditions are those existing in the atmospheric surface layer. The present model quite reasonably predicts the observed variations of the normalized variables with respect to the similarity variable, the ratio of the vertical height to the Monin-Obukhov length.[9] However, this cannot be used as independent verification of the model because of the use made of these data in determining the model coefficients.

Another stable flow which has been predicted by the model is that of shear layer entrainment in a stratified fluid. Calculations were made to simulate the experiment of Kato and Phillips.[16] They used dye to visually measure the rate of spreading of shear-generated turbulence into a region of fluid with a stable density gradient. Comparisons between the present model predictions and the observations have been made in Ref. 12. Since this represents little more than a qualitative comparison, it is not repeated here.

3.3 Free convection

Free convection is a flow that is quite different from the flows used to determine the model coefficients. The turbulence is produced by the unstable buoyancy force without influence from any mean shear stress. Willis and Deardorff[17] have measured the velocity and temperature fluctuations in an unstable layer bounded above by a stable density gradient and below by a surface with a positive heat flux. Their experiment called for establishing an initial stable temperature gradient between two surfaces and then applying a heat flux to the region through the lower surface. With mean velocities restricted to a minimum, free convection occurs in a mixed layer above the lower surface. The thickness of this mixed layer increases with time, but the fluctuating velocity distributions exhibit self-similarity when normalized by the characteristic velocity

$$w^* = \left(\frac{g \overline{w\theta}_0 z_i}{\theta} \right)^{1/3} \qquad (11)$$

where $\overline{w\theta}_0$ is the surface heat flux and z_i is the depth of the mixed layer.

Figure 3 compares our model predictions for the normalized vertical velocity fluctuations with the experimental observations. For the model predictions, we assumed no mean velocity and a constant surface heat flux to simulate the laboratory experiment. The agreement between predictions and observations is heartening, particularly since no model constant adjustments were involved.

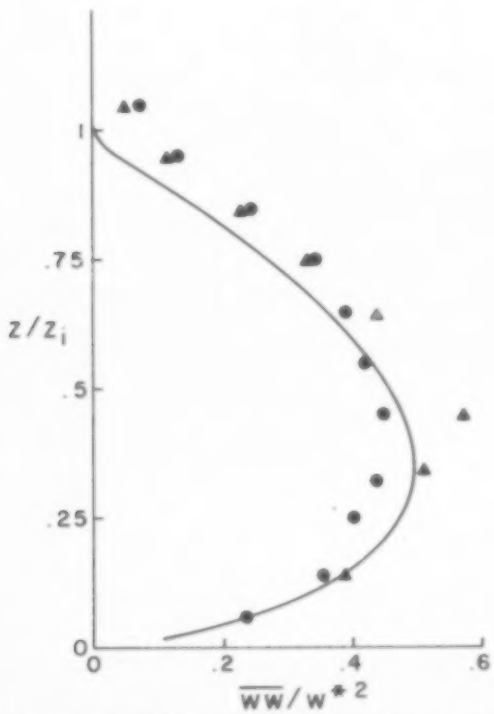

Figure 3. Similarity profiles of vertical velocity fluctuation in an unstable mixed layer; data from Ref. 17

The horizontal velocity fluctuations are given in Figure 4. Here the comparison with experiment is not as close since the observations show a peak near the lower surface that is not evidenced in the model results. The distributions of temperature fluctuations are shown in Figure 5. The agreement between model and experiment is very good except near the top of the mixed layer where the observations show a much stronger local maximum than is predicted. This may be due to the fact that inertial oscillations exist in this region. Overall, the comparison between model predictions and experimental observations is quite favorable.

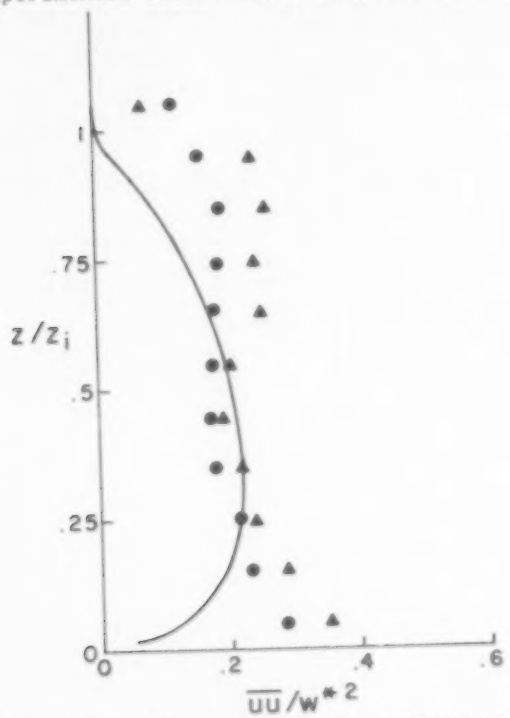

Figure 4. Similarity profiles of horizontal velocity fluctuations for the conditions of Figure 3

The favorable comparisons of Figures 3-5 are in spite of the fact that the modeled vertical flux of kinetic energy is significantly different from the experimental observations, as shown in Figure 6. This is consistent with our basic assumption that the second-order correlations calculated from their conservation equations are given more accurately than the accuracy to which the third-order correlations are approximated.

3.4 Diurnal variations in the planetary boundary layer

Over homogeneous terrain, the atmospheric boundary layer may be considered a function of time and altitude only. The results of calculations for a fixed geostrophic wind and upper level temperature lapse rate with a cyclic surface heat flux

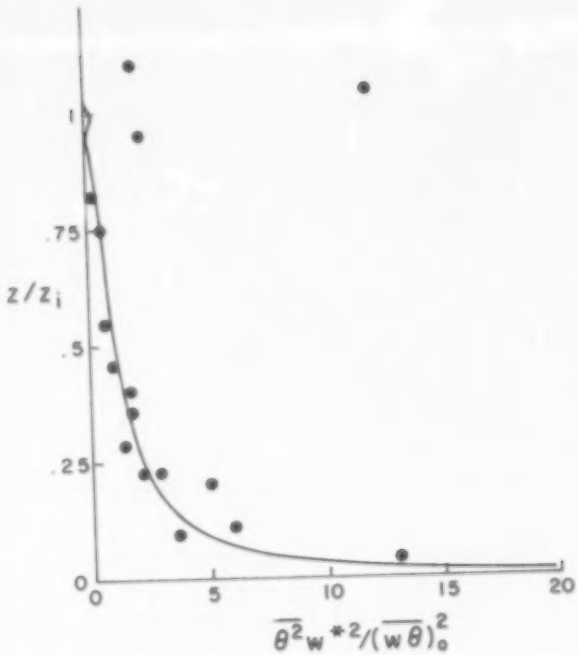

Figure 5. Similarity profiles of temperature fluctuations for the conditions of Figure 3

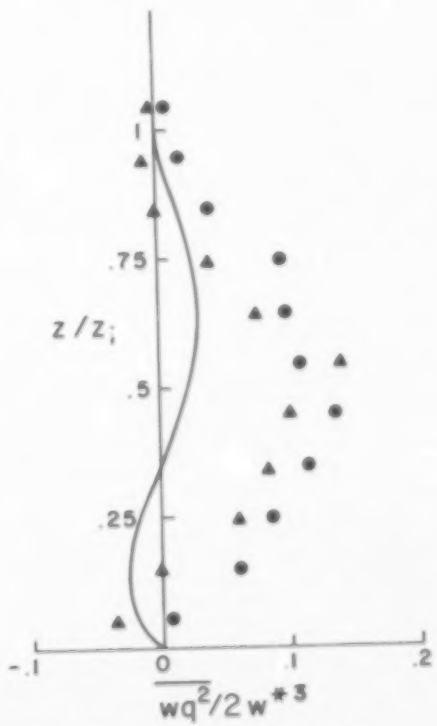

Figure 6. Similarity profiles of vertical flux of kinetic energy for the conditions of Figure 3

approximating conditions over the Midwestern plains during summer[18] are presented in Ref. 19. These results were obtained using a quasi-equilibrium approach to the equations and a gross feature approach to the scale. The results presented here were obtained using the full equations as presented in Section 2.

The predicted contours of constant turbulent fluctuations are presented in Figure 7 as a function of time and altitude. The boundary layer thickness grows during the day and shrinks during the evening and morning hours. The turbulent kinetic energy reaches a maximum of 4.8% of the geostrophic mean kinetic energy in the midafternoon at an altitude of approximately 500 meters. As the sun sets, the turbulence begins to decay until in the early morning hours its maximum kinetic energy is ≈0.25% of the mean kinetic energy. The biggest difference between the results presented here and those in Ref. 19 occurs during the early morning hours. The full equations with a

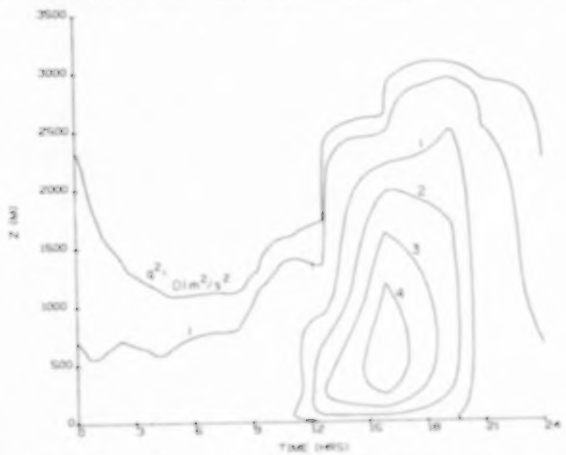

Figure 7. Isopleths of turbulent energy in a diurnal planetary boundary layer

dynamic scale predict a slower decay of q^2 and consequently considerably larger q^2 in the altitude range from 100 m to 1 km in the morning hours. But even this larger value is still quite small compared with afternoon values. Both model representations predict such features as the temperature inversion and local wind jet observed to occur nocturnally at low levels.

The variation of the angle between the direction of the geostrophic wind above the boundary layer and the direction of the surface wind is given in Figure 8 as a function of time of day. Some data points averaged over a summer for another location by Hoxit[20] are also included as a qualitative comparison. Since the average includes days with atypical surface heat flux and other influences such as baroclinicity, geostrophic wind variation, and moisture transport between the surface and the atmosphere, it is consistent to expect the model to predict a wider spread between the large angle at night and the small angle around noon. It is not clear whether there

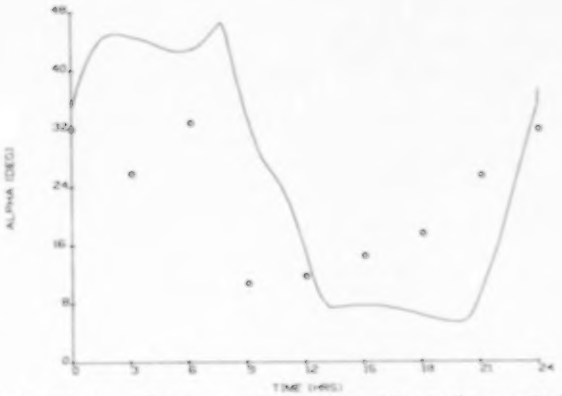

Figure 8. Diurnal variation of surface wind angle; data from Ref. 20

is sufficient shift in the surface heat flux variation to account for the apparent shift of approximately 3 hours in the rapid transition from high to low angle at sunrise.

Surface shear velocity is plotted as a function of the stability variable $\kappa u^*/fL$ in Figure 9. Data points for $Re \approx 10^7$, as taken from Tennekes' summary,[21] are included in the plot. The model predictions show a hysteresis loop with the surface shear stress significantly larger when the surface heat flux is decreasing rather than increasing. The data show considerable scatter but tend to be biased towards the upper bound. The factor of two difference in u^* at neutral conditions demonstrates the influence of unsteady dynamics on the atmospheric boundary layer.

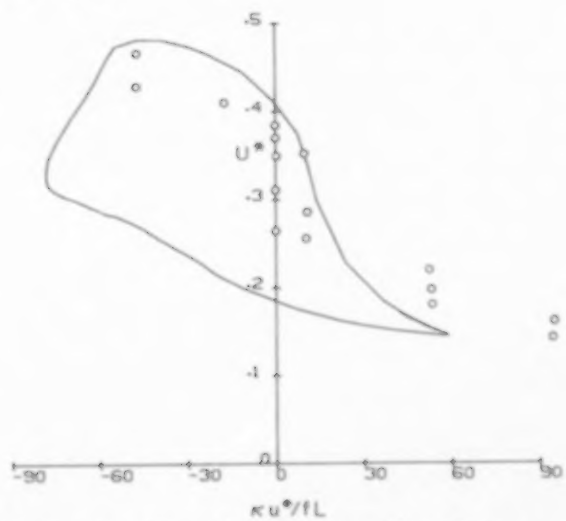

Figure 9. Diurnal variation of surface shear velocity as a function of stability; data from Ref. 21

3.5 Stratified wake

The passage of a body through a stratified fluid generates a turbulent wake containing kinetic and potential energy. The buildup of potential energy is caused by the co-mixing of heavier density fluid above the lighter density fluid. In the initial stages of wake development in a weakly stratified medium, the turbulent kinetic energy dominates the potential energy, and the wake spreads. This spreading in turn increases the potential energy until, at a time comparable to the natural oscillating period of the fluid, inertial waves are generated. Computations for this flow using a quasi-equilibrium version of the present model have been reported in Ref. 12.

Figure 10 shows typical contours of the turbulent kinetic energy and secondary flow stream function at two instances of time following wake initialization. Time is normalized by the characteristic Brunt-Väisälä period of the fluid

$$t_c = 2\pi[(g/\theta)\partial\theta/\partial z]^{-1/2} \qquad (12)$$

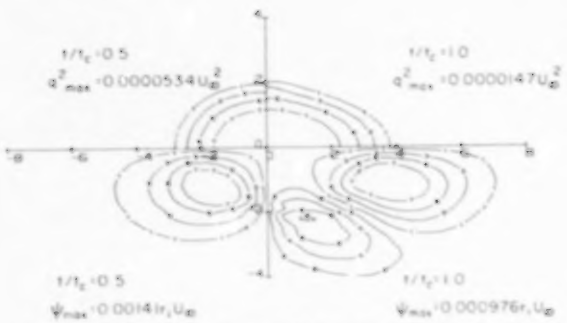

Figure 10. Contours of turbulent energy and secondary flow for two instances of time after wake initialization for Ri_o = 0.00925. 1 = +10% of maximum value for that quadrant; 2 = -10%; 3 = +30%; 4 = -30%; etc.

The flow is symmetric about both axes so that only one quadrant is shown for each variable at each time. At t/t_c = 0.5, the secondary flow exhibits a simple collapsed motion, while at t/t_c = 1, a second wave mode has been added. At both times the secondary flow extends well outside the region of turbulence.

Figure 11 is a summary plot showing the sensitivity of the wake shape to initial Froude number, $Fp = Ut_c/D$, or initial Richardson number of the turbulence, $Ri_o = (2\pi r_1/q_{max}t_c)^2$, along with a qualitative comparison with laboratory flow visualization results.[22]

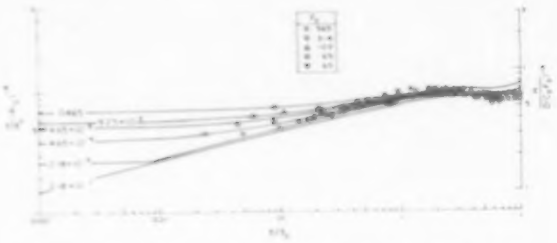

Figure 11. Vertical spread of stratified wake; data from Ref. 22

4. Concluding Remarks

The explicit appearance of buoyancy terms in the equations for Reynolds stress and turbulent heat flux are sufficient to account for many of the effects observed in variable density flows. The only direct influence of buoyancy included in the modeled terms required for closure is its influence on the macroscale parameter $\bar{\lambda}$. The predictions of this relatively simple second-order closure model appear to be reasonably consistent with available observations, although there still exists a need for unambiguous experiments under relatively stable flow conditions. One can expect continued model development, but the model appears sufficiently accurate to permit practical calculations to proceed concurrently.

5. References

[1]Donaldson, C.duP., "Calculation of Turbulent Shear Flows for Atmospheric and Vortex Motions," AIAA Journal, Vol. 10, No. 1, January 1972, pp. 4-12.

[2]Donaldson, C.duP., "Atmospheric Turbulence and the Dispersal of Atmospheric Pollutants," AMS Workshop on Micrometeorology (D.A. Haugen, ed.), Science Press, Boston, 1973, pp. 313-390.

[3]Mellor, G.L., "Analytic Prediction of the Properties of Stratified Planetary Surface Layers," J. Atmos. Sciences, Vol. 30, 1973, pp. 1061-1069.

[4]Daly, B.J. and Harlow, F.H., "Transport Equations in Turbulence," Phys. Fluids, Vol. 13, No. 11, 1970, pp. 2634-2649.

[5]Wyngaard, J.C., Coté, O.R. and Rao, K.S., "Modeling the Atmospheric Boundary Layer," Advances in Geophysics, Vol. 18A, Academic Press, New York, 1974.

[6]Launder, B.E., "On the Effects of a Gravitational Field on the Turbulent Transport of Heat and Momentum," J. Fluid Mech., Vol. 67, Part 3, 1975, pp. 569-581.

[7]Meroney, R.N., "Buoyancy Effects on a Turbulent Shear Flow," Project THEMIS Report No. 28, Colorado State University, April 1974.

[8]Lewellen, W.S., Teske, M.E., and Donaldson, C.duP., "Application of Turbulent Model Equations to Axisymmetric Wakes," AIAA Journal, Vol. 12, No. 5, 1974, pp. 620-625.

[9]Lewellen, W.S. and Teske, M.E., "Prediction of the Monin-Obukhov Similarity Functions from an Invariant Model of Turbulence," J. Atmos. Sciences, Vol. 30, 1974, pp. 1340-1345.
[10]Bradshaw, P., "The Understanding and Prediction of Turbulent Flows," Aeronautical Journal, 1972, pp. 403-418.
[11]Mellor, G.L. and Herring, H.J., "A Survey of Mean Turbulent Field Closure Models," AIAA Journal, Vol. 11, No. 5, 1973, pp. 590-599.
[12]Lewellen, W.S., Teske, M.E., and Donaldson, C.duP., "Turbulent Wakes in a Stratified Fluid," Aeronautical Research Associates of Princeton, Inc. Report No. 226, September 1974.
[13]Freymuth, P. and Uberoi, M.S., "Structure of Temperature Fluctuations in the Turbulent Wake Behind a Heated Cylinder," Phys. Fluids, Vol. 14, No. 12, 1971, pp. 2574-2580.
[14]LaRue, J.C. and Libby, P.A., "Temperature Fluctuations in the Plane Turbulent Wake," Phys. Fluids, Vol. 17, No. 11, 1974, pp. 1956-1975.
[15]Webster, C.A.G., "An Experimental Study of Turbulence in a Density-Stratified Shear Flow," J. Fluid Mech., Vol. 19, Part 2, 1964, pp. 221-245.
[16]Kato, H. and Phillips, O.M., "On the Penetration of a Turbulent Layer into Stratified Fluid," J. Fluid Mech., Vol. 37, Part 4, 1969, pp. 643-656.
[17]Willis, G.E. and Deardorff, J.W., "A Laboratory Model of the Unstable Planetary Boundary Layer," J. Atmos. Sciences, Vol.31, 1974, pp. 1297-1307.
[18]Wyngaard, J.C., "Notes on Surface Layer Turbulence," AMS Workshop on Micrometeorology (D.A.Haugen, ed.), Science Press, Boston, 1973, pp. 101-149.
[19]Lewellen, W.S., Teske, M.E., and Donaldson, C.duP., "Turbulence Model of Diurnal Variations in the Planetary Boundary Layer," Proc. 1974 Heat Transfer and Fluid Mechanics Institute (L.R.Davis and R.E.Wilson, eds.), Stanford University Press, Stanford, 1974, pp. 301-319.
[20]Hoxit, L.R., "Diurnal Variations in Planetary Boundary-Layer Winds Over Land," Boundary Layer Meteorology, Vol. 8, 1975, pp. 21-38.
[21]Tennekes, H., "Similarity Laws and Scale Relations in Planetary Boundary Layers," AMS Workshop on Micrometeorology (D.A. Haugen, ed.), Science Press, Boston, 1973, pp. 177-216.
[22]Lin, J.T. and Pao, Y.H., "Turbulent Wake of a Self-Propelled Slender Body in Stratified and Nonstratified Fluids: Analysis and Flow Visualizations," Flow Research Corp. Report No. 11, 1973.